Conceptual simplifications for long-term sediment transport simulations

-Application to Iffezheim reservoir, Germany

vorgelegt von

Qing Zhang, M.Sc.

geb. in Heilongjiang, China

von der Fakultät VI – Planen Bauen Umwelt
der Technischen Universität Berlin

zur Erlangung des akademischen Grades
Doktor der Ingenieurwissenschaften
- Dr.-Ing. -

Genehmigte Dissertation

Promotionsausschuss:

Vorsitzender:	Prof. Dr.-Ing. Matthias Barjenbruch
Gutachter:	Prof. Dr.-Ing. Reinhard Hinkelmann
Gutachterin:	Prof. Dr.-Ing. Silke Wieprecht
Gutachterin:	Dr.-Ing. Gudrun Hillebrand
Gutachter:	apl. Prof. Dr.-Ing. Frank Molkenthin

Tag der wissenschaftlichen Aussprache: 13. Februar 2018

Berlin 2018

Dedicated to

my beloved parents and my lovely fiancé

Abstract

The aim of this PhD thesis is to assess the long-term evolution of the fine sediment budget in the Iffezheim reservoir, which is the last barrage of the impounded section of the Rhine River. Based on the observed flow and suspended sediment concentration as well as echo-sounding data, various methods were proposed to estimate long-term riverbed changes. The application of a high-resolution 3D model was one focus in order to capture the multi-dimensional flow effects upstream of the barrage as accurately as possible and to represent the local deposition and erosion in a realistic manner.

Since practicable computation time for long-term predictions using high-resolution 3D models has not yet been considered to be satisfactory with the current technique, methods for reducing the computational effort while maintaining similar accuracy were developed. First, the reduction of the high-resolution model was carried out by coarsening the grid in space and time and decreasing the number of sediment fractions. The reduced 3D model contributed to large savings of computation time by 76 %, while the solution accuracy remains similar (5 % deviation) when compared to high-resolution results. Secondly, an upscaling approach was developed, where long-term instationary simulations of riverbed volume changes were replaced by a series of precalculated stationary ones. For this purpose, the boundary conditions of the numerical model - the discharges and the suspended sediment concentrations - are grouped into classes and for each class a representative computation for one day was carried out. The amount of the riverbed change for a certain period was obtained by adding up the number of days per class multiplied with the precalculated representative volume change of this class. Using this approach, the reduction of CPU time was considerable with 97 %, while the results for long-term (years) simulations matched well with the measurements (+3 % and 20 %). In order to obtain projected boundary conditions of the numerical model, time-series analysis and synthesis and artificial neural networks (ANN) were applied. In the context of the time series the ARIMA model performed the best and showed a reasonable agreement between predicted and observed values for 5 years forecasting monthly inflow. Based on projected discharges from the KLIWAS program the ANN model predicted the daily suspended sediment concentration until 2100 and considerably

improved the results in comparison to a usual sediment rating curve.

Ultimately, a coupled concept was developed linking advantages of the above-mentioned approaches. It was possible to determine a reasonable prediction of the sediment volume changes in the study area for the near future (2020-2049) and far future (2070-2099) with a reasonable computation time. The results reveal that for the chosen climate scenario for the near future 33 % and for the far future 63 % more sediment volume changes, mainly deposition, than currently are expected leading to more extensive dredging measures.

Kurzfassung

Zielstellung dieser Arbeit ist die Abschätzung des langfristigen Feinsedimenthaushalts der Staustufe Iffezheim, welche die letzte Staustufe im staugeregelten Oberrhein darstellt. Basierend auf vor Ort gemessenen Abflüssen und Schwebstoffkonzentrationen sowie Peilmessungen zur Sohlentwicklung wurden verschiedene Methoden zur Prognose der langfristigen Sohlhöhenveränderungen entwickelt. Ausgangspunkt war ein hochauflösendes 3D-Modell, mit dem die mehrdimensionalen Strömungseffekte im Stauraum und die lokalen Depositionen und Erosionen möglichst realistisch abgebildet werden konnten.

Da praktikable Berechnungszeiten für Langzeitvorhersagen mit hochauflösenden 3D-Modellen mit dem heutigen Stand der Technik noch nicht zufriedenstellend möglich sind, wurden Methoden zur Reduzierung des Berechnungsaufwandes unter Beibehaltung einer vergleichbaren Genauigkeit entwickelt. Im ersten Schritt wurde das hochaufgelöste Modell räumlich und zeitlich vergröbert und die Anzahl der Sedimentfraktionen reduziert. Das reduzierte 3D-Modell führte zu einer großen Rechenzeitersparnis von 76 %, während die Genauigkeit der Ergebnisse im Vergleich zum hochaufgelösten Modell ähnlich blieb (5 % Abweichung). Danach wurde ein Skalierungsansatz entwickelt, bei dem langfristige instationäre Simulationen von Sedimentvolumenänderungen durch eine Reihe von vorberechneten stationären Simulationen ersetzt wurden. Dafür wurden die Randbedingungen des Modells (Abflüsse und Schwebstoffkonzentrationen) in Klassen eingeteilt und für jede Klasse wurde eine repräsentative Berechnung für einen Tag durchgeführt. Die Gesamtvolumenänderung für einen bestimmten Zeitraum wurde dann durch Summieren der Anzahl der Tage in jeder Klasse multipliziert mit der vorberechneten repräsentativen Volumenänderung dieser Klasse ermittelt. Mit dieser Vorgehensweise war die Reduzierung der Rechenzeit mit 97 % beträchtlich, während die Ergebnisse für Langzeitsimulationen (Jahre) gut mit den Messungen übereinstimmten (+3 % und 20 %). Um Vorhersagen für die Randbedingungen des numerischen Modells zu erhalten, wurden die Methoden Zeitreihenanalyse und -synthese sowie Künstliche Neuronale Netzwerke (KNN) angewendet. Bei den Zeitreihen lieferte das ARIMA Modell die besten Ergebnisse und zeigte eine gute Übereinstimmung zwischen den vorhergesagten und beobachteten Werten bei einer

5 Jahres-Vorhersage der monatlichen Zuflüsse. Basierend auf projizierten Abflüssen aus dem KLIWAS-Programm prognostizierte das KNN Modell die täglichen Schwebstoffkonzentrationen bis zum Jahr 2100 und führte zu erheblich verbesserten Ergebnissen im Vergleich zu einer üblichen Transport-Abfluss-Beziehung.

Letztlich wurden die genannten Methoden unter Nutzung ihrer jeweiligen Vorteile zu einem Gesamtkonzept verknüpft. Damit war es möglich, eine brauchbare Vorhersage der Sedimentvolumenänderungen im Untersuchungsgebiet für die nahe Zukunft (2020 - 2049) und auch für die ferne Zukunft (2070 - 2099) mit einer effizienten Berechnungszeit zu ermitteln. Die Ergebnisse zeigen, dass für das gewählte Klimaszenario für die nahe Zukunft 33 % und für die ferne Zukunft 63 % mehr Sedimentvolumenänderungen, hauptsächlich Deposition, als zurzeit zu erwarten sind, was zu umfangreicheren Baggermaßnahmen führen wird.

Acknowledgements

This dissertation summarizes my work at the Chair of Water Resources Management and Modeling of Hydrosystems, Department of Civil Engineering, Technische Universität Berlin and at the Department M3, Groundwater, Geology, River Morphology, Federal Institute of Hydrology, Koblenz in the years 2012-2017.

First of all, I would like to express my sincere gratitude to Prof. Reinhard Hinkelmann for his outstanding supervision and inspiring attitude during the time I have been working at the chair. I would like to thank him for the financial support and giving me the freedom to realize my ideas and to achieve my goals. I would like also to thank Prof. Hans Moser for providing valuable advice and help.

I am deeply grateful for Dr. Gudrun Hillebrand. Many thanks for sharing her profound knowledge of modelling sediment transport, experience of field work and providing field data used in this study. She continuously supported me no matter how busy she was. I am also grateful to Dr. Thomas Hoffmann for the valuable discussions and contributed ideas. I would like to thank Prof. Nils Reidar B. Olsen for his support of solving problems with the 3D numerical code SSIIM.

A huge thanks is addressed to all my colleagues I met at the Federal Institute of Hydrology in Koblenz: Frauke König, Axel Winterscheid, Birgit Astor, Stefan Vollmer, Ulrich Looser. Further I would like to show my appreciations to all my colleagues and friends: Theresa Speckter, Vikram Notay, Clara Scheer, Irina Klassen, Ralf Duda. I could not express my thanks with only a few words to my friends in Germany and abroad for the great courage and memory of joy. Last but not least, I would like to take this opportunity to express my great gratitude and blessings to all those people around the world who have ever helped me in any respect of this thesis.

Contents

List of Figures

List of Tables

Nomenclature

Abbreviations

1D one-dimensional

2D two-dimensional

3D three-dimensional

a.s.l. above see level

ACF Auto Correlation Function

ADCP Acoustic Doppler Current Profiler

AI Artificial Intelligence

AIC Akaike Information Criterion

ANN Artificial Neural Networks

approx. approximately

BC Riverbed Volume Change

BfG German Federal Institute of Hydrology

BFGS Broyden-Fletcher-Goldfarb-Shanno

CFL Courant-Friedrichs-Lewy (Courant)

COV Coefficient of Variation

CPU Central Processing Unit

CSF Corey Shape Factor

DC Coefficient of Determination

DEM Digital Elevation Model

FAM Finite-Area-Method

FEM Finite-Element-Method

FFBP Feed-Forward Back Propagation

FVM Finite-Volume-Method

GIS Geographic Information System

HCB Hexachlorobenzene

KLIWAS Impacts of climate change on waterways and navigation – Searching for options of adaptation (Auswirkungen des Klimawandels auf Wasserstraßen und Schifffahrt – Entwicklung von Anpassungsoptionen)

LOESS Locally Weighted Scatterplot Smoothing

MAH Monocyclic Aromatic Hydrocarbons

MBE Mean Bias Error

MLR Multiple Linear Regression

MNLR Multiple Non-Linear Regression

NF Neuro-Fuzzy

PACF Partial Auto Correlation Function

PAH Polycyclic Aromatic Hydrocarbons

PCB Polychlorinated Biphenyls

R Correlation Coefficient

RMSE Root Mean Square Error

SBM Sediment Budget Method

SIMPLE Semi-Implicit Method for Pressure-Linked Equations

SRC Sediment Rating Curve

TCM Topographic Change Method

WANN Wavelet Artificial Neural Networks

WSV Federal Waterways and Shipping Administration

Greek Symbols

δ_{ij} Kronecker delta

ν kinematic viscosity

$\rho\overline{u_i u_j}$ turbulent Reynolds stresses

ρ_s sediment density

ρ_w water density

σ standard deviation

τ bed shear stress

τ^* non-dimensional shear stress

τ_c critical shear stress

ε turbulent dissipation

Ξ Yalin parameter

ξ exposure factor

κ von Karman constant

v_T turbulent eddy viscosity coefficient

Latin Symbols

a reference level

C_d drag coefficient

c_i concentration of suspended load for i^{th} fraction

d diameter of the sediment particle

d_0	diameter of the reference sediment particle
d_i	sediment particle diameter for i^{th} fraction
d_{max}	maximum grain size
$f_{a,0}$	initial fraction of active layer
f_a	fraction of active layer
f_d	fraction of the deposited material
FF	shape factor
g	gravitational acceleration
H	water level
h	water depth
k	turbulent kinetic energy
k_s	roughness
P	power value of roundness
p	dynamic pressure
Q_s	sediment transport rate
R_i	power roundness parameter
Re	Reynolds number
Re^*	grain Reynolds number
S	sediment source term
Sc	Schmidt number
u_*	shear velocity
U_i	averaged velocity
w_s	settling velocity
z_a	height of active layer

z_d	height of deposition
D_*	dimensionless nominal diameter
w	vertical velocity
sec	second

Chapter 1

Introduction

1.1 Problem statement

The Rhine River is one of Europe's most important waterways. The Rhine is about 1,233 km long. Following its source in the Swiss Alps, it flows through France and Germany, finally emptying into the North Sea in the Netherlands. To guarantee navigation, flood protection and for the generation of energy, ten barrages have been constructed in the Upper Rhine between Basel and Iffezheim during the last century (see Figure 1.1). The construction of these barrages has heavily restricted the sediment transport processes. Particularly, this is the case at the Iffezheim barrage, which is the last of a series of ten barrages (see Figure 1.1). Its issue has been connected in the joint research project "Estimation long-term evolution of fine sediment budget in the Upper Rhine", which was carried out by the German Federal Institute of Hydrology (BfG), the Karlsruhe Institute of Technology and the Technische Universität Berlin. The long-term estimation of the fine sediment budget, which describes the balance between quantities of sediment input, sediment output and accumulated sediment in the study area itself (BfG, 2016; Gehres et al., 2016), is of great importance for canalized and impounded rivers such as the Upper Rhine.

This doctoral thesis focuses on the problems of the aforementioned barrage - namely, the Iffezheim barrage. There, several problems of weir system, i.e., those due to sediment transport, can be found. On the one hand, erosion occurs immediately downstream of the last barrage in the Upper Rhine. This is counteracted by an annual artificial bed load supply of approx. 180,000 m^3 to maintain the water level (Boettcher, 2001), as agreed upon with France. On the other hand, about 60 % of the total dredging volume in the Upper Rhine is assigned to Iffezheim reservoir, according to the analysis of dredging volume in the Upper Rhine barrages from 1991-2004 by Vollmer and Goelz (2006).

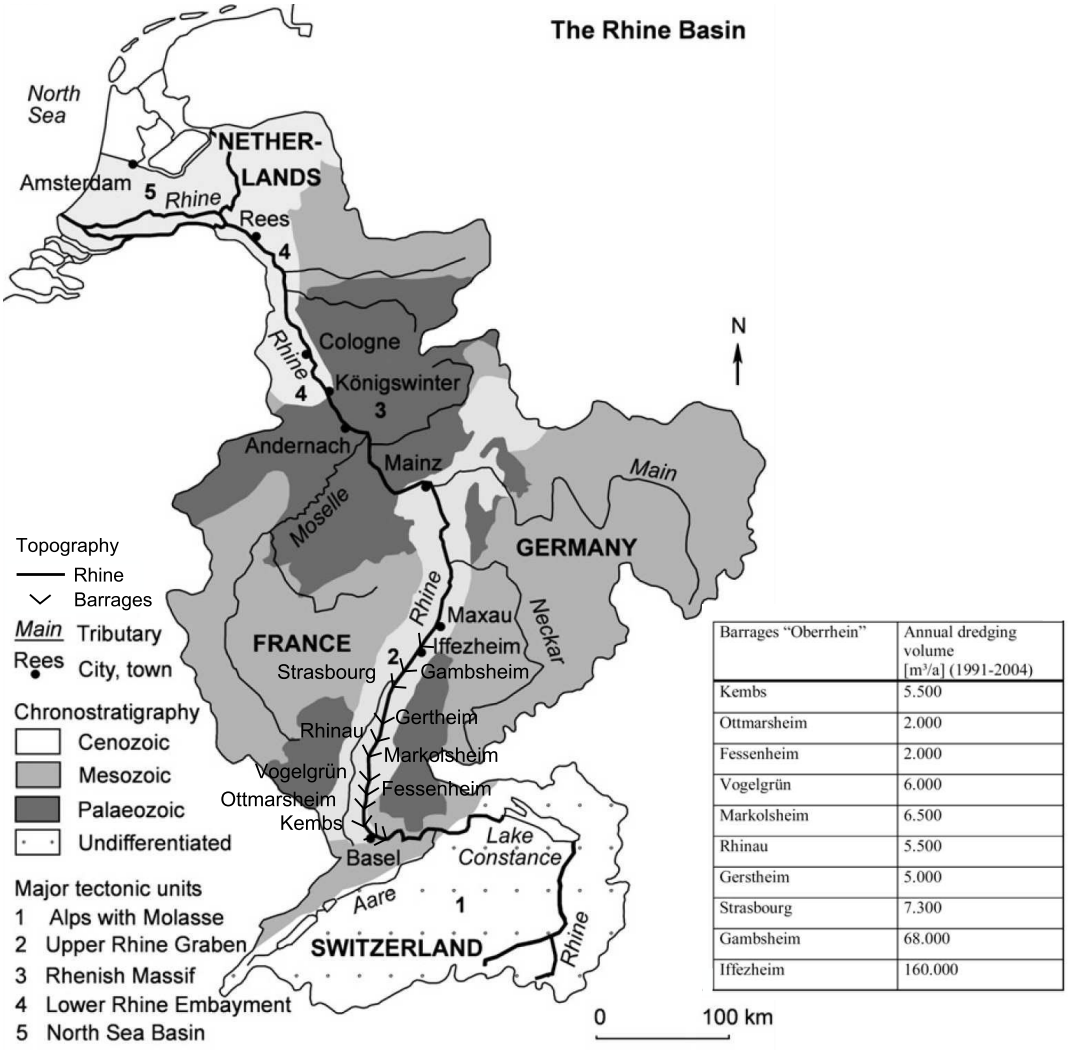

Barrages "Oberrhein"	Annual dredging volume [m³/a] (1991-2004)
Kembs	5.500
Ottmarsheim	2.000
Fessenheim	2.000
Vogelgrün	6.000
Markolsheim	6.500
Rhinau	5.500
Gerstheim	5.000
Strasbourg	7.300
Gambsheim	68.000
Iffezheim	160.000

Figure 1.1: Catchment area of the River Rhine, ten impoundments at the Upper Rhine and annual amounts of dredged sediment between 1991 and 2004 (modified from Frings et al. (2014) and Vollmer and Goelz (2006)).

Figure 1.2: Iffezheim reservoir and Plittersdorf gauging station in the downstream (modified from Köthe et al. (2004)).

Annually approximately between 50,000 m^3 and 160,000 m^3 of fine sediments have accumulated in the weir channel since the construction of the barrage in 1977 (Huber, 2005; Karnahl, 2008). The accumulation of fine sediment upstream of the barrage is the main topic of this thesis, as this phenomenon is common to all barrages in the Upper Rhine.

The accumulated fine sediments lead to both economic and ecological consequences, i.e., it reduces reservoir storage capacity for flow regulation and also adversely affects the flood protection by increased water levels. In order to keep the dam stable and maintain the capacity of the weir channel, dredging measures have to be undertaken. This leads to high costs. Moreover, polluted fine sediment is found from the dredging material at different barrages in the Upper Rhine. The contaminants include heavy metals, arsenic, monocyclic (MAH) and polycyclinc aromatic hydrocarbon (PAH), and other organic compounds like polychlorinated biphenyl (PCB). However, the contamination load of the Rhine River has been constantly decreasing since the 1960s. Only the chemical compound hexachlorobenzene (HCB) causes still problems for fish and environmental health. In the 1970s and 1980s, HCB was induced to the Rhine River through industrial wastewater. The chemical compound occurred as a by-product in the production of pentachlorophenol and chlorsilanes. HCB can attach to fine sediment particles due to the strong adsorption power and their high specific surface area. This contaminant is

bioaccumulative, hardly biodegradable and thus persistent in the environment (Pohlert et al., 2011). Due to the slow flow velocities, reservoirs in the barrages upstream are long-term sinks of this kind of contaminated fine sediments. In case of high contamination, it is not allowed to relocate dredged and contaminated sediment to other river sections.

In order to assess the long-term fine sediment budget, it is important to understand the long-term sediment dynamics. To achieve this goal, **long-term model studies**, which should simulate sediment transport, riverbed erosion and deposition processes, are necessary. In this way, the frequency and amount of cost-intensive dredging requirements in the reservoir can be assessed more accurately.

1.2 State of the art

Over the past years, models for long-term forecasting have been of particular interest in operational hydrodynamics and morphodynamics. Hydrodynamics is the study of fluid in motion, whereas morphodynamics indicates the response of bathymetry to hydrodynamic processes as well as their mutual interaction, e.g., the water movement, sediment dynamics (Wright and Thom, 1977; Zhou, 2011). Models can be classified into physical models, numerical models and data-driven models.

Physical models are based on physical laws, i.e., they imitate hydrodynamic and sedimentary processes in a representative or physical way. Physical models are often carried out at a much smaller spatial scale and provide the opportunity to study morphodynamic systems using controlled settings (Zhou et al., 2014). However, finding a reasonable scaling factor which can be applied with confidence to relate physical experiments to natural systems is a typical difficulty; extensive setup techniques require significant time to complete. From the practical point of view, physical models are desirable for in situ observation, but not suitable for long-term assessment and consequently, not included in this thesis.

Numerical modelling has attracted many research studies because of satisfactory results and their efficiency. A numerical morphodynamic model can simulate the morphodynamic processes in a reservoir as a function of the hydrodynamic processes. Many parameters from laboratory and field measurements are required for model setup. Once calibrated and subsequently validated, a numerical model can be a powerful technique for investigating various possible natural or anthropogenic scenarios for predicting a range of plausible sediment yields in the future, e.g. fine sediment budget prediction (van Rijn et al., 2001). Numerical morphodynamic models include 1D, 2D and 3D models. 1D

numerical models, e.g., SOBEK, can be applied to assess bed evolution and calculate the transported sediment loads. However, they are inherently limited to 1D flow and sediment transport problems, such as section integrated erosion and deposition processes in a straight and homogeneous river reach (Rüther, 2006). 2D numerical models can accurately predict morphological changes, when 3D flow effects are of minor importance, such as in many straight open channel flows, the vertical velocity component is much smaller than the horizontal components because of the large width-to-depth ratio (Rüther, 2006). The advantage of a 3D model is the possibility of modeling many processes in any river geometry with complex flow effects, e.g., curved channels with helical flow. In such cases, the application of a 3D model should give better results compared to 2D and 1D models. But their disadvantage is the long computation time due to the large number of cells.

Data-driven models are based on the analysis of previously observed data and try to improve associations between input and output variables, without considering the fundamental physical laws, and consequently, can generate future time series. Recently, they have been used for modeling hydromorphodynamic processes, because of their simplicity, rapid development time, minimum information requirements and ease of real-time implementation (Tayyab et al., 2016; Zhang et al., 2015b). Data-driven models can be broadly divided into three groups: regression-based models, time series models and artificial intelligence (AI)-based methods.

Regression analysis is a statistical process for estimating the relationships among variables, e.g. a first order Markov-model (Maniak, 1997), a Fiering model (Fiering, 1972), multiple linear regressions (MLR), multiple non-linear regressions (MNLR). The regression analysis is often employed in such a way as to test theories that the current values of one or more independent time series affect the current value of another time series. They have been applied successfully in solving hydrological problems (Ho and Xie, 1998; Yousif et al., 2016; Zhang, 2003), e.g. the Fiering model works well with monthly flow data.

After the publication of Box et al. (1976), Box-Jenkins or ARIMA (autoregressive integrated moving average) models became one of the most used time series models in forecasting process changes, especially in hydrological forecasting (Karamouz and Araghineja, 2012).

In recent years, AI-based techniques are capable of analyzing long time-series, large-scale data and non-linear systems. They have become increasingly popular. Compared to regression-based methods and time series models, AI-based models have the advantage to capture the complex behaviour of non-uniform data from dynamic and non-linear

natural systems well (Nourani et al., 2014). There are a few studies dealing with sediment volume estimation in reservoirs. Jothiprakash and Vaibhav Gang (2009) estimated the volume of sediment retained in the Gobindsagar reservoir in India by artificial neural network (ANN), using 32 years time series of annual rainfall, annual inflow and capacity of the reservoir as inputs. Uenes et al. (2013) estimated the Tahtaköprü reservoir volume evolution in Turkey by ANN, using monthly precipitation, monthly total volume of evaporation, dam spillway discharge volume, released irrigation water amount and periodicity. The data were collected over 29 years. As shown above, AI techniques require many input parameters and long data sets for predicting sediment quantities. Until now, most studies are about modelling of river flow records (Khashei and Bijari, 2010; Zhou et al., 2008). AI models proved a superior prediction performance in forecasting suspended sediment concentrations (Cigizoglu and Alp, 2006; Cigizoglu and Kisi, 2006; Kumar et al., 2016; Liu et al., 2013; Rajaee, 2011; Zounemat-Kermani et al., 2016).

For predicting long-term evolution of the fine sediment budget in Iffezheim reservoir, methods for direct targets, i.e., the total volume change and for intermediate objectives, e.g. the boundary conditions of numerical model - discharge and suspended sediment concentration are employed in this investigation. Here numerical and data-driven models are applied in terms of accuracy and efficiency. A further detailed literature review about 3D numerical morphodynamic models worldwide is described in section 4.1. Some literature research about data-driven models for appropriate objectives are summarized in section 7.1 and section 8.1.

1.3 Study area

1.3.1 Historical background of the river engineering in the Upper Rhine

Since the beginning of the 18th century, the Upper Rhine has changed immensely due to anthropogenic influences that consequently characterize present flow and transport processes.

The Upper Rhine was originally a diverse network of large and small watercourses that were continuously changing over time. The mild climate brought there a diverse flora and fauna. Nevertheless, humans were at high risk from flooding or epidemics during low-water periods. Consequently, to improve the flood protection and to reclaim land, the river was straightened between Basel and Mannheim (see Figure 1.1). Following the plans of the German engineer Johann Gottfried Tulla (Henze, 1989), this

process of straightening was accomplished between 1817 to 1876. The highly branched and meandering river was restricted to the main river channel. To realize this, river sinuosity was filled up and river bend cutoffs were created. Additionally, dams have been constructed for flood protection. Thereby, the Rhine River has been shortened by one quarter (ca. 80-90 km) of its original length between Basel and Mannheim. The shortening led to higher flow velocities and stronger bed erosion. The Rhine River dug constantly deeper into a new riverbed layer. As a result, groundwater level sunk by several meters, which made the surrounding landscape dry. Wells had to be dug deeper and forests in the floodplain died (BAW, 1980). A further problem arose in the downstream area of the Upper Rhine, as the flood risk rose due to the missing retention areas.

The construction of groynes from 1912 until the beginning of the Second World War (Kreus, 2008) lead to the narrowing of the waterway and made it possible to navigate even when the water level was low. But it also aggravated the effect of degradation and this in turn additionally affected the groundwater level.

Apart from the regulation of the Rhine River using groynes, the construction of the "Grande Canal d'Alsace" (side-channel of the Rhine) began in 1928. In the Treaty of Versailles, France secured sole use of the hydropower generated at the Rhine River along the German border and reimbursed Germany half the value of the actual gained energy. The side-channel has a depth of approx. 9 m and a width of 80 m at the riverbed and 130 m at the water surface (FGG Rhein, 2015). The discharge up to 1400 m^3/s is drained in the side-channel for energy generation and safe navigation. At the same time, the remaining discharge in "Tullas riverbed" was regulated by an average discharge of 20 to 30 m^3/s for approx. 300 days per year. The channel built on the left hand side of the river between Basel and Strasbourg (see Figure 1.1). The riverbed was covered in concrete entirely to avoid the problem of erosion. After finishing the first part of the channel, with a pause in construction caused by the Second World War, the consequences became clear. Due to the impermeable riverbed, the groundwater level decreased further. This led to negative effects on nature and agriculture. Moreover, the flood wave was further accelerated through the construction. Continuing the channel construction to Strasbourg would have exacerbated the situation and disconnected German harbours in the navigable section of the Rhine. Thus, Germany proposed the preventative "Schlingen" resolution (compromise) to France. Recorded by the treaty in 1956, this agreement involved the section of the Rhine River stretching from Breisach to Strasbourg (see Figure 1.1). To reach an agreement with France, Germany agreed to the channelization of the Mosel River and also gave up half of their share of the generated power that was

already agreed upon in the Treaty of Versailles in 1919.

Following the "Schlingen" approach, four barrages were built between Breisach and Strasbourg between 1960 and 1970. As a result, the waterway for navigation runs alternatively along the Rhine, and it passes along a half loop ("Schlingen") in the sections with the barrages. The loops include the hydropower plants and shipping locks. In the Rhine River, sills and weirs were built to keep the water level high and to keep the groundwater level. Due to the low flow velocity in the re-regulated Upper Rhine, the problem of deep erosion was reduced in this part of the river. But this problem still existed downstream of Strasbourg. Basically, the bed load transport was interrupted by the barrages, while strong riverbed erosion was observed directly downstream of the barrages. To counteract this, France and Germany decided to build the barrages of Gambsheim (1974) and Iffezheim (1977) that were also used for energy generation. For planning the barrages, instead of the constructional loop concept - "Schlingen" resolution, the barrages were built directly on the Rhine River (see Figure 1.2). The old riverbed was locked by a cross-dam. Right next to the cross-dam, a movable weir was located on one side and a power plant and two ship locks on the other side. It was already known in the planning phase that the problem of degradation would only be transferred further downstream. Therefore, to avoid the need for construction of further barrages, bed loads are artificially filled directly downstream of the Iffezheim reservoir.

The observations of the last two centuries show a chain of events that can appear due to the alteration of the river. At the end of this series of barrages stands the Iffezheim barrage, which is the focus of this study. The Iffezheim barrage and its upstream reservoir, which is located between Rhine km-309.1 to 334.0, at the French-German Border between Karlsruhe and Strasbourg, together form the largest impoundment of the Rhine. The Iffezheim barrage divides the downstream part of the reservoir in three channels. The middle channel leads the water to the hydropower plant. The orographic left channel is the channel to the weir and the right is a lock channel for ships (see Figure 1.2).

1.3.2 Morphological evolution after the construction of the Iffezheim barrage

In the years after the construction of the Iffezheim barrage, the bed load and suspended load downstream of the barrage are reduced. Both, the monitoring and the statistical analysis of dredging quantity, confirm that the Iffezheim barrage has a significant effect as a sediment trap. The amount of dredging material was increased significantly. However,

this could be reduced through the construction of moles in the up- and downstream (Huber, 2005), which serve as hydraulic structures on the one hand and deposition places for dredging material on the other hand. Till the year 2005, the possibility of accommodation is exhausted (Huber, 2005).

In the past years, a decrease in the deposition of fine sediment has been observed. Vollmer and Goelz (2006) analyzed the dredging volumes in the Upper Rhine from 1991-2004 and concluded that depending on hydrology, approx. between 150,000 and 200,000 m^3 of fine material are expected to be deposited annually in the reservoir. According to observations between in the 21st century, an annual average of about 1 to 2 million m^3 of suspended sediment transport passes through the Iffezheim barrage, whereby less than 10 %, i.e., approx. 115,000 m^3 settle in the upper weir channel (Hillebrand et al., 2015). Due to historic emissions, fine sediment deposits in the reservoir are contaminated. Relocation within the river system is thus impossible.

With regard to flood protection requirements and contaminants in the sediment, the responsible water ways and shipping authority (WSV) has to monitor the morphodynamic evolution in the riverbed and perform regular dredging in this area. Figure 1.3 presents an example of the upstream riverbed evolution from December 2005 to April 2007. At this location, in total about 246,000 m^3 of sediment were deposited during this period. In section 3.3 the morphological riverbed evolution by erosion and sedimentation is analyzed for years based on bed level surveys by the WSV.

1.4 Aim and outline of the work

This thesis aims to apply long-term model studies in order to gain a better understanding of long-term sediment dynamics in the Iffezheim reservoir. Applying a 3D numerical model investigating the sediment transport processes and developing alternative methods to assess morphological changes in the Iffezheim reservoir over long-term periods are essential parts of this thesis.

The structure of this thesis is as follows: Chapter 1 presents a general introduction to the research topic and defines the problem. The state of the art in research methods for solving the problem is provided as well. In order to obtain a more comprehensive understanding of the study area, the introduction begins with the historical background of the river engineering in the Upper Rhine. The morphological evolution of the study area after its construction is described afterwards. The aim and outline are also defined in this chapter. Chapter 2 presents the fundamentals of sediment transport processes in nature. Chapter 3 introduces the available field data and their statistics analysis. The

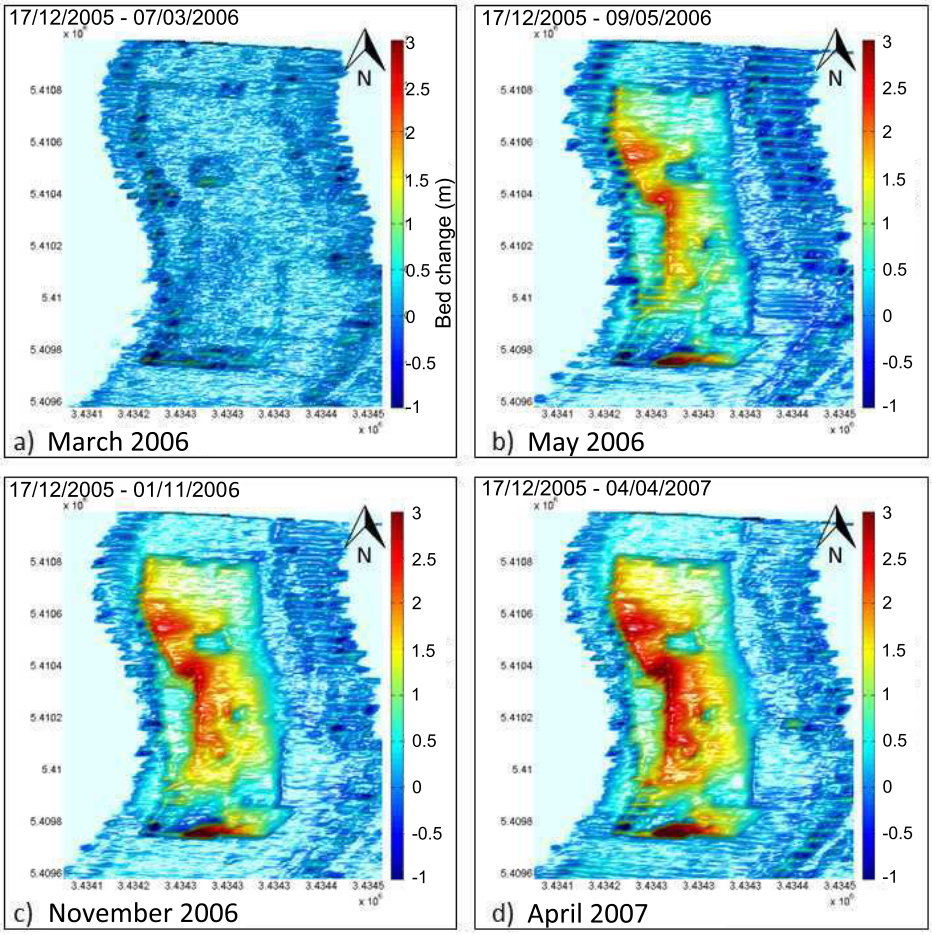

Figure 1.3: Riverbed evolution after dredging in the weir channel of the Iffezheim reservoir from Rhine km-330 to Rhine km-334 after December, 2005.

theory of numerical modeling of flow and sediment transport processes is presented in chapter 4. Here, the set up of a high-resolution 3D numerical model and its calibration is presented. Chapter 5 and chapter 6 discuss upscaling approaches to model long-term sediment dynamics. Chapter 5 provides the approach to upscale a high-resolution model based on coarsening the grid and optimising the model parameters and the number of grain size fractions. Chapter 6 discusses a reduced complexity approach called "classification of discharge and suspended sediment concentration boundary conditions". Using this approach, the instationary simulations of riverbed volume change are replaced by a series of stationary simulations. Chapter 7 and 8 provide alternative methods to indirectly assess the morphological evolution in the riverbed. Here, they are applied to create the boundary conditions for the long-term studies. Chapter 7 introduces the statistical methods of time series analysis and synthesis and applies this method to forecast monthly inflow discharges of the Iffezheim reservoir. Chapter 8 presents the concept of artificial neural networks and, as an extension the wavelet artificial neural networks, to simulate the long-term suspended sediment concentration based on the discharge time series. In chapter 9, all approaches that have been applied in the Iffezheim reservoir case are summarized regarding their benefits and drawbacks and transferability to the Upper Rhine. Then a coupled model approach is developed. With this approach, a long-term riverbed evolution is simulated until the year 2100, and the results are assessed, taking into consideration the impact of climate change. Finally, this thesis draws conclusions in chapter 10 and gives recommendations for future research.

Chapter 2

Fundamentals of sediment transport in surface waters

In this chapter, the basic and most significant sediment transport processes in surface waters are discussed. The ideas will be applied to the modelling of sediment transport in the Iffezheim reservoir in chapter 4. The goals of this chapter are to 1) describe the processes that govern the transport of sediments in surface waters, 2) focus on suspended sediment transport, which is considered as main problem in the Iffezheim reservoir, and 3) describe deposition processes in modelling sediment transport.

Section 2.1 provides a brief overview of sediment transport processes in rivers. In section 2.2, general properties of sediment-particle sizes and variation in size of natural suspended sediments, especially in the River Rhine, are introduced. Section 2.3 describes settling velocities of sediment particles. The vertical distribution of suspended sediment concentration is discussed in section 2.4, the purpose is to illustrate some of the significant characteristics of distribution of different types of sediment material. The theory in this section provides a basis for the numerical model set up (see subsection 4.3.2) and is a prerequisite of spatial coarsening of model grids (see subsection 5.2.2). Section 2.5 introduces erosion processes related to incipient motion of sediment and critical bed shear stress. This thesis focuses on modelling of the sediment inflow and predicting the rate of accumulation within the Iffezheim reservoir, therefore, deposition processes are more important. Their application in modelling are described in the last section.

2.1 Sediment transport classification and processes

Sediment transport in the river is the movement of solid particles, due to the movement of the fluid in which the sediment is entrained. Sediment transport can be classified in

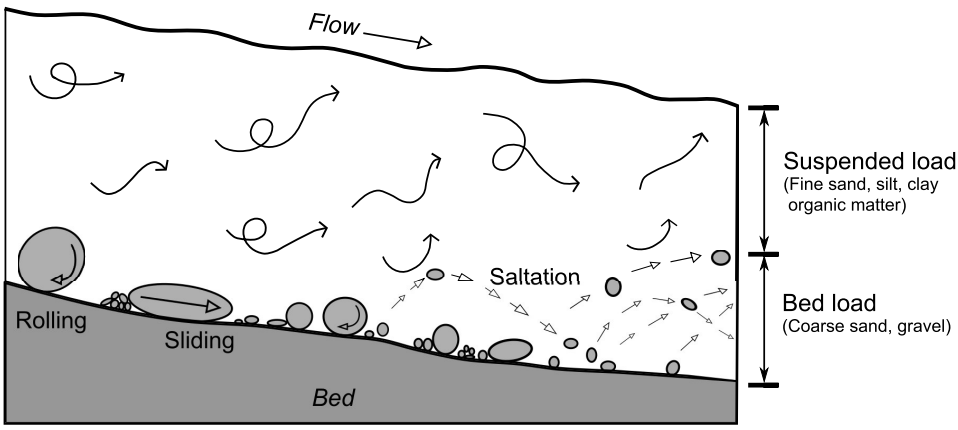

Figure 2.1: River systems: natural transport systems.

different ways. Commonly, it is separated into two classes based on the mechanism by which grains move: 1) **bed load**, wherein grains roll, slide, or move in saltation and move only in a zone close to the bed surface, and 2) **suspended load**, wherein grains are picked up off the bed and move through the water column in generally wavy paths defined by turbulent eddies in the flow (see Figure 2.1). In general and for ordinary flows in rivers, grains smaller than a certain diameter tend to mainly travel in suspension, grains coarser than a certain diameter tend to mainly travel as bed load, and grains in between these sizes travel as either bed load or suspended load, depending on the strength of the flow (Chien and Wan, 1999). Wilcock et al. (2009) give an experience value for a certain diameter of about 1/8 mm based on many field investigations in the USA. Kresser (1964) concluded from four European rivers that the critical diameter that differentiates bed load and suspended load is defined as follows:

$$\frac{U^2}{gd} = 360 \tag{2.1}$$

in which U is the average velocity of flow. d is the diameter of the sediment particle.

Sediment transport can be distinguished in another way based on the source of the grains: (1) **bed material load**, which is composed of particles whose statistical properties are fully represented in the bed, e.g., coarser sand and gravel; and (2) **wash load**, which is composed of finer grains found in only small (less than a percent or two) amounts in the bed. Wash load typically includes colloidal particles (<0.1 μm) of clay and light-weight organic particles, which have a small settling velocity. Once introduced into the channel, wash-load grains are kept in suspension by the flow turbulence and essentially pass straight through the stream with negligible deposition or interaction

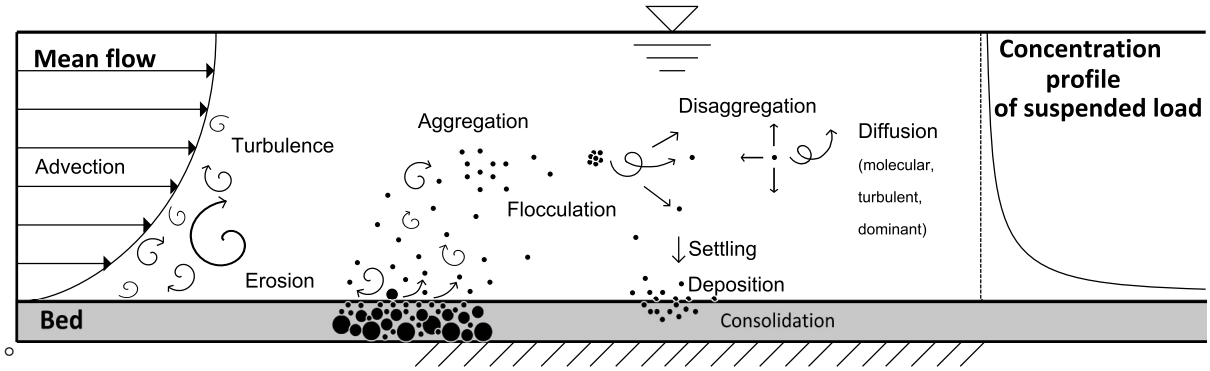

Figure 2.2: Sediment transport processes.

with the bed (Wilcock et al., 2009).

For modelling of sediment transport processes, the most commonly used classification depends on the mechanisms of sediment transport.

Figure 2.2 presents sediment transport processes. On the left hand side, the flow velocity profile is shown. If flow is at high velocity, it is turbulent and has eddies of various sizes. A particle is then picked up by turbulence or a particle jumps from the bed and enters such an eddy, thus erosion occurs. A suspended particle may be carried away far from the bed. It depends on the relationship between the size of the eddy and the size of a particle. If the size of the eddy is much greater than a particle, the eddy may carry the particle for a long time; if an eddy is of about the same size as a particle, the latter is liable to fall out of the eddy. By the time the particle falls out of the eddy, it may already have been carried into the region of the main flow, where it may even enter another eddy and be carried further along. Obviously, the transport of suspended particles is mainly the effect of large-scale eddies (Chien and Wan, 1999). In case of fine sediment particles, they flocculate and therefore drop out of suspension when they become too heavy. They can, however, disaggregate by collision or turbulence. If flow is at low velocity, the eddies close to the bed are very small; thus they can not cause the suspension of particles. In many cases, a parabolic concentration profile is formed by the particle distribution in the surface water, as illustrated on the right hand side.

In addition, the suspended particle in the water would sink and settle on the riverbed. The cohesive riverbed, e.g. in the Iffezheim reservoir, because of presence of organic material or silty particle, will consolidate over the time. It means that the pore water is gradually forced out of the cohesive soil and the sediment material in the riverbed gets condensed.

Generally, suspension of particles takes a certain amount of energy from the turbulent

flow. On the one hand, flow turbulence carries sediment particles into suspension, and on the other hand, the existence of suspended load reduces the turbulence intensity (Chien and Wan, 1999). This effect could possibly be taken into consideration of numerical modelling. In the case of ignoring this effect, it should be noticed in assessing the simulation results, especially for the high-concentration flow.

If the sediment has non-uniform distribution[1] in the riverbed, 1. the original top layer of bed material becomes finer due to deposition; and 2. a size gradation due to sorting during deposition causes the top layer to become finer and finer with increasing transport distance to the barrage. Namely, the closer to the barrage the finer is the material. The larger the distance from the barrage, the coarser is the deposited material. A detailed study of non-equilibrium sediment transport[2] in a reservoir can be found in Han (1979).

2.2 Sediment characteristics

The most obvious property of the sediment is the size of its particles. Most particles are irregular in shape. The unique size is thus difficult to define. However, a conceptually useful and unique size diameter can be defined as the diameter of a sphere with the same volume as the particle (Wilcock et al., 2009).

Particle sizes were first classified using the Wentworth scale (Wentworth, 1922). After that, several classification schemes and their subsequent modifications have been adopted to describe the approximate relationship between the size fractions (Folk, 1954, 1974; Schlee, 1968; Shepard, 1954). However, due to different limitations these schemes have not been used widely, e.g., Shepard's original classification scheme does not allow for sediments with significant amounts of gravel. The scheme derived by Folk (1954) uses the term mud instead of silt and clay. Hence, the United States Geological Survey Open-File Report 2006-1195 conforms to the definition of Wentworth and completes the definition of particles sizes and their characters, which is shown in Table 2.1. In Germany, the grain size classification is after DIN EN ISO 14688[3], which is based on the decadic logarithm. Both grain size classifications are similarly graduated and vary in subgroups and limits of grain diameters for each group.

According to this classification, gravel-sized particles have a nominal diameter from 2 mm to 32 mm after Wentworth (1922), while the size range of gravel is from 2 mm to 20 mm after DIN 4022; sand-sized particles have nominal diameters from 63 µm to 2 mm; silt-sized particles have nominal diameters from 2 µm to 63 µm; and clay is <2 µm. Fine sediment includes fine sand, silt and clay. Cohesive sediment is usually referred to as

Table 2.1: Grain size classification. Left: from Doeglas (1968) slightly modified after Wentworth (1922) with limit in µm/mm and the Krumbein Φ scale (Krumbein and Aberdeen, 1937). The Φ scale is a logarithmic scale computed by the equation $\Phi = -log_2 d/d_0$, where d is the diameter of the particle in millimeters and d_0 is a reference diameter, equal to 1 mm. Right: after DIN 4022 with limit in µm/mm.

Grain size classification from:						
Wentworth and Doeglas				DIN 4022		
Size (metric)	Φ scale	Aggregate name		Aggregate name		Size (metric)
63 *mm*	-6		**cobble**	**cobble**		63 *mm*
32 *mm*	-5	very coarse	**gravel**	coarse-	**gravel**	20 *mm*
16 *mm*	-4	coarse		medium		6,3 *mm*
8 *mm*	-3	medium				
4 *mm*	-2	fine		fine		2 *mm*
2 *mm*	-1	very fine				
1 *mm*	0	very coarse	**sand**	coarse	**sand**	630 μm
500 μm	1	coarse				
250 μm	2	medium		medium		200 μm
125 μm	3	fine		fine		63 μm
63 μm	4	very fine				
32 μm	5	very coarse	**silt**	coarse	silt	20 μm
16 μm	6	coarse				
8 μm	7	medium		medium		6,3 μm
4 μm	8	fine				
2 μm	9	very fine		fine		2 μm
	10		**clay**	**clay**		

grain size up to 63 μm.

The natural stream demonstrates typically a wide range of particle sizes in the riverbed, often from less than a micrometer to as much as centimeters. Because a particular measuring technique is only valid for a limited range of particle sizes, more than one measurement technique may be necessary to measure the complete size distribution of a sediment mixture.

The most common measurement techniques are sieving, the use of laser diffractometer, the use of an electrical impedance particle sizer and particle imaging system. Sieving is done by means of a series of stainless steel sieves. The sediments generally are dried, disaggregated, and passed through a series of these sieves; the residue on each sieve is then weighted. Because fine sieves tend to become clogged rather rapidly, sieving generally is useful only for coarse sediments with d >63 μm (Wilcock et al., 2009). An accurate and convenient procedure for measuring particle sizes over a wide range is by laser diffractometer. In this instrument, light is passed through low concentrations of the sediment-water mixture and is diffracted by the particles. The particle size distribution is then determined from the diffraction pattern (Wilcock et al., 2009), e.g., LISST (Optical laser diffraction instruments) estimates the size distribution of an ensemble of particles using forward scattering of a laser beam measured with a series of 32 annular detectors and it can measure particle sizes from about 1 to 500 μm (Reynolds et al., 2010). The Malvern Particle Sizer (Nano Sight Linie) can measure the particle sizes even from 10 nm to 2000 nm (Malvern, 2017). The Coulter technology is an electrical impedance particle sizer. The technology was principally developed to count blood cells quickly by measuring the changes in electrical conductance as cells suspended in a conductive fluid pass through a small orifice (Beckman Coulter Life Sciences, 2017). This method can also be used to measure suspended sediment in an electrolyte solution. Particles as small as 0.2 μm and as large as 1600 μm can routinely be measured by Beckman Coulter Counter.

Additionally, the particle size and its distribution can be measured by a particle imaging system, e.g. FlowCam system (FlowCam, 2017). This system uses an ultra-high-precision computer controlled syringe pump to pull the fluid sample through a flow cell perpendicular to an optical path (FlowCam, 2017). The particle imaging system is known to be a powerful technique for imaging and identification of relatively large

[1]A non-uniform distribution is any distribution where the fractions of grain size are spatially not the same.

[2]Non-equilibrium sediment transport refers to cases where the outflowing sediment discharge from a reach does not equal the inflowing sediment discharge to that reach (Griffin, 1995).

[3]DIN EN ISO 14688 replaces DIN 4022 for the designation of the grain size fractions, whose names are very common in the German speaking countries.

particles in natural samples. It gives statistically relevant results quickly, e.g., tens of thousands of particle images can be captured per minute using FlowCam. Its range is from 2 µm to 2 mm.

The particle size distribution for the sediment from the Rhine River is measured by laser diffractometer. The detailed description of the sediment samples in the River Rhine and Iffezheim reservoir are presented in subsection 3.2.

From the perspective of morphological grain size distribution in a reservoir, sediment grain size vary rapidly in the horizontal direction from gravel, even cobble to fine-grained muds. The large sediments are located where stream flow and wave action are strong, whereas the fine sediments are located where stream flow and wave action are small. The sediment distribution can also change rapidly in the vertical direction. For example, during a flood event, the flow brings large quantities of sediment, which may deposit on the top layer of fine sediments in the riverbed. After the flood, the flow velocity is relatively low, finer sediments may deposit and may cover this coarse layer (Wilcock et al., 2009).

2.3 Settling velocities

The settling velocity of a particle w_s in water flow depends on the size, shape, density of the particle, density and viscosity of the fluid as well as the permeability of the aggregate (Simoes, 2014). The dynamic of a solid idealized spherical particle in standing water can be determined essentially from the diameter and the density of the particle. Incorporating both properties, many equations are available to determine the settling velocity, e.g. Stokes (1850), Zanke (1982), Dietrich (1982), van Rijn (1989), Cheng (1999) and Wu and Wang (2007)'s formula. These formulae are shown in Table 2.3.

Stokes (1850)'s formula is under the assumption of the regular sphere shape for all particles and also limited to laminar flow. The formula is limited to small grain sizes. For larger sediment sizes, other formulae should be applied.

Settling velocities measured in field are somewhat lower than those given by Stokes's law, because most naturally occurring particles are irregularly shaped and the flow around them is not ideally steady, and their hydrodynamic drag is greater than for steady flow. Hence, many researchers have developed equations on the basis of experimental data for natural particles.

In 1977, Zanke developed a general settling velocity formula for spherical particles depending on drag coefficients of Stokes flow with $Re < 1$, Newton flow with $Re > 10^3$ and for any $Re < 2 \cdot 10^5$ as approximate solution. In 1982, Zanke modified the formula

Table 2.3: Formulae for definition of settling velocity.

Researcher, year	Formulae	Scope
Stokes, 1850	$w_s = \frac{gd^2}{18\mu}(\rho_s - \rho_w)$	laminar flow
Zanke, 1982	$w_s = 11\frac{v}{d}\left(\sqrt{1+0,01D_*^3}-1\right)$	laminar and turbulent flow
Dietrich, 1982	$w_s* = R_3 \cdot 10^{R_1+R_2}$	laminar and turbulent flow
van Rijn, 1989	$w_s = \frac{1}{18}\frac{\triangle g d^2}{\nu}$ $w_s = 10\frac{v}{d}\left(\sqrt{1+0,01d^3}-1\right)$ $w_s = 1.1\sqrt{\triangle g d}$	d < 0.01 cm d = 0.01 ~ 0.1 cm d > 0.1 cm
Cheng, 1997	$w_s = \frac{v}{d}\left(\sqrt{25+1.2d^2}-5\right)^{1.5}$	Stokes flow to high Reynolds numbers
Wu & Wang, 2007	$w_s^{**} = \frac{Mv}{Nd}\left[\sqrt{\frac{1}{4}+\left(\frac{4N}{3M^2}D_*^3\right)^{\frac{1}{n}}}-\frac{1}{2}\right]^n$	laminar and turbulent flow

*

$R_1 = -3.76715 + 1.92944(logD_*) - 0.09815(logD_*)^{2.0} - 0.00575(logD_*)^{3.0} + 0.00056(logD_*)^{4.0}$

$R_2 = (log(1-\frac{1-CSF}{0.85})) - (1-CSF)^{2.3}tanh(logD_* - 4.6) + 0.3(0.5-CSF)(1-CSF)^{2.0}(logD_* - 4.6)$

$R_3 = \left[0.65 - (\frac{CSF}{2.83}tanh(logD_* - 4.9))\right]^{(1+(3.5-P)/2.5)}$

with Corey shape factor (CSF), dimensionless nominal diameter (D_*), power value of roundness (P)

**

M and N are constant coefficients.

with a shape factor $FF = \frac{c}{\sqrt{ab}}$. The shape factor is oriented with an a, b and c as the space axes on an ellipsoid, which is idealized by the actual grain. Here a is the largest value and c is the smallest value. For natural sediments FF has the value of 0.7 (see Table 2.3). The formula delivers satisfying results. Only between laminar and turbulent flow the settling velocity is overestimated.

Dietrich (1982) introduced an empirical formula which includes additionally a power roundness parameter related to the particle shape and a smoothness coefficient. However, the power roundness parameters R_i is rarely measured in practice and thus only used rarely.

Based on the theory of Zanke, van Rijn developed the settling velocity equations with fine classified groups.

Cheng (1999) connected previous formulae to establish a general relation between the drag coefficient C_d and the Reynolds number $Re = w_s d/\nu$ for natural sediment that can also be fitted to experimental data for intermediate Reynolds numbers. Differing C_d at low and high Re and using a dimensionless particle diameter the author received an equation to estimate the settling velocity for natural sand particles. Wu and Wang (2007) reevaluated the graphical $C_d - Re$ relation of the U.S. Interagency Committee for $Re > 1000$ by a wider rage of data and a nominal diameter. The coefficients used in their formula are only depending on the Corey shape factor. In contrast, in the research of van Rijn (1989) the settling velocity only differs by the particle size d. For natural non-cohesive particles, a Corey shape factor of 0.7 is recommended (Cheng, 1999; Wu and Wang, 2007).

In addition, there are many other formulae for calculating settling velocities, which can e.g. consider the flocculation aspects for fine sediments.

2.4 Vertical distribution of a suspended sediment concentration

Sediment particles, mainly silt and sand, with small settling velocities can be kept in suspension by the upward flux of turbulence generated at the riverbed. The upward currents must equal or exceed the particle settling velocities for suspended sediment load to be sustained. Sediment particles, because of their greater specific weight, tend to move toward the riverbed. As the result, the sediment concentration is typically higher near the bed and distributes in the vertical water column as illustrated in Figure 2.2 on the right hand side.

Vertical distribution of a suspended sediment concentration depends on the grain

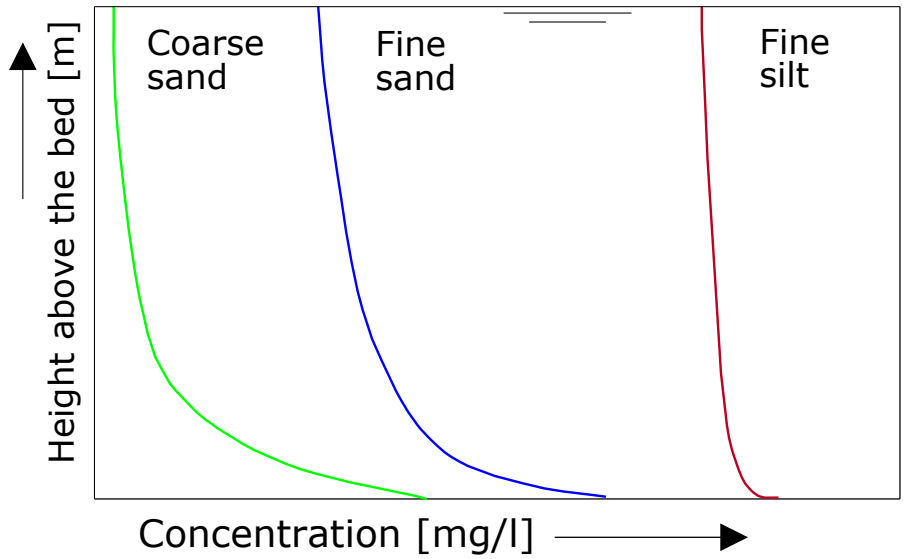

Figure 2.3: Typical vertical profiles of suspended sediment concentration in terms of sediment material (schematic).

size and turbulent flow conditions. Relating the suspended sediment size to its distribution under a certain turbulent condition, various concentration profiles are shown in Figure 2.3. Coarser sands cause especially the non-uniform distribution and have a higher concentration near the bed. The declination rate is much faster than the one of fine sands. Fine silt is easily suspended and is nearly uniformly distributed in a vertical section. Detailed information for vertical distribution of different sediment sizes under variable turbulent conditions can be found in Malcherek (2006).

To calculate the vertical distribution of sediment concentration for various particle sizes, the diffusion theory and the gravitation theory have been proposed (Chien and Wan, 1999). The commonly used equation - Hunter Rouse equation - belongs to the diffusion theory, which has been described with detailed comments by Zhang (1963). Rouse (1937) used a series of grids moving in simple harmonic motion in a cylinder and suggested that the vertical concentration profile of suspended load can be expressed for the case of low concentrations as follows:

$$\frac{S_v}{S_{va}} = \left(\frac{h-y}{y} \frac{a}{h-a} \right)^z \tag{2.2}$$

in which

$$z = \frac{w}{\kappa u_*} \tag{2.3}$$

where S_v is the instantaneous concentration and S_{va} is a reference concentration of the suspension at distance "a" above the bed; κ is the von Karman constant in the

logarithmic formula for the velocity distribution; z is the Rouse number; u_* is the shear velocity; h is the water depth, y is the height in the water and w is the vertical velocity. This formula is used for steady uniform flow of both water and sediment.

2.5 Initiation of motion for non-cohesive and cohesive particles

The incipient motion of a single grain is determined during the bed load transport by an imbalance between current force and weight force acting on the riverbed grain. Incipient motion and bed load motion are closely related to the phenomenon of flow turbulence, velocity and pressure fluctuations caused by turbulence near the bed surface (Chien and Wan, 1999). One incipient motion problem is to determine the flow at which a given particle size moves. Many researchers have developed empirical incipient motion criteria based on the mathematical theory and a large amount of experimental data (Shields, 1936; Simoes, 2014; Vollmer and Kleinhans, 2007; Zanke, 2003). The most commonly used methods are employed as an approach similar or identical to the Shields diagram for non-cohesive particles (Shields, 1936).

Shields (1936) expressed the critical shear stress τ_c for the initiation of motion as a relation between the non-dimensional shear stress τ^*, also called the Shields parameter, and the grain Reynolds number depending on the shear velocity, Re^*, defined as:

$$\tau^* = \frac{\tau}{(\rho_s - \rho_w)gd} \tag{2.4}$$

$$Re^* = \frac{u_* d}{\nu} \tag{2.5}$$

$$U^* = \sqrt{\tau/\rho_w} \tag{2.6}$$

where τ is the bottom shear stress; ρ_w and ρ_s are the water and sediment densities, respectively; ν is the kinematic viscosity of water; g is the acceleration due to gravity; d is the diameter of the sediment particle; and u_* is the shear velocity.

Yalin and da Silva (1979) suggested eliminating U^* from the abscissa through a combination of τ^* and Re^*, the Yalin parameter: $\Xi = Re^{*2}/\tau^* = D_*^3$, with D_* being the dimensionless grain diameter defined as

$$D_* = \left[\frac{(s-1)g}{\nu^2}\right]^{\frac{1}{3}} d$$

where s is the specific gravity of the sediment with $s = \rho_s/\rho_w$. The use of D_* eliminates simultaneous use of U^* in the abscissa and the ordinate of the Shields diagram, reducing data scatter and eliminating the need for an iterative process to find τ^* for a particular set of hydraulic and sediment processes (Simoes, 2014).

Once single grains are in motion, they bump into each other rolling or jumping on the riverbed. As the grain size decreases, the influence of the stabilizing gravity force decreases as well, but electrochemical forces of attraction and other physical interactions become more important. Due to the cohesive forces, single grains form a unit floc, so that the individual grain character is lost.

The erosion of cohesive sediment differs significantly from the motion of rolling soils. Three types of erosion are distinguished. Surface erosion or flake erosion describes the breakage of single grains or floccules. This erosion type occurs at very low shear stresses, in contrast to the mass erosion, in which the whole layer of soil is torn out of the ground and the riverbed mechanically collapses. The eroded layer of soil disintegrates in turbulent flow and is sustained in suspension. The third type of erosion is the fluidization of the sediment under the influence of waves, also known as entrainment. The cohesive character of sediment is determined by diverse influences. The cohesive erosion is influenced by Van der Waals forces, the clay content, the Born-interaction[4], the Ph value, and the salinity (Hillebrand, 2008). Moreover, the degree of sediment consolidation plays an important role, because the lower the pore water content, the smaller is the distance between the single particles and the higher is the stability of the riverbed.

The erosion rate is generally determined from experiments, and effects due to turbulent fluctuations are inherently included in the erosion measurements. In case of this study (see Chapter 4), erosion rates and critical shear stresses for erosion were measured by the University of Stuttgart on core samples from the Iffezheim reservoir. The results were used in the calibration of an erosion law (Hillebrand et al., 2015; Noack et al., 2015).

2.6 Processes and parameters affecting deposition

This section focuses the discussion on deposition in sediment sinks, i.e. reservoirs. Various processes and parameters that affect deposition rates are as follows: fluid turbulence, particle size distributions, flocculation.

[4]Born force is a kind of repulsive force. His influence is negligible with larger particle distances and only increases strongly at very small particle distances. It represents a kind of geometric repulsion and prevents the interpenetration of particles (Hillebrand, 2008).

First, the tendency of particles to deposit during transport is countered by upward diffusion due to the turbulent movement of fluid particles (Mehta, 2013). Thus, whether a given size fraction is sustained in suspension depends on the flow velocity.

Second, particle sizes of suspended sediment in the Iffezheim reservoir range from three to four orders of magnitude (see subsection 3.2). Considering of fine sediment deposition, this range varies by as much as five to six orders of magnitude. The particle size distribution causes a major influence on deposition rates, e.g. due to the different settling velocities (see subsection 2.3 and 4.2.2) and must be considered in the modeling of deposition rates.

Third, flocculation becomes increasingly significant for deposition rates as particles become smaller and more cohesive. Flocculation is a dynamic process that causes changes with time in the size and density of flocs as well as their settling speeds. Therefore, the spatial and temporal variations of flocs have to be considered (Lick, 2009). The flocculation effect is currently studied using the numerical model SSIIM and has been investigated in the Iffezheim reservoir (Klassen, 2017).

In the modeling of sediment transport and deposition quantity, various parameters, including these mentioned above, should be considered. Some of them should be taken into account in the interpretation of laboratory results, but they are probably not of importance in the interpretation of modeling results, e.g., the partial coverage of previously deposited sediments by recently deposited sediments. In turn, some of them are significant and must be included in analyses and modeling, e.g. effects of particle size distribution and effects of flocculation for cohesive sediments. In addition, as sediments are deposited, they consolidate over time (see section 2.1). This affects the height of the riverbed in the modeling, subsequently the flow velocity and even the rate of accumulation over time.

Chapter 3

Field data and statistics

3.1 Hydrodynamic conditions

Discharge till the year 2013

Daily time series of discharges from January 1924 to December 2013 were collected by the German Federal Waterways and Shipping Administration (WSV) at the Plittersdorf station (see Figure 1.2), which at a distance of 6.2 km is the closest downstream station to the Iffezheim reservoir.

Table 3.1 and Figure 3.1 show the mean monthly discharge[1] at Plittersdorf station from 1924 to 2013. The average discharge per month is 1166 m^3/s for the entire period of record. The maximum mean monthly discharge is of 2888 m^3/s recorded in May 1999, and the minimum mean monthly discharge is of 339 m^3/s recorded in November 1947. The observed long-term trend of the mean annual water discharge of Rhine River has slightly increased since 1930s, as shown in Figure 3.2.

KLIWAS projected discharge till the year 2100

The research program KLIWAS (Impacts of climate change on waterways and navigation - Searching for options of adaptation) was launched to determine and evaluate the impact of climate-induced changes of flows and water levels in navigable waterways by the Federal Ministry of Transport and Digital Infrastructure (BMVI) (BMVI, 2015). The discharge of the Rhine river was projected considering various climate change scenarios with several model combinations.

[1]The mean monthly discharge is the average discharge for a given month of the year. For example, the average discharge for January 2013 is based on the daily discharge for that month, whereas, the long-term mean monthly flow for January is based on the average for all January from 1924 to 2013 at Plittersdorf station.

Table 3.1: Statistics of mean monthly water discharges (data from Plittersdorf station, 1924-2013).

	Mean monthly discharge (m^3/s)	Standard deviation (m^3/s)	Max discharge (m^3/s)	Min discharge (m^3/s)
Jan	986	363	2117	449
Feb	1015	404	2217	359
Mar	1073	362	2373	442
Apr	1197	371	2282	577
May	1360	404	**2888**	635
Jun	1595	401	2715	738
Jul	1485	388	2505	644
Aug	1270	345	1934	497
Sep	1087	319	1966	462
Oct	954	341	2083	**339**
Nov	966	396	2541	348
Dec	1006	401	2080	404
Monthly	**1166**	**374**	**2888**	**339**

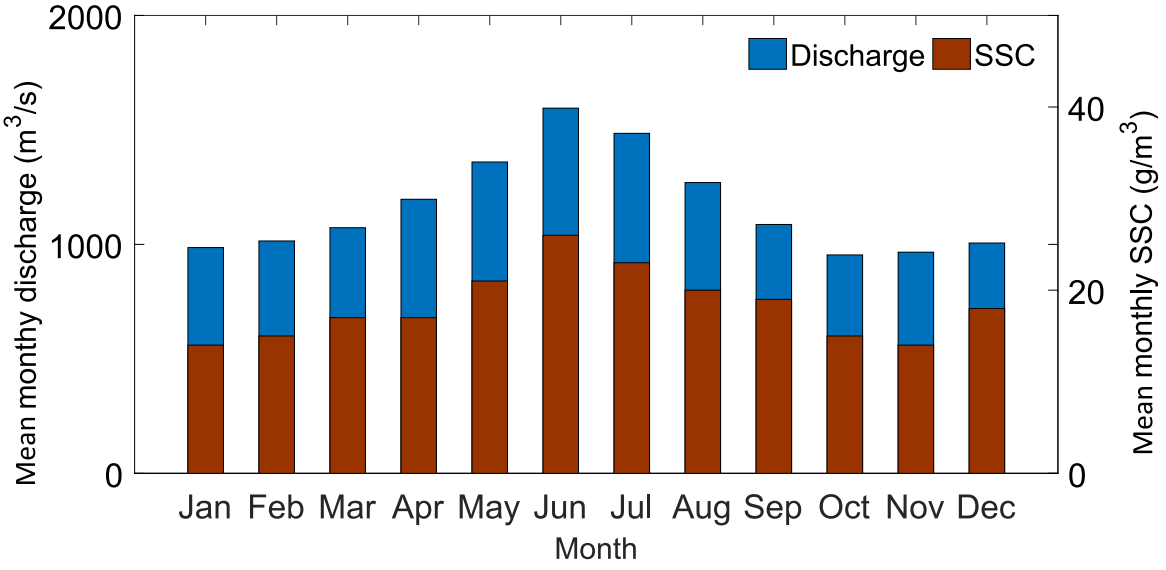

Figure 3.1: Mean monthly discharges from 1924-2013 and suspended sediment concentrations (SSC) from 1978-2013 at Plittersdorf station.

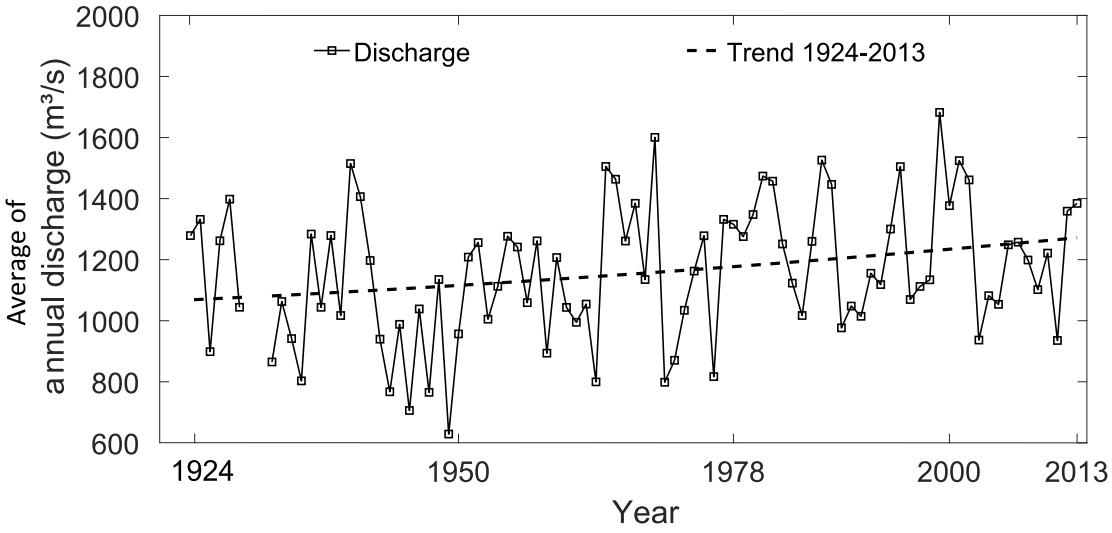

Figure 3.2: Annual average of discharges (data from Plittersdorf station, data in 1930 and 1931 are not available.).

The hydrological model HBV (Bergström, 1995) was used to simulate the discharge of the River Rhine. Using the 1D hydrodynamic model SOBEK-RE, the projected discharge downstream of the Iffezheim reservoir was calculated into water depths and flow velocities. Emission scenario A1B[2] was applied. The bathymetry from year 2004 and 2009 were applied to the instationary simulations and based on the historical time series from 1961 to 2010, the discharge was projected till the year 2100 (Nilson et al., 2014).

The projections of discharges at the Maxau gauging station are used in this study. Maxau is one of the oldest gauging stations in River Rhine and is located approx. 25 km downstream of the Iffezheim reservoir. The average discharge in Maxau is about 40 m^3/s higher compared to at the Plittersdorf station (Nilson et al., 2014).

Figure 3.3a shows the historical discharges from 1924 to 2013, while Figure 3.3b presents the projected discharges from 2014 to 2100. Comparing both hydrological regimes, higher frequencies and intensities of extreme events are more often observed in the years from 1980 to 2013, which are then shifted into the future scenario. The

[2] "A1 describes a future world of very rapid economic growth, global population that peaks in mid-century and declines thereafter, and rapid introduction of new and more efficient technologies. The three A1 groups are distinguished by their technological emphasis: fossil intensive (A1FI), non-fossil energy sources (A1T), or a balance across all sources (A1B)." - IPCC, 2007

monthly water discharge increased in winter (Nov.-Mar.), whereas the projected average discharge in summer (May-Oct.) shows no significant change. The discharge maximum shifted more and more towards the winter period, caused by climate change. A slight increase of average discharge over the whole period was found.

Water levels in the Iffezheim reservoir

At the Iffezheim reservoir, the regulation of the weir and the hydropower station is based on a control curve, which defines the water level depending on the inflow value (Klassen, 2012). The bed volume change in the weir channel is very sensitive to the water level H. Therefore, all simulations should be precisely maintained by the control curve, as described below:

$$
\begin{aligned}
Q < 1700\,m^3/s: &\quad H = 123.6\,m \\
1700\,m^3/s < Q < 1900\,m^3/s: &\quad H = 123.6 - 5.0 \cdot 10^{-4} \cdot (Q - 1700)\,m \\
1900\,m^3/s < Q < 3600\,m^3/s: &\quad H = 123.5\,m \\
3600\,m^3/s < Q < 4800\,m^3/s: &\quad H = 123.5 - 4.2 \cdot 10^{-4}(Q - 3600)\,m \\
Q > 4800\,m^3/s: &\quad H = 123.0\,m
\end{aligned}
$$

3.2 Sediment conditions

Suspended sediment concentration

In the Iffezheim reservoir, the suspended sediment comes from the upstream of the Rhine River and its tributaries, such as the largest tributary Aare River and many small tributaries. The suspended sediment concentration (SSC) is measured by the WSV and BfG at permanent stations by primarily filtering a 5 l water sample every working day, afterwards weighting the solids (Vollmer and Goelz, 2006). In addition, Acoustic Doppler Current Profiler (ADCP) are used to analyze spatial distributions of flow velocity and suspended sediment concentration for several cross-sections along the Upper Rhine River, also in the Iffezheim reservoir. Echo intensities of the ADCP back-scatter signals correlate with SSC. By analyzing water samples and comparing them to measured back-scatter intensities, distributions of SSC at observed cross sections can be derived (Hillebrand et al., 2012b). Recently, LISST has been used to measure the suspended sediment concentration. For more information about LISST see subsection 2.2.

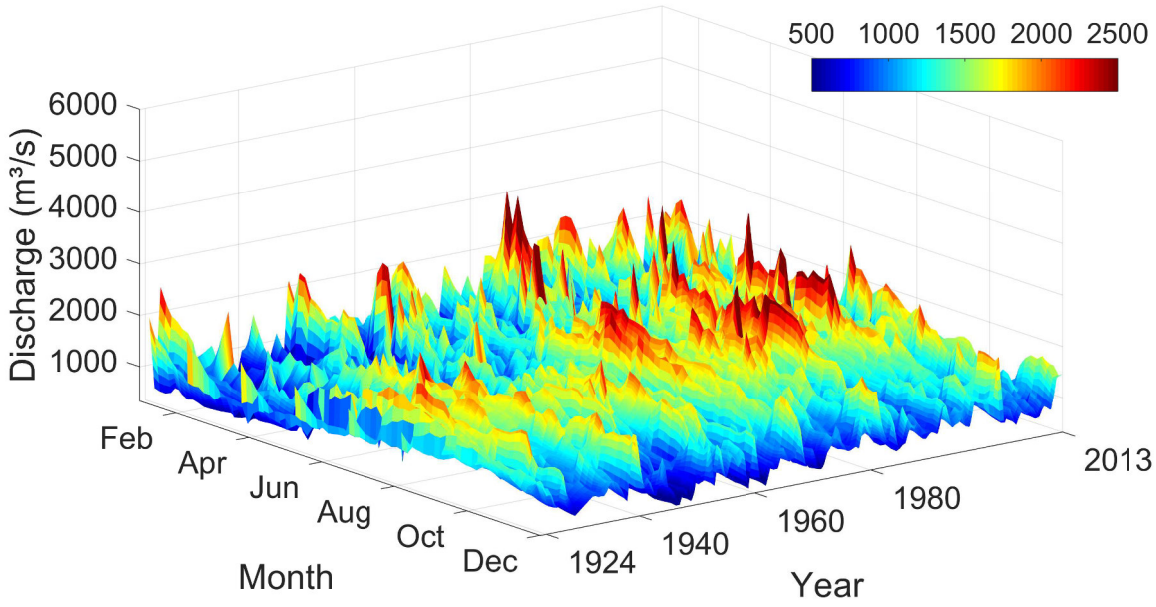

(a) Historical discharge from 1924-2013 (Q_{mean}= 1126 m³/s).

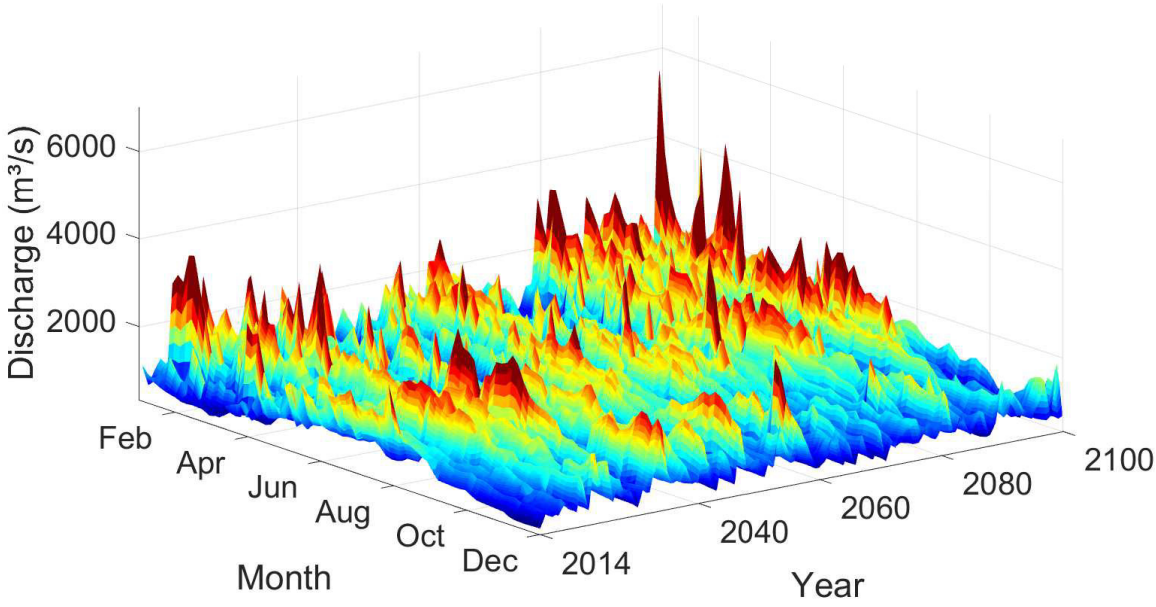

(b) Projected discharge from 2014-2100 (Q_{mean}= 1190 m³/s).

Figure 3.3: Long-term daily discharge at Plittersdorf station in the past and in the future.

Table 3.2: Statistics of monthly sediment concentration and discharge (data from Plittersdorf station, 1978-2013).

	Mean monthly SSC (g/m^3)	Standard deviation (g/m^3)	Max SSC (g/m^3)	Min SSC (g/m^3)	Sediment transport rate (g/s)
Jan	14	6	28	5	1501
Feb	15	9	48	5	1645
Mar	17	11	58	6	2175
Apr	17	8	38	6	2062
May	21	14	71	6	3034
Jun	26	15	92	12	4200
Jul	23	10	47	5	3121
Aug	20	9	42	6	2250
Sep	19	8	48	6	1921
Oct	15	6	30	3	1507
Nov	14	9	41	3	1510
Dec	18	10	43	5	1999
Monthly	**18**	**10**	**92**	**3**	**2244**

The daily suspended sediment concentration (SSC) at Plittersdorf station was collected from 1978 until 2013. Based on the statistics of the data, the average monthly suspended sediment transport rate, also called the sediment discharge Q_s, is 2244 g/s, while the average sediment concentration is 18 g/m^3. The maximum concentration measured was 369 g/m^3 on October 8, 2007. The mean monthly SSC are shown in Table 3.2 and Figure 3.1.

Figure 3.4 shows the annual variation of sediment concentrations and sediment discharge from 1978 to 2013. The whole time series displays a mild decrease.

Water samples taken for the suspended sediment were investigated by a particle size analysis of the ADCP and detailed information can be found in Astor et al. (2014).

Grain size distributions of riverbed and suspended load

A precise grain size distribution means that not only the exact grain size fractions but also the spatial distribution of the material within the study area have to be considered and investigated regarding the effect on the hydraulic roughness and the stability of the riverbed. The grain size distribution relates to the riverbed and the suspended sediment load. Due to the spatial distribution of the material in the riverbed, the analysis of grain size distribution curves was carried out at the entrance of the investigation area and in

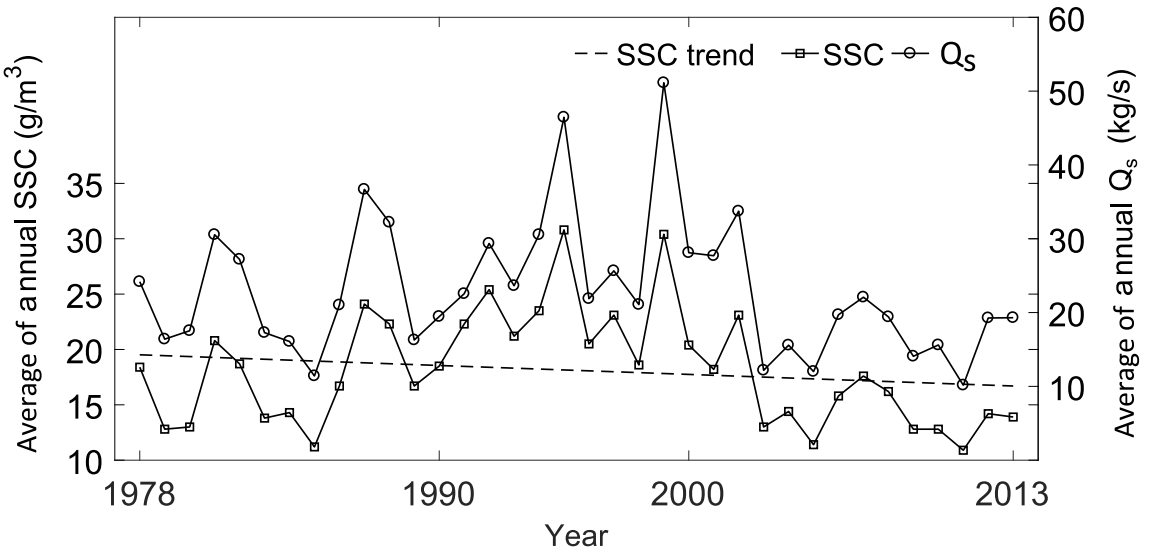

Figure 3.4: Annual average of sediment concentration and suspended sediment transport rate (data from Plittersdorf station).

the weir channel.

Along the riverbed, the non-uniform grain size distributes in non-uniform spatial patterns depending on the measurement location. Figure 3.5 shows the grain size distribution close to the entrance of the Iffezheim reservoir. Fraction of particles by mass in a particular size class is plotted as a function of the diameter of that size class in a semi-logarithmic graph. The three samples are taken in 2014. They are from close to the right bank of river sections in different depths. The cross sections Rhine-km 317.75 is located upstream of the entrance of the model[3]. The distribution at the measuring point Rhine-km 317.75 shows a finer material for the deeper sample than for the upper layer. The material at cross sections between Rhine-km 317.75 and 330.50 in flow direction becomes increasingly finer. Additionally, the riverbed near the model boundary is coarsened from left-hand to right-hand side, from finer sediment to coarse gravel.

Sediment samples taken from the riverbed in the weir channel, beginning at Rhine-km 332.9 show a wide range of sediment sizes. On the left-hand side of the weir channel, fine-grained cohesive sediment dominates the channel bed, resulting from the deposition of the suspended sediment within the weir channel that started after the construction of the barrage in 1977. The deposited sediments largely consist of silt with varying portions of clay and sand (see Figure 3.6). The analysis results of summation curves of the grain size distribution at the riverbed of the weir channel are derived from 113

[3]The upstream model boundary starts at Rhine-km 330.00.

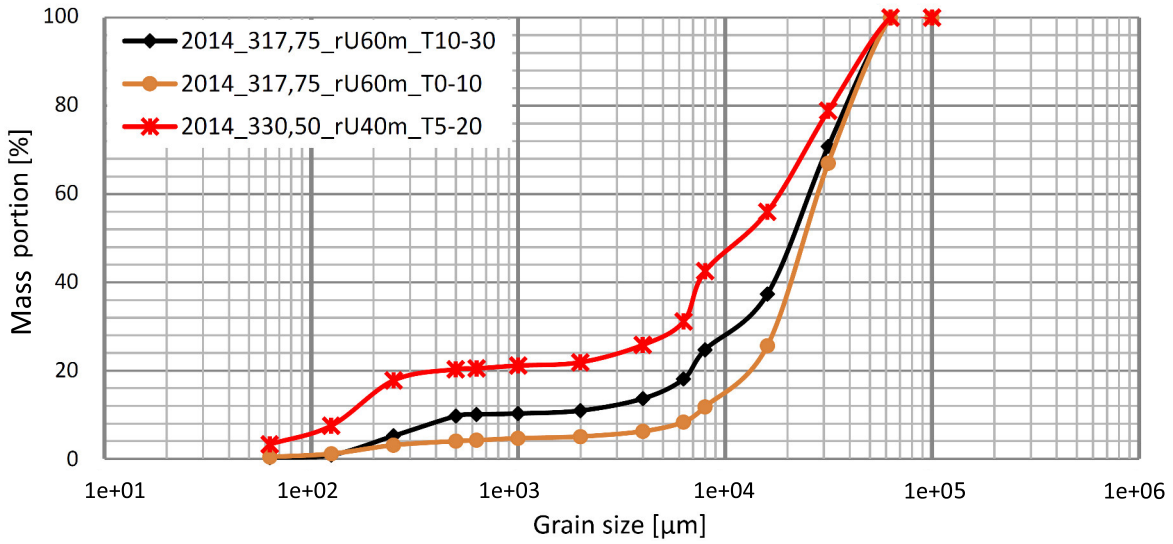

Figure 3.5: Sieve analysis results of sediment samples at the upstream of Iffezheim reservoir. For example, 2014_317.75_rU60m_T10-30 indicates that the sample is taken from Rhine-km 317.75, 60 m away from the right bank in depth between 10 to 30 cm at the riverbed in 2014 (data from BfG, 2014).

Figure 3.6: Observed sediment grain size at Rhine-km 330.5 at the left and right hand side, 500 m downstream of the upstream model boundary (BfG, 2014).

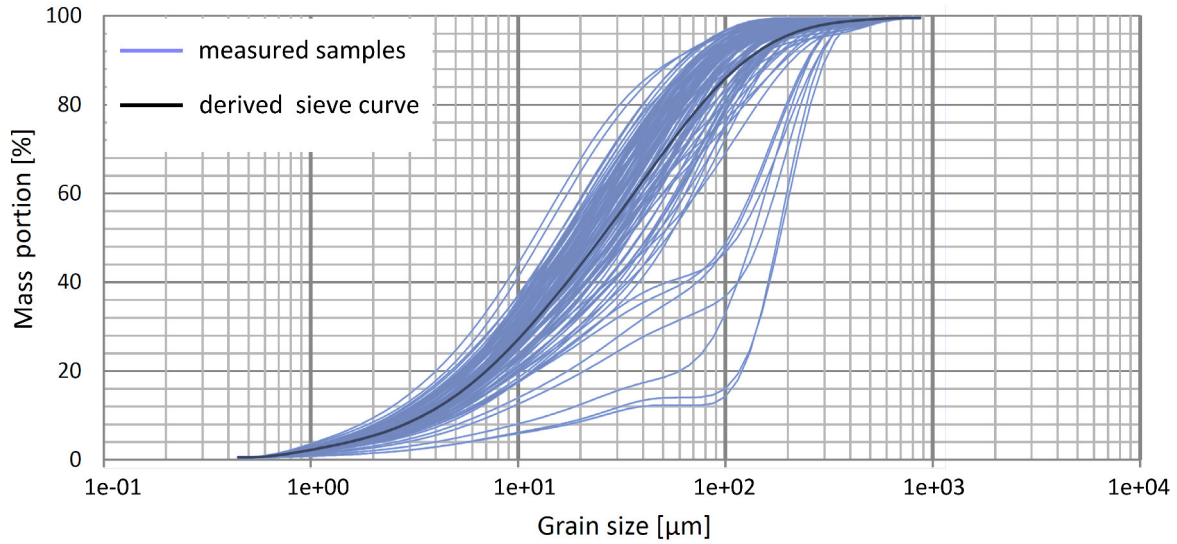

Figure 3.7: Analysis results of summation curves of grain size distribution at initial stage at the left hand side of the weir channel (Noack et al., 2014).

samples (Noack et al., 2014) and are shown in Figure 3.7.

The analysis of measurements of the riverbed material allows the assumption that on the right-hand side of the weir channel, part of the original gravel river bed representing the bed material of the river channel before the construction of the barrage prevails (Hillebrand et al., 2012a). Figure 3.8 shows the original channel bed using soil samples taken in 1968. For the simulations in the further research, the average grain size distributions in the riverbed are taken for the entrance and the weir area, respectively. The mean grain diameter d_{50} is between 0.01 and 19 mm.

The grain size distribution of suspended load is taken from measurements at Rhine-km 330.0 in July 2012. The material consists of silt and sand.

3.3 Morphological evolution analysis

Long-term morphological evolution analysis

Engineering techniques for assessing and understanding the sediment transport and delivery mainly depend on field surveys. The morphological bed evolution of the Rhine River has also been studied for years based on bed level surveys and transport measurements through German WSV. The riverbed evolution in the Iffezheim reservoir was observed by echo sounding within the weir channel from Rhine km-332.0 to Rhine km-333.9 with intervals of 20 m. Approximately quarterly measurements of cross-sectional soundings

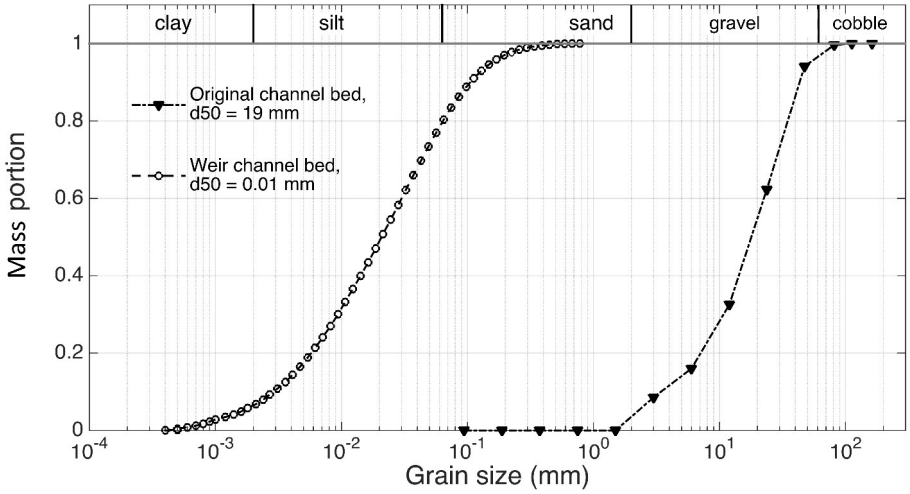

Figure 3.8: Sediment summation curve of the grain size distribuzion of the original channel bed using soil samples taken in 1968 (sand and fines were excluded in the measurements) and cumulative frequency distribution of the grain sizes in the weir channel based on laser diffraction measurements.

have been carried out. Thirty-seven sets of sounding data, which were obtained between July 2000 and February 2011, were used in this research for the determination of present situation and historical changes.

The echo sounding measurement reveals that most of the deposition occurred on the left-hand side of the weir channel. Average deposition rates between 2002 and 2011 in this area were in a range of 50 to 60 cm/yr omitting dredging periods. On the right-hand side of the weir channel, no net deposition took place (Hillebrand, 2012).

In order to quantitatively estimate the deposition or erosion amount in the weir channel, a section of the weir channel between Rhine km-332.0 and 333.8 was chosen in this study. Common methods to calculate the amount of deposition and erosion are Sediment Budget Method (SBM), Topographic Change Method (TCM) by Geographic Information System (GIS) and Digital Elevation Model (DEM) (Zhou, 2011). Here, the TCM is applied. The Cartesian grid in 3D space is replicated to produce the coordinates of a rectangular grid. The storage capacity of each grid is calculated by the area of the grid and the height of the local bed change. Based on the changes of all storage capacities, the amount of deposition and erosion can be calculated. The method is hereby fulfilled with MESHGRID function in MATLAB and a grid resolution of 1 m is used.

Figure 3.9 shows the data set for echo sounding measurements between July 2000 and February 2011. Thirty-seven sets of echo sounding data are marked with green arrows. The values between the sounding data are the measured volume changes in

Table 3.3: Dredging periods, dredging quantities and the appropriate time period.

Dredging period	Dredging quantities ($\times 10^3$ m^3)	Time period
07/2000 - 03/2001	355.3	1, 2
11/2003 - 03/2004	105	12
01/2005 - 09/2005	290	16, 17

the selected area of the weir channel. The blue arrows represent the periods in which the deposition is dominant. In contrast, the red arrows show negative volume changes. Dredging periods, which are listed in Table 3.3, are marked with a grey box.

The investigation is divided into 36 periods, each of them is located between two successive echo sounding measurements. Each period is called short-term period. Several short-term periods form a long-term period. These periods are applied for the developed upscaling approach described in chapter 6.

In order to investigate a possible relationship between various discharge conditions and the riverbed volume change, the statistical parameters of discharge and volume change in the weir channel have been analyzed. They are listed in Table 3.4. The statistical parameters contain the duration of each short-term period, average, minimum and maximum discharge and standard deviation σ, which is calculated with equation 3.1 and is used to compare the daily discharges with the average discharge in a period:

$$\sigma = \sqrt{\frac{\sum_{i=1}^{N}(Q_i - Q_{mean})^2}{N}} \tag{3.1}$$

with N = number of days in the investigated period, Q_i is daily discharge and Q_{mean} is average discharge during a period.

Table 3.4 indicates that most of the time periods have a positive volume change, i.e. deposition. These periods have an average inflow higher than the average discharge of the entire period of 1200 m^3/s. Usually, high discharges lead to a positive sedimentation, because rivers basically carry a lot of sediment during a flood event. Strong flood events exert merely a special short-term impact on the sediment budget in the study area (Winterscheid and Svenson, 2016). The existence of negative volume changes in the observed area is due to two reasons. Firstly, dredging event lead to larger negative volume changes (see Figure 3.9). Secondly, the smaller negative volume changes are probably not only erosion, but possibly include consolidation effects. The consolidation effects are difficult to quantify and are more dominant compared to the rather minor

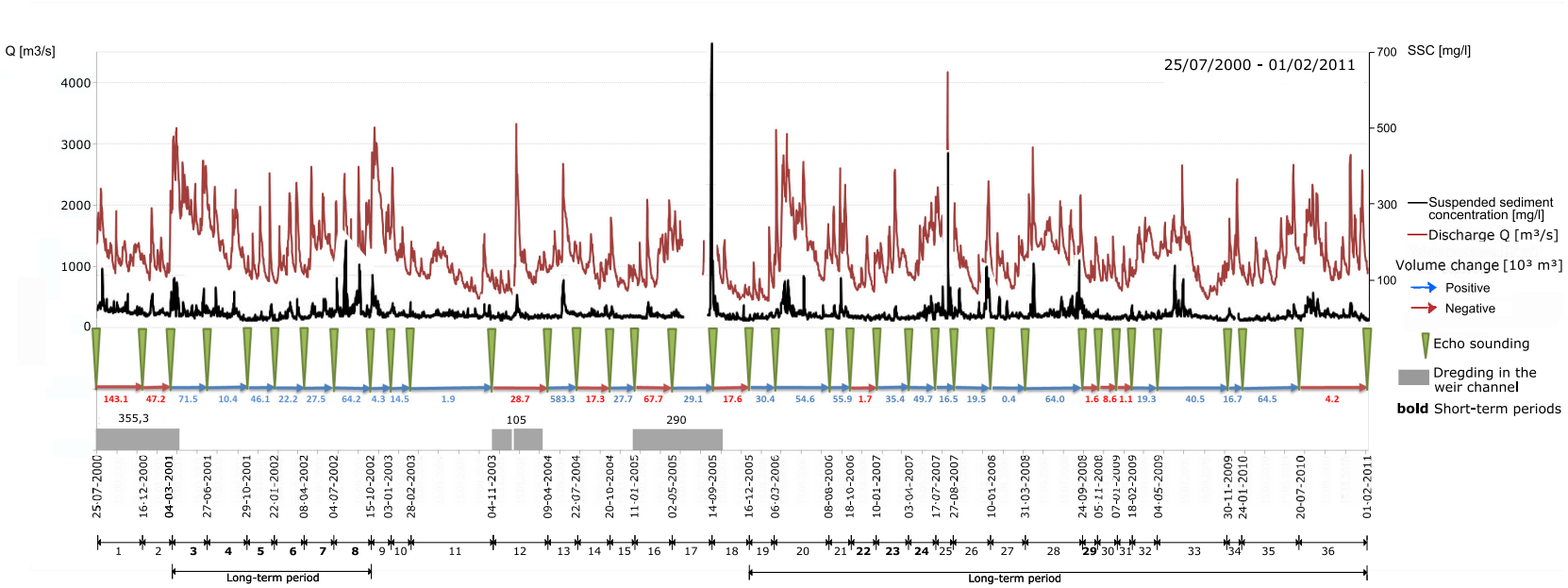

Figure 3.9: Time series of discharge (red line) and suspended sediment concentration (black line) measurement at the Plittersdorf gauging station, dates of the sounding data measurement (green arrows) and dredging periods (gray boxes) in the weir channel.

deposition during the low flow phases (Hillebrand, 2012), which include, for example, the short-term periods 22, 29, 30 and 31 with smaller negative volume changes.

Monthly morphological evolution analysis

It was supposed that the amount of volume change for each period is evenly distributed in months, as shown in Table 3.5. Dredging periods are not taken into account. Table 3.5 reveals the averaged volume change, maximal and minimal volume changes and the standard deviation for each month within 10 years. On average, the measured monthly deposition is 9800 m^3 and the annual deposition is 118,000 m^3. This value is in good agreement with the assessment from other studies (Freiburg, 2011; Hillebrand et al., 2015).

3.4 Summary

Morphodynamic information is of very essential interest. The Iffezheim reservoir in the Upper Rhine is affected by the morphodynamic parameters including river discharge, sediment discharge and bathymetry evolution. For understanding the historical morphodynamical changes at the Iffezheim reservoir, this chapter analyzes the in situ measurement data, which were collected by the Federal Institute of Hydrology (BfG) and the Water and Shipping Administration (WSV).

In order to understand hydrodynamic conditions, the water discharge time series from 1924 to 2013 were analyzed. The average monthly discharge is 1166 m^3/s. Maximum and minimum mean monthly discharges during the period of record are 2888 m^3/s and 339 m^3/s, respectively. The months with much higher discharge are concentrated from April to September, which account for 60 % of the total discharge. A slight increasing trend was found in the water discharge in the past 90 years. Comparing the historical discharge and the predicted discharge from KLIWAS program until the year 2100, the average discharge is slightly increased. The frequency and intensity of extreme events with become larger. The monthly water discharge increases in winter and no significant change of discharge is found in summer.

In order to understand sediment conditions, we analyzed the suspended sediment concentration time series from 1978 to 2013 and soil samples taken from the reservoir. The average annual sediment transport rate is 2244 g/s, while the average sediment concentration is 18 g/m^3. A slight decreasing trend is observed in the behavior of sediment discharge. The average d_{50} is 19 mm in the riverbed on the right-hand side and 0.01 mm on the left-hand side of the reservoir.

Table 3.4: Data analysis of each short-term period: duration, mean, minimum, maximum inflow, RMSE and the volume change in the section of Rhine-km 332.0 to 333.8.

	Time period	Duration (day)	Qmean (m^3/s)	Q_{min} (m^3/s)	Qmax (m^3/s)	s (m^3/s)	$\triangle V_{total}$ ($\times 10^3$ m^3)
1	25/07/2000 - 16/12/2000	145	1276	890	2270	253	-146.3
2	17/12/2000 - 04/03/2001	79	1079	772	1950	260	-192.0
3	05/03/2001 - 27/06/2001	115	2155	1520	3260	420	108.6
4	28/06/2001 - 29/10/2001	124	1415	886	2300	343	10.5
5	30/10/2001 - 22/01/2002	86	1014	727	2520	338	43.1
6	23/01/2002 - 08/04/2002	76	1278	777	2370	403	21.6
7	09/04/2002 - 04/07/2002	87	1400	820	2630	363	26.2
8	05/07/2002 - 15/10/2002	103	1395	918	2630	351	60.0
9	16/10/2002 - 13/01/2003	91	1996	1220	3270	563	15.0
10	14/01/2003 - 28/02/2003	46	1155	863	1640	193	13.1
11	01/03/2003 - 04/11/2003	249	914	472	1530	226	1.3
12	05/11/2003 - 09/04/2004	158	951	514	3324	456	-84.4
13	10/04/2004 - 22/07/2004	104	1282	901	2677	335	57.0
14	23/07/2004 - 20/10/2004	90	1006	636	1530	179	-16.1
15	21/10/2004 - 11/01/2005	84	889	602	1796	258	24.5
16	12/01/2005 - 02/05/2005	111	1126	663	2088	361	-203.6
17	03/05/2005 - 14/09/2005	135	817	876	3144	811	-12.1
18	15/09/2005 - 16/12/2005	93	716	460	1434	227	-16.0
19	17/12/2005 - 06/03/2006	81	660	444	1640	249	27.0
20	07/03/2006 - 08/08/2006	155	1637	769	3230	576	84.4
21	09/08/2006 - 18/10/2006	71	1407	918	2600	367	52.0
22	19/10/2006 - 10/01/2007	85	852	589	1500	231	-1.6
23	11/01/2007 - 03/04/2007	83	1235	734	2580	352	34.2
24	04/04/2007 - 17/07/2007	105	1352	771	2290	413	50.0
25	18/07/2007 - 27/08/2007	41	1822	1260	4170	565	12.6
26	28/08/2007 - 10/01/2008	137	1052	553	2390	387	18.8
27	11/01/2008 - 31/03/2008	81	993	640	1500	214	0.5
28	01/04/2008 - 24/09/2008	177	1456	999	2940	299	64.5
29	25/09/2008 - 05/11/2008	42	980	746	1480	204	-1.5
30	06/11/2008 - 07/01/2009	64	927	678	1490	197	-7.4
31	08/01/2009- 18/02/2009	42	845	607	1330	174	-0.4
32	19/02/2009 - 04/05/2009	75	1321	833	1800	249	18.3
33	05/05/2009 - 30/11/2009	210	1089	467	2650	403	36.7
34	01/12/2009 - 24/01/2010	55	1205	826	2420	348	16.0
35	25/01/2010 - 20/07/2010	196	1026	687	2660	353	58.6
36	21/07/2010 - 01/02/2011	177	1489	772	2820	494	-0.7
		3853	**1200**	**444**	**4170**	**345**	**171.8**

Table 3.5: Statistics of monthly riverbed evolution (Data from Iffezheim reservoir, 2000-2010); BC: Riverbed volume change.

	Average BC ($\times 10^3$ m^3)	Standard deviation ($\times 10^3$ m^3)	Max BC ($\times 10^3$ m^3)	Min BC ($\times 10^3$ m^3)
Jan	10.0	6.6	19.5	1.2
Feb	6.5	2.8	9.3	0.6
Mar	10.0	9.3	27.4	1.4
Apr	10.8	8.7	30.8	1.2
May	9.3	3.6	13.9	2.0
Jun	18.3	11.8	34.7	12.1
Jul	15.8	16.5	56.5	1.4
Aug	11.1	10.7	28.8	0.4
Sep	9.3	10.3	26.0	0.3
Oct	6.0	7.6	24.0	0.8
Nov	4.2	4.9	15.9	0.4
Dec	6.6	6.1	17.9	1.0
Monthly	**9.8**	**8.2**	**56.5**	**0.3**
Annual	**118.0**			

For an analysis of morphological changes, we considered the echo sounding data from 2000 to 2011. The 37 echo sounding measurements reveal that most of the deposition occurred on the left hand side of the weir channel. So far on the right hand side of the weir channel, deposition has not occurred. During flood events, the riverbed is even eroded at this section. Probably the eroded sediments are the same material, which was deposited during the low discharge. There is no deepening of the riverbed in the long-term. In the past 10 years, three dredging events took place in 2000/2001, 2003/2004 and in 2005. The average bed change is 118,000 m^3/yr and obvious temporal changes of the sediment placement are not observed.

Chapter 4

3D high-resolution numerical modeling

4.1 3D numerical morphodynamic models

There are many developed models to display morphodynamics in different areas, e.g. for estuarine, channel and reservoir evolution or reservoir flushing. These include TELEMAC-SISYPHE, Delft3D, MIKE21, ECOMSED, TIMOR3, SSIIM, OpenFOAM etc.

SISYPHE is part of the TELEMAC system and was developed by the Laboratoire National D'Hydraulique et Environment of Electricité de France (EDF). SISYPHE model provides realistic estimates of bed movements and sediment transport patterns driven by currents in coastal environments, rivers, lakes or estuaries. The model is internally coupled to the depth-averaged shallow water flow (TELEMAC 2D) or to the Reynolds-averaged Navier-Stokes flow module (TELEMAC 3D). The bottom evolution equation is solved, using either a finite element (FEM)(Hervouet, 2007) or a finite volume method (FVM). The usage of the TELEMAC 3D model to simulate complex hydrodynamic and morphodynamic situations like secondary currents in curved channels, sand grading effects in waterways and wave-induced littoral drifts is presented in Villaret et al. (2013). For strong recirculation flow a 3D model becomes necessary and the development of a feedback method of the friction factor is applied to reduce uncertainties. Langendoen et al. (2016) report on a depth-averaged, non-linear river morphodynamic model, which is more accurate in simulating near-bank flow. Hence, the study presents an improvement of the near-bank sediment transport, the bed evolution and consequently the platform adjustment by utilizing the TELEMAC 3D SISYPHE model. The current version of SISYPHE simulates suspended sediment transport only with one fraction.

Delft3D by Deltares (Lesser et al., 2004) in the Netherlands is the open source soft-

ware which covers a wide range of hydrological processes from hydrodynamics, sediment transport and morphology to water quality for fluvial, estuarine and coastal areas. The model handles non-steady flow by solving unsteady shallow water equations and transport phenomena of tidal or meteorological processes. Moreover, they include an extensive feature to simulate dredging and dumping scenarios. In practice the Delft3D model is proposed, e.g. to assess the influence of alongshore variability in the initial bathymetry as well as the variability in incident cross-shore hydrodynamic forcing. More precisely, a model has been applied to estimate the variation in wave and tidal forcing conditions. The formation and development of estuarine turbidity in partially mixed estuaries can be another application (Han et al., 2014).

MIKE3, developed by Danish Hydraulic Institute (DHI) in Denmark is a three-dimensional modelling package for the simulation of flows, waves, sediments and ecology in rivers, lakes, estuaries, bays, coastal areas and seas. MIKE 3 software includes three sediment modules that enable to model all aspects of sediment transport. They are sand transport, mud transport and particle tracking module. Using mud transport module, erosion, transport and deposition of cohesive and cohesive/granular sediment mixtures can be modeled (MIKE, 2017).

Another 3D hydrodynamic and sediment transport model is ECOMSED, which is developed by HydroQual to apply marine and freshwater systems. ECOMSED is a component model that links the output from one component to another. Therefore, the models need to share the same grid structure. The capabilities of the model range from the simulation of transport and fate of suspended sediment to dissolved tracers and neutrally-buoyant particles in shallow water systems such as estuaries, rivers, lakes and coastal oceans. Amongst others, problems of optics and spill tracking can be studied. In Nie et al. (2012) the model is used to simulate the water level during a typhoon storm surge that landed on the coast of Zhejiang in China. This morphological model was used to capture the flow structure and resistance of sand dunes and bed forms similar to the Lower Mississippi River (Kheiashy et al., 2010).

The software OpenFOAM by CFD Direct, an open-source software package, has the capability to numerically solve a wide range of fluid dynamic related problems. The turbulence of fluids is depicted by Reynolds-averaged Navier-Stokes equation, coarse grid structure or numerical simulations as FVM, FEM or FAM (Finite Area Method). OpenFOAM has an extensive range of features to solve problems from complex fluid flows, involving multi-fluid (Hirt and Nichols, 1981), chemical reactions, turbulence and heat transfer, to acoustics, solid mechanics and electromagnetics. An OpenFOAM based numerical model is used to estimate the coastal structures that are influenced by the

normal incident irregular wave fields (Jacobsen et al., 2015). In the fields of sedimentary geology, OpenFOAM has recently become more popular. Liu (2008) applied the fluid flow solver from the original turbulence flow solver, added a sediment transport solver and studied a three-dimensional numerical model with free water surface and mesh deformation for local sediment scour (Liu and Garcia, 2008). However, the open source program needs further pre-processing and post-processing tools.

The Institute of Hydraulics and Water Resources of the Technical University of Darmstadt, Germany developed a quasi 3D hydrodynamic and morphodynamics model, TIMOR 3. Flow and sediment transport in lakes, estuaries, harbors and coastal waters can be simulated under the forcing of tides, freshwater inflow, winds etc. The model is based on FEM using triangular elements. A 3D bed evolution and suspended sediment transport is included, based on the shallow water equations. A long-term morphological response to the water and sediment change in the area of the Yangtze Estuary was established by the morphodynamic TIMOR 3 model (Zheng et al., 2012).

Additionally, many individual researchers worked on the development and improvement of morphodynamics models. For example, Willis and Krishnappan (2004) reviewed many numerical models and gave an overview of the knowledge base required for developing a 3D sediment transport model. Wu et al. (2000) developed a 3D numerical model for calculating flow and sediment transport in open channels. Both suspended sediment and bed load transport processes were considered. The hydrodynamic model and the suspended load sediment transport model are both investigated in laboratory channels. The agreement with measurements was generally good. Jia et al. (2010) developed a 3D numerical model to simulate morphological changes in alluvial channels during the period from October 1996 to October 1998 due to bank erosion in the Shishou bend of the middle Yangtze River in China. Simulated processes of bank erosion agreed with field observations. Jia et al. (2013) used this 3D numerical model again and investigated the sedimentation processes of fine-grained particles in a 14 km long section upstream of the Three Gorges Dam for the period from March 2003 to October 2006. The calculated total amount of deposits agreed well with measurements.

Olsen (2014) developed the fully 3D numerical model SSIIM, which is an abbreviation for Sediment Simulation In Intakes with Multiblock options. The program SSIIM was developed for use in River/Environmental/Hydraulic/Sedimentation/Engineering and simulates the hydraulic and sediment transport in rivers, channels and reservoirs. A grid generator, a morphodynamic calculation module and visualization of results are implemented in this program. Olsen (2014) studied the application of a FVM on an unstructured non-orthogonal 3D grid. This model is especially suitable for complex

natural geometries. With the grid generator module the topography of the riverbed can even be updated in a user-friendly manner. This represents a particular advantage when a large number of echo-sounding data are applied for modeling, which is the case for the Iffezheim reservoir in this study.

In addition, concerning the 3D simulation of flow and sediment transport, SSIIM presents many nature sediment transport features, including multiple sediment sizes, sorting, bed load and suspended load, bed forms and effects of sloping beds, even algae growth on the water surface, and it has the option to enhance the accuracy of scour depth estimation. Many researchers have successfully applied SSIIM to simulate morphodynamics processes in their study area, e.g., Fischer-Antze et al. (2008) studied the bed changes in a section of the river Danube during a flood. The results accorded reasonably well with regular bed level surveys before and after the flood for approximately 45 days. Haun et al. (2013) computed suspended sediment distribution and deposition patterns in a hydropower reservoir in Costa Rica over 250 days. A reasonable agreement between the measurements and computed results was obtained.

Regarding the many nature sediment transport features and simple adaptation of bathymetry, 3D-SSIIM model is chosen in this thesis to simulate the morphodynamic evolution in the Iffezheim reservoir. As can be seen, most research studies have applied 3D models only for a relatively short-term period. For long-term studies, the model is generally limited due to the huge computational effort.

4.2 Model concepts of 3D SSIIM

In this work, the fully 3D hydro- and morphodynamic SSIIM model, developed by Prof. Olsen (Olsen, 2014), has been used to simulate the morphological changes in the Iffezheim reservoir. SSIIM simulates the flow and sediment transport in three steps: Firstly, a water flow simulation with steady state conditions is conducted as initial condition. The results (e.g. flow velocities, water level) are saved, after the water flow simulation has converged or reached the maximum number of iterations. Secondly, the results from the previous step of the water flow computation are read back and a sediment transport simulation with steady state conditions is started. The computation results from this simulation are used to determine initial conditions for unsteady transport simulations. Finally, the sediment computation under unsteady flow conditions is performed. The theory about the hydrodynamic and morphodynamic model are described in subsections 4.2.1 and 4.2.2.

4.2.1 Hydrodynamic model

The three-dimensional Reynolds averaged Navier-Stokes equations for turbulent flow are solved to obtain the water velocity and pressure (Olsen, 2014). The Navier-Stokes equations for non-compressible and constant density flow are:

$$\frac{\partial U_i}{\partial t} + U_j \frac{\partial U_i}{\partial x_j} = \frac{1}{\rho_w} \frac{\partial}{\partial x_j}(-p\delta_{ij} - \rho_w \overline{u_i u_j}) \tag{4.1}$$

With subscript i = 1, 2, 3; where U_i is the averaged velocity, x is the coordinate direction, ρ_w is the water density, p is the dynamic pressure, δ_{ij} is the Kronecker delta and $\rho_w \overline{u_i u_j}$ are the turbulent Reynolds stresses. On the left-hand of the equation, there is a transient and a convective term. The model employs an element-based finite volume approach in space and an implicit scheme for time discretization. The convective term is solved by a second order upwind scheme. On the right-hand of the equation, there are the pressure and Reynolds stress terms. The SIMPLE method (Semi-Implicit Method for Pressure-Linked Equations (Pantankar, 1980)) is used for pressure-correction, the $k - \varepsilon$ model is used to calculate the turbulence (see Equation 4.3) (Olsen, 2014).

To model the Reynolds stress term SSIIM uses the Boussinesq approximation:

$$-\overline{u_i u_j} = v_T \left(\frac{\partial U_i}{\partial x_j} + \frac{\partial U_j}{\partial x_i}\right) + \frac{2}{3} k \delta_{ij} \tag{4.2}$$

The first term in bracket on the right side of the equation behaves as the diffusive term in the Navier-Stokes equation. The second term on the right side is incorporated into the pressure. It is very small, and usually not of any significance. In equation 4.2, the turbulent eddy viscosity coefficient v_T is given by:

$$v_T = c_\mu \frac{k^2}{\varepsilon} \tag{4.3}$$

where k is the turbulent kinetic energy, defined by: $\mathrm{k} \equiv \frac{1}{2}\overline{u_i u_j}$, ε is the turbulent dissipation; with constant $c_\mu = 0.09$. The above equation is complemented by two additional convection-diffusion-reaction equations for the computation of k and ε (Olsen, 2014):

$$\frac{\partial k}{\partial t} + U_j \frac{\partial k}{\partial x_j} = \frac{\partial}{\partial x_j}\left(\frac{v_T}{\delta_k} \frac{\partial k}{\partial x_j}\right) + P_k - \varepsilon \tag{4.4}$$

$$\frac{\partial \varepsilon}{\partial t} + U_j \frac{\partial \varepsilon}{\partial x_j} = \frac{\partial}{\partial x_j}\left(\frac{v_T}{\delta_\varepsilon} \frac{\partial \varepsilon}{\partial x_j}\right) + C_{\varepsilon 1} \frac{\varepsilon}{k} P_k - C_{\varepsilon 2} \frac{\varepsilon^2}{k} \tag{4.5}$$

where the coefficient P_k is given by

$$P_k = v_T \frac{\partial U_j}{\partial x_i}\left(\frac{\partial U_j}{\partial x_i} + \frac{\partial U_i}{\partial x_j}\right) \tag{4.6}$$

$C_{\varepsilon 1}$, $C_{\varepsilon 2}$ and δ_k are constants in the $k-\varepsilon$ model and have the following standard values: $C_{\varepsilon 1} = 1.44$; $C_{\varepsilon 2} = 1.92$; $\delta_k = 1.0$; $\delta_\varepsilon = 1.3$.

The velocity gradient towards the wall is often very steep. Instead of assigning many grid cells, a wall law is used. This means that it is assumed that the velocity profile follows a certain empirical function (see Equation 4.7), e.g. in case of cells close to the bed, the wall laws are used to derive analytical expressions for the source terms. When computing the velocities, the wall law is used to calculate the bed shear stress. The bed shear stress was used as a sink term at the bed for the Navier-Stokes equations. The shear stress multiplied with the area of the cell side bordering the wall is used as a sink term in the velocity equation (Olsen, 2014). The wall law in 3D SSIIM is given as an empirical formula for rough walls by Schlichting (1979):

$$\frac{U}{u_*} = \frac{1}{\kappa} ln\left(\frac{30y}{k_s}\right) \tag{4.7}$$

The shear velocity is denoted u_* and κ is a constant equal to 0.4. The distance to the wall is y and the roughness k_s is equivalent to a diameter of particles on the bed.

In this research, a constant wall roughness of 2 cm was used, similar to the maximum observed sediment size.

4.2.2 Sediment transport model

The computation of the suspended sediment transport is performed by solving the transient convection-diffusion equation (Olsen, 2014):

$$\frac{\partial c_i}{\partial t} + U_j \frac{\partial c_i}{\partial x_j} + w_f \frac{\partial c_i}{\partial z} = \frac{\partial}{\partial x_j}\left[\Gamma \frac{\partial c_i}{\partial x_j}\right] + S \tag{4.8}$$

where c_i is the concentration of suspended load for the i^{th} fraction. S is a sediment source term, which is used to assign a pick-up flux from the bed or release in the water column. Γ is the turbulent diffusivity, which is taken from the $k-\varepsilon$ model.

$$\Gamma = \frac{\nu_T}{Sc} \tag{4.9}$$

where Sc is the Schmidt number, set to 1.0 as default.

For problems involving resuspension of sediments, a boundary condition near the

bed is necessary. For this an empirical formula of van Rijn (1987) is used in SSIIM:

$$c_i = 0.015 \frac{d_i}{a} \frac{(\frac{\tau - \tau_{c,i}}{\tau_{c,i}})}{(d_i(\frac{(\rho_s/(\rho_w - 1)g}{\nu^2})^{1/3})^{0.3}} \tag{4.10}$$

$$c_{a,i} = 0.015 f_{silt,i} \frac{d_i \cdot T_i^{1.5}}{a \cdot D_{*,i}^{0.3}} \tag{4.11}$$

where the dimensionless particle diameter of the fraction i is given by:

$$D_{*,i} = [\frac{(\rho_s \cdot \rho_w)g}{\rho_w \cdot \nu^2}]^{1/3} \cdot d_i \tag{4.12}$$

where $c_{a,i}$ is the concentration of suspended load near the bed for the i^{th} fraction. The sediment particle diameter for the appropriate fraction is denoted as d_i. τ is the bed shear stress. $\tau_{c,i}$ is the critical bed shear stress for the i^{th} fraction. In equation 4.10 the parameter a is the reference level set equal to half the height of the cell closest to the bed. $f_{silt,i}$ is the fraction of the silt. T_i is the dimensionless bed shear stress parameter. ρ_s represents the density of sediment. ν is the kinematic viscosity of water and g is the gravitational acceleration.

In the case of non-uniform sediment transport, interactions exist among different size classes of bed material. Coarse particles have a higher chance of exposure to the flow, while fine particles are more likely sheltered by coarse particles. To determine T_i for graded beds, the hiding and exposure approach introduced by Egiazaroff (1965) for non-uniform sediment transport was taken into account.

$$T_i = \frac{(\tau_0 - \xi_i(d_i/d_{50})\tau_{c,d_{50}})}{(d_i/d_{50})\tau_{c,d_{50}}} \tag{4.13}$$

where d_{50} is the median sediment diameter. τ is the bed shear stress. $\tau_{c,d_{50}}$ is the critical bed shear stress of median sediment diameter. The exposure factor ξ_i is defined by

$$\xi_i = [\frac{log19}{log(19 \cdot \frac{d_i}{d_{50}})}]^2 \tag{4.14}$$

The critical shear stress for cohesive beds (in this case defined as containing a clay content of $\geq$8 %) was calculated by using the equation reported by Chien and Wan (1998):

$$\tau_{cr} = \frac{1}{77.5}[3.2(\rho_s - \rho_w)gd_{50} + (\frac{\rho_b}{\rho_{b,0}})^{10}\frac{k}{d_{50}}] \tag{4.15}$$

where ρ_b and $\rho_{b,0}$ are the bulk density of the active layer and of the consolidated bed, respectively, and k is a calibration coefficient, which is here equal to $2.9 \cdot 10^{-2}\, kg/s^2$ for the deposition dominant case (Hillebrand et al., 2012a).

In addition to the suspended load, the bed load can also be calculated by SSIIM. Van Rijn's formula for bed load is used (van Rijn, 1987). For the calculation of the Iffezheim reservoir, only suspended load transport is considered. Hence, the description of bed load is ignored in this section and detailed information can be found in van Rijn (1987) and Olsen (2014).

Settling velocity

The settling velocity of the particles is one of the most important parameters for sediment transport simulation. Suspended load varies vertically in the water. A sediment particle can be transported in suspension if only its settling velocity is less than the vertical component of hydraulic turbulence, which is defined as the Rouse number z (Rouse, 1937) in equation 4.16:

$$z = \frac{w_s}{k \cdot u_*} \tag{4.16}$$

where w_s is the settling velocity of the particle, k a constant equal to 0.4 and u_* the shear velocity of the main flow. $k \cdot u_*$ denotes the force of the turbulence preventing the particle from sinking. If z is smaller than 1.2, the particles are in suspension; if z is larger than 2.5, the particles are transported as bed load; if z is between 1.2 and 2.5, the particles move as both suspended load and bed load (Whipple, 2004). Based on this, it can be known that the settling velocity affects the particle movement behavior, which subsequently leads to deviations in calculating bed changes.

Figure 4.1 illustrates a case where bed load and suspended load transport modes are calculated in a computational domain in SSIIM model. In SSIIM, the settling velocity has to be given for each fraction by an appropriate diameter. For quartz particles with a density of 2650 kg/m^3 the settling velocity can be estimated by distinct equations (see subsection 4.4.2). The estimation of settling velocity for fine particles is more difficult due to the influence of cohesive forces. Additionally, the particle settling velocity is also affected by suspended sediment concentration. Thus, a sensitivity analysis of the impact of settling velocity on sediment transport processes is required, which has been done in subsection 4.4.2.

Active layer

Layered structures are becoming more popular to describe the sediment bed, especially when fractional transport is computed. SSIIM simulates the bed-material sorting using a multiple-layer approach. The riverbed is divided into two layers in the vertical to account for the heterogeneity of bed material (see Figure 4.1). The first layer is the active layer that interacts with the flow and suspension. The active layer has a constant value of thickness over the simulation time. It is used to limit the amount of sediment that can be eroded, so that not all of the sediment can be eroded at once. The bottom layer is the inactive layer, which serves as source and sink of sediments for the active layer. The height of the inactive layer was set to a large value in order to supply the active layer with a sufficient amount of sediments. The entrainment rate for each time step in each cell is limited by the available amount of sediment of each grain size fraction in the active layer.

Sorting mechanisms were considered in the model. The bed layers are modified at each time step to account for deposition and erosion. The deposition and erosion processes considering the control volume of the bed layers are presented in Figure 4.2 and are calculated in the SSIIM model as follows:

Deposition of sediment causes an upward displacement of the active layer from time n+1 to n+2. Material on the riverbed is mixed, then removed from the active layer and transferred into the inactive layer. In SSIIM, the material is first added and mixed with the active layer from the deposition. Each fraction in the active layer $f_{i,a}$ is computed for the next computation step (Rüther, 2006):

$$f_{i,a} = \frac{f_{i,a,0} \cdot z_a + f_{i,d} \cdot z_d}{z_a + z_d} \tag{4.17}$$

where z_a is the thickness of the active layer, z_d is the height of the deposition, $f_{i,a}$, $f_{i,a,0}$ denote the i^{th} fraction in the current time step and the i^{th} fraction in the active

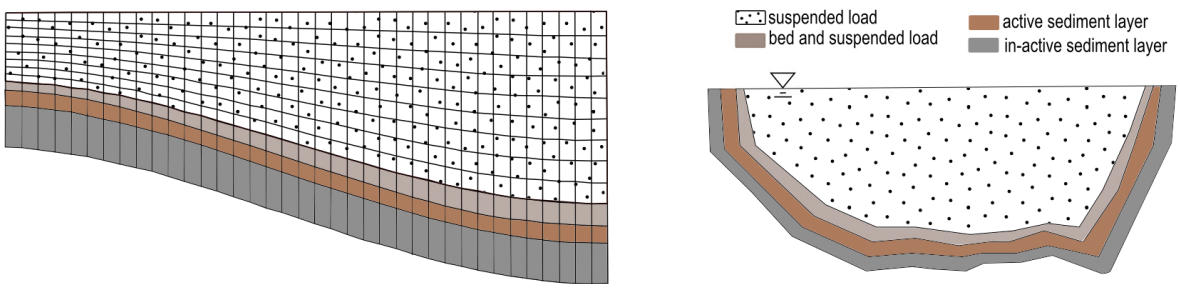

Figure 4.1: Longitudinal and cross-section cut through the computational domain.

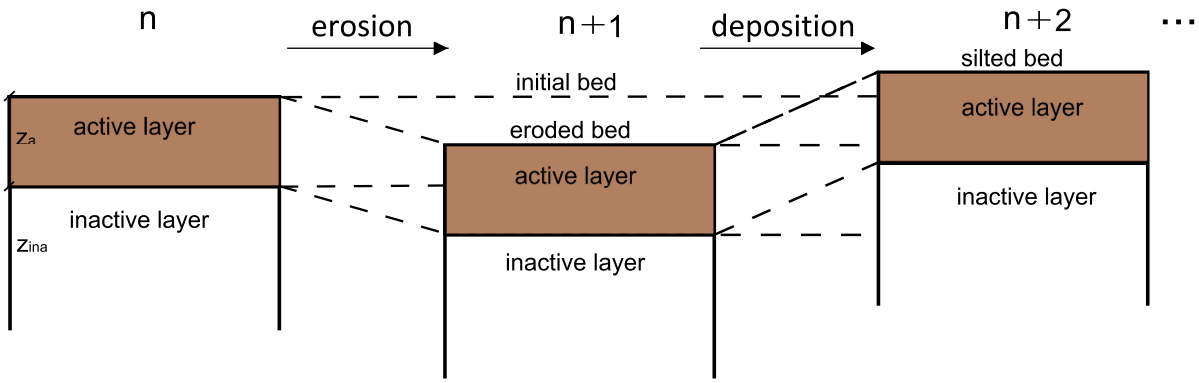

Figure 4.2: Active layer definition sketch: during the erosion top layer thickness is increased to re-adjust the active layer thickness from time step n to n+1, during deposition top layer thickness is decreased to readjust the active layer thickness from n+1 to n+2.

layer in the last step, respectively. Because the vertical magnitude of the active layer remains constant, material has to be transferred to the inactive layer to re-adjust the top layer to the defined active layer thickness. Thus, the fraction in the inactive layer $f_{i,ina}$ is computed (Rüther, 2006):

$$f_{i,ina} = \frac{f_{i,ina,0} \cdot z_{ina} + f_{i,d} \cdot z_d}{z_{ina} + z_d} \tag{4.18}$$

where the index *ina* denotes the inactive layer, z_{ina} is the height of the inactive layer.

Erosion processes were treated in an analogous way.

4.3 Model setup

4.3.1 Model area and grid generation

The Iffezheim model area is shown in Figure 4.3. The polygon depicts the model boundary with a length of about 4 km from Rhine km-330.0 to 333.9. The width of the domain ranges from 300 to 650 m, and the water elevation is ranging from 108 m a.s.l. to 126 m a.s.l.. The barrage consists of a flexible weir, a hydropower plant and a ship lock. The weir controls the flow. The weir channel is the main area of deposition, which is marked in green.

Grid generation is a backbone for any computational approach in fluid dynamics and is also essential in SSIIM model. The size and alignment of the cells strongly influence the accuracy, the convergence as well as the computational time (Olsen, 2014). Using SSIIM grid generator, the Iffezheim study area is discretized by unstructured (tetrahedral and hexahedral) and non-orthogonal grid cells having dimensions of approximately 5 to

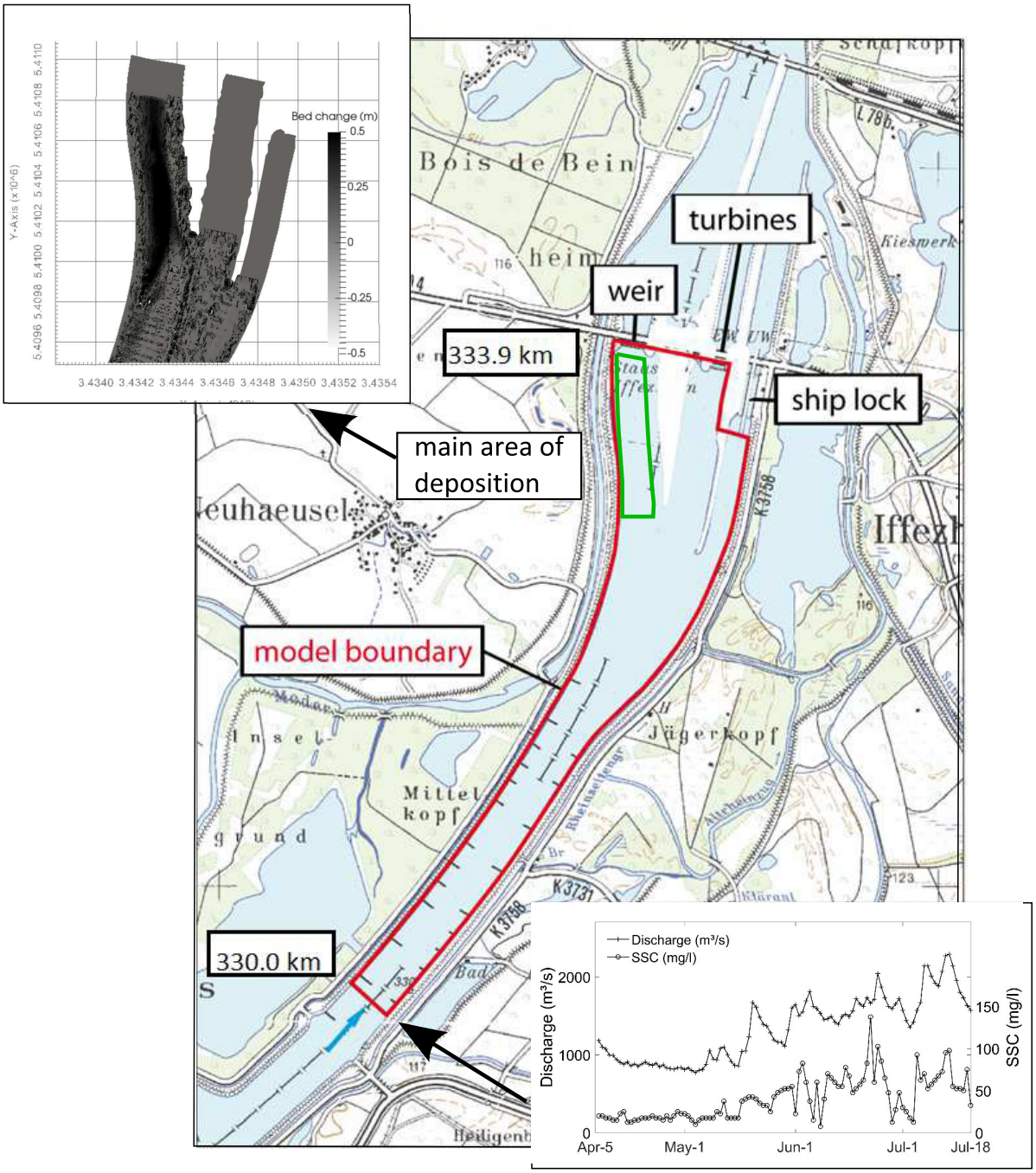

Figure 4.3: Overview map of the Iffezheim reservoir (background map: Federal Agency for Cartography and Geodesy) and reference period from April 5 to July 18, 2007 for model set up. Bottom right: Time series of discharge and SSC for the model boundary. Upper left: Riverbed change derived between subsequent echo sounding data.

10 m in the horizontal direction. 9 layers in vertical direction were set up initially for a water depth of about 13 m (see Figure 5.3). The initial grid has 301,478 cells in total. Because of grid adaptation, the number of cells in the vertical direction varied during computation according to the water depth. More details about the grid generation are given by Olsen (2014).

4.3.2 Model input - boundary conditions

The model input data include bathymetry data, hydrological conditions, sediment conditions, initial grain size distribution in the riverbed, sediment grain size classification and physical coefficients. The input data are taken from the field, which has been described in detail in chapter 3. Different time series of field data are chosen as model input for different purposes and approaches. This is announced separately before each approach in chapters.

For the model setup and calibration, a reference time period from April 5 to July 18, 2007 lasting 105 days was chosen. The bathymetry data taken from the echo sounding survey in April 2007 were set as the initial riverbed. The time series of discharge and sediment concentration through the upstream boundary in this period were chosen (see Figure 4.3). A homogenous initial grain size distribution for the whole domain was firstly set up in the riverbed. Afterwards, a sensitivity analysis was carried out to investigate the impact of the initial grain size distribution on the riverbed changes and subsequently the state most closely to nature (see subsection 4.4.4). For the fractional sediment transport computation, the continuous sediment sieve curve was decomposed into 9 size fractions (see Figure 5.6 and Table 5.5).

In addition, to define a concentration profile of suspension at the model boundary, a function with polynomial regression was developed. Generally, the boundary cross section profile can be obtained by the Hunter-Rouse equation through mean concentration (see subsection 2.4). Figure 4.4b shows the concentration profile with the mean concentration at the cross section of 32 g/m^3. It is observed that using the Hunter-Rouse equation the determined concentrations are distributed homogenously on the riverbed. However, due to the left bend of the channel, sediment is concentrated on the left-hand side (see Figure 4.3), as shown in Figure 4.4a and measured at Rhine-km 330,945 on June 10, 2010. In order to represent the measured distribution profile, polynomial regression was used to describe the relationship between the concentration, location and

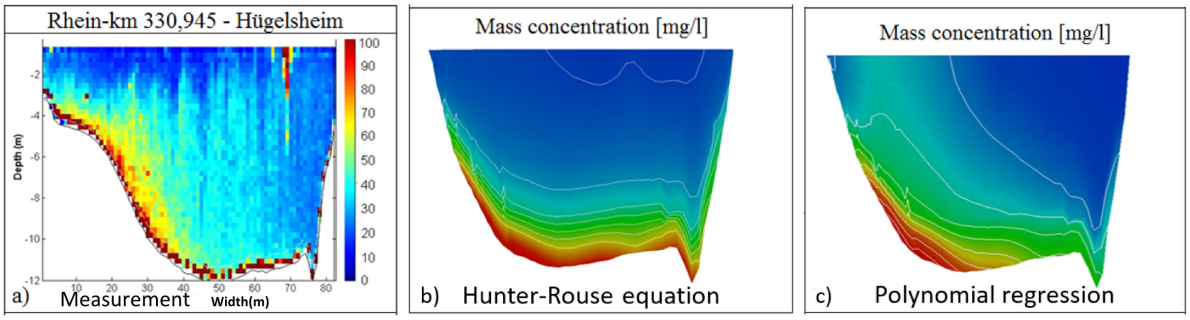

Figure 4.4: Sediment concentration at the Rhine-km 330.945 (Hügelsheim, see Figure 5.1) a) Measurement b) Hunter-Rouse distribution c) Sediment concentration distribution with polynomial regression.

water depth:

$$SSC = k_{1+}k_2x + k_3y + k_4h + k_5x^2 + k_6y^2 + k_7h^2 + k_8xy + k_9xh + k_{10}yh \qquad (4.19)$$

where SSC is the suspended concentration, $k_1 - k_{10}$ are coefficients, x, y, are the Gauss-Krüger coordinates and h is the vertical coordinate. Figure 4.4c shows the sediment concentration distribution using Equation 4.19. The 10 coefficients in Equation 4.19 are given in a special file (*inspace file*) in the SSIIM model. A detailed description of creating the *inspace* file based on the measurements is appended in Figure 4.5.

4.3.3 Model input - initial conditions

Besides the model boundary conditions, proper initial conditions are also important. Some of the initial conditions are only needed to set an initial value according to the available experience, and they will become stable during the simulation. Some of them are in an empirical formula and need to be adjusted and studied through a sensitivity analysis in order to improve the applicability of the model. Table 4.1 gives the input parameters, including numerical and physical ones. All numerical parameters were determined through a sensitivity analysis (Zhang et al., 2013, 2015a) and the key information is summarized in the subsection 4.4.1 and 4.4.3. Some of the physical parameters are experience values according to the current research knowledge, e.g. sediment density, Schmidt number and critical shear stress for bed particles. Some of them are from in-situ field measurements, e.g., sediment fractional components and fraction of compacted sediments in riverbed deposits. For choosing the settling velocity formula, a sensitivity

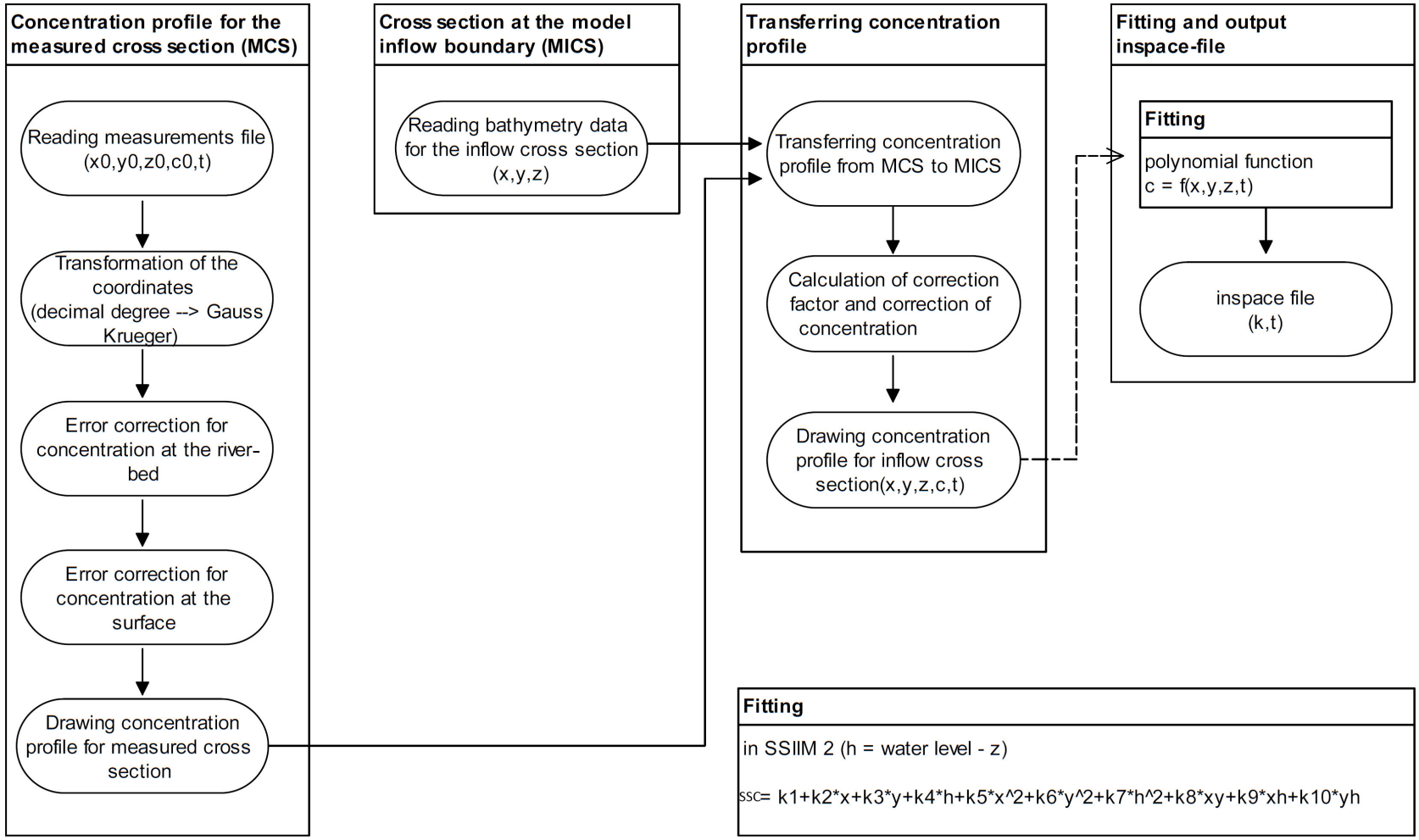

Figure 4.5: Flow chart for creating the inspace file in SSIIM based on measurements.

Table 4.1: Settings of input parameters in SSIIM.

Numerical parameters	
Time step for hydrodynamic simulation (sec)	200
Time step for sediment simulation (sec)	600
No. of inner iterations for hydrodynamic simulation	30
No. of inner iterations for sediment transport simulation	5
Active layer thickness (m)	0.1
Inactive layer thickness (m)	10
Physical parameters	
Sediment grain size density (kg/m^3)	2650
Schmidt number (-)	1.5
9 fractional sediment components in suspension and in riverbed	see Table 5.5
Settling velocity formula	Zanke (1982), see Table 2.3
Critical shear stress for bed particles	Shields (1936) and Chien and Wan (1998)
Fraction of compacted sediments in bed deposits	0.24

analysis was carried out (Zhang et al., 2015a) and the results are presented in subsection 4.4.2.

4.4 Sensitivity studies

For the sensitivity analysis, both time independent and time dependent simulations were carried out. For time independent simulations, a constant discharge of 1550 m^3/s and a constant concentration of suspended sediments of 20 g/m^3 were used. The influence of time step size, number of iterations for both hydrodynamics and morphology and the thickness of the active layer were investigated in stationary simulations. For the

Table 4.2: Chosen combinations of time step and number of iterations from the hydraulic simulation.

Combinations	**Comb. 1**	Comb. 2	Comb. 3	Comb. 4
Time step [s]	**200**	300	400	500
Number of iterations [-]	**30**	40	50	60

instationary sediment transport simulation, the discharge and the suspended sediment concentration recorded over 105 days in the reference period were used (see Figure 4.3). The sensitivity study about the initial grain size distribution on the sediment transport was carried out in stationary simulations.

4.4.1 Time step and iterations

Hydrodynamic simulation

Since the results of the hydraulic computation affect the subsequent sediment simulations, it must be performed accurately to ensure correct results for further steps. The size of the time step used in explicit time integration is limited by the CFL (Courant-Friedrichs-Lewy [Courant]) condition. In the SSIIM program an implicit solver is used, which has no inherent limit on the size of the time step. The time steps used in explicit time integration is generally smaller than those used in implicit time integration. However, it is well known that a numerical model is less stable with large time steps and a small number of inner iterations. To achieve high accuracy, a short time step and a high number of iterations are needed. However, the smaller the time step is, the more calculations are required to model the same time period. A high number of calculations leads to increased CPU time. Restricted CPU time is often the limiting factor for the accuracy of the results. When modeling any case, it has to be modeled within a reasonable amount of time and still be adequately accurate.

Zhang et al. (2013) have focused on the hydraulic modeling of the Iffezheim reservoir regarding aspects of solution stability and CPU time through various tests with steady state conditions and found out, the following combinations of time steps and number of iterations successfully delivered stable hydraulic results, listed in Table 4.2. Among them, a time step of 200 sec with 30 iterations is recommended, because the velocities were correct and stable, the results converged fast and required the least CPU time. Additionally, the study demonstrated that the velocity did not converge to an acceptable value in the model with time steps larger than 600 sec.

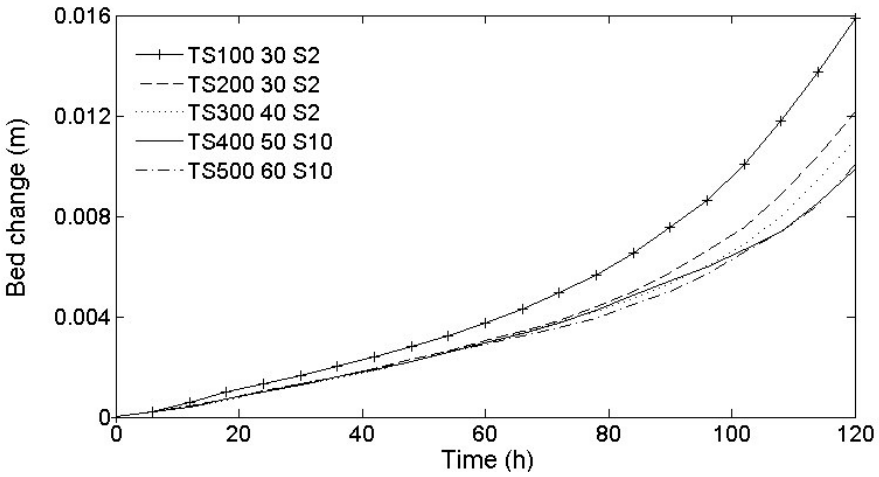

Figure 4.6: Bed change of survey points in the weir channel with varied time step and number of iterations using constant sediment inflow. TS100_30 S2 means time step 100 sec with 30 iterations for the hydraulic and 2 iterations for the sediment transport computation.

Morphodynamic simulation

As in the hydrodynamic simulation, the numerical parameters, e.g., time step size and number of inner iterations used in the sediment calculation affect the bed change volume and CPU time. A large time step encourages the water-flow simulation to become unstable and would have led to more inner iterations. For very small sediment sizes (due to the long settlement process) and low velocities more inner iterations would be required. Hence, Zhang et al. (2015a) studied the fractional sediment transport in the Iffezheim reservoir and carried out a sensitivity analysis, including the time step size for sediment transport simulation and number of iterations in relation to riverbed change.

The combinations from the last section in Table 4.2 were further investigated. A morphodynamic iteration was appended for the sediment transport simulation to find the optimal combination considering CPU time and accuracy. For this purpose, the bed change of a large number of nodes in the weir channel was investigated and analyzed, e.g., the bed change of one node at km-333.5 near the weir was investigated. All the tests were carried out for 5 simulation days. It was found that the number of sediment iterations did not affect the results significantly. The difference in bed change between 2 and 50 iterations was very small (Zhang et al., 2013). Figure 4.6 presents the optimum number of the iterations for the sediment transport equation. The choice of a larger number of iterations did not change the calculation results significantly. The results showed that the smaller the time step, the higher are the bed changes in the riverbed.

Table 4.3: Investigated combinations of time step and number of iterations from the hydraulic simulation (see Table 4.2), compared with the combination of time step of 100 sec and 30 iterations.

Combinations	Number of iterations for morphodynamics	Bed change error [-]	CPU time ratio [-]
Comb. 1	2	0.23	0.78
Comb. 2	2	0.31	0.61
Comb. 3	10	0.36	0.60
Comb. 4	10	0.36	0.55

However, this trend was not clearly observed if a time step larger than 300 sec was used. For a time step of 400 sec and 50 hydraulic iterations and for a time step of 500 sec and 60 hydraulic iterations, the bed change did not differ.

It can be assumed that the smaller time step led to more accurate results. A time step of 100 sec with 30 iterations for the hydraulics and 2 iterations for the sediment transport was considered as reference. The bed change in the study area and the CPU time after 5 simulation days were compared in Table 4.3. Bed change error was the ratio of the other combinations to time step 100 sec and 30 iterations. The CPU time ratio was the ratio of the CPU time of other combinations to time step 100 sec and 30 hydraulic iterations. Table 4.3 indicates that the use of a finer time step improved the results; however, the computational time increased. Using a time step of 500 sec and 60 hydraulic iterations combined with 10 iterations for sediment simulation, the bed change varied by 36 % and the CPU time is ratio is 0.55.

4.4.2 Settling velocities

In order to assess the general effect of the settling velocity on the suspended sediment transport simulation, several tests were performed by Zhang et al. (2015a). There are many equations used to determine the settling velocity and the grain diameters are incorporated, as described in section 2.3. In this study the equations of Zanke (1982), Dietrich (1982), van Rijn (1989), Cheng (1999) and Wu and Wang (2007) are examined.

During the comparison of these equations, it has been found that the settling velocities using different formulae were only similar for the small particle sizes less than 0.01 mm, and greatly differed for larger particles. The settling velocity of Cheng's formula has similar values as Wu and Wang's formula. Thus, in this study only the equations of Zanke, Dietrich, van Rijn and Wu and Wang are examined.

The bed change of a longitudinal profile in the weir channel after 5 simulation days

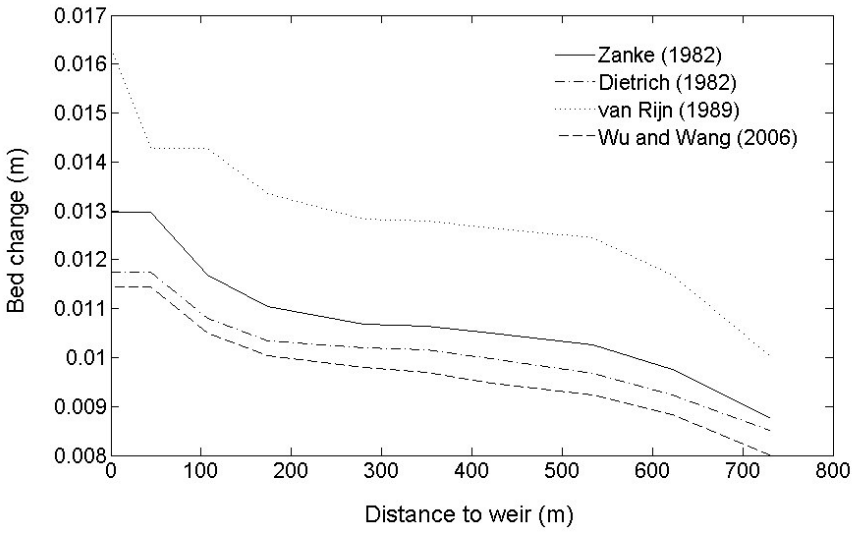

Figure 4.7: Longitudinal bed change in the weir channel using different settling velocities.

under steady state conditions is shown in Figure 4.7. Using the van Rijn's formula resulted in a high value of deposition. The settling velocity of Wu and Wang (2007) has the smallest value which leads to smaller bed changes in comparison with the other formulae. The simulation results are sensitive to the variation of the settling velocity. The results show that the settling velocity could be used as a calibration parameter during the subsequent simulations. The formulae of Zanke and Dietrich, which lead to neither the bed change maximum nor the bed change minimum can be further used. Zanke's formula is applied in following cases.

4.4.3 Thickness of the active layer

The choice of the thickness of the active layer has a significant impact on the erosion and deposition in the sediment transport simulation (see subsection 4.2.2).

If sediment particles are eroded from the active layer, the percentage of this fraction will be decreased in the active layer. Since the thickness of the active layer has a constant value over the entire simulation period, sediments have to enter from the inactive layer. The filling is proportional to the composition of grain sizes in the inactive layer. On the one hand, the thickness of the active layer should not be chosen too large. In case of the existence of an armoring layer, the bed armoring would last longer at the riverbed, and therefore the erosion rate is influenced. On the other hand, the thickness of the active layer should not be too small, as this means that it may contain less material available

than the real amount that could be eroded during the current time step.

If sediment deposition occurs, the deposited sediment within the active and the inactive layer will be mixed, erroneous results for the subsequent erosion may be obtained. In many researches, this is one of the most sensitive parameters (Kopmann and Schmidt, 2010; Warner et al., 2008). However, the thickness of the active layer z_a has an individual value for a natural river, which depends on the deposition and erosion ratio. Regularly, the value z_a is based on assumptions. Kopmann and Schmidt (2010) assumed that this active layer thickness is limited between 0.017 and 0.3 m in River Danube. Villaret et al. (2013) assumed an active layer of 10 cm thickness in the application to a 22.4 km long stretch of the River Danube model. Rüther (2006) supposed that the active layer thickness could be thought to scale in the order of the largest grain size.

In the literature, some formulae are available for calculating a dynamic thickness of the active layer considering the individual grain size fractions, the flow intensity (Lick, 2009), bed shear stresses and the erosion rates. In SSIIM model, a constant thickness over the whole simulation time is required. Two simplified approaches were thus considered as a reference, first the formula after Hunziker (1995):

$$z_a = 5 \cdot d_{max} \tag{4.20}$$

where d_{max} is the maximum grain size in the riverbed.

Secondly, Einstein (1950) assumed the thickness of the bed surface layer to be about twice the mean sediment diameter. This assumption only applies if the intensity of sediment movement is not strong:

$$z_a = 2 \cdot d_{50} \tag{4.21}$$

Using the formulae by Hunziker and Einstein, active layer thicknesses of 0.1 m and 0.02 m were tested. Simulations of two larger thicknesses of 0.3 m and 0.5 m were also carried out, respectively. Figure 4.8 illustrates the bed change of a chosen cross section at Rhine-km 333.0 after 5 simulation days. Strong deviations were obtained with variation of the active layer thickness. The thicknesses of 0.3 m and 0.5 m have the same tendency. The smaller thickness leads to higher deposition, the larger thickness leads to higher erosion. The results indicate the same trend as the one mentioned above. For the Iffezheim reservoir, the thickness of the active layer after Hunziker (1995) is considered further to be applied for the simulation. Erosion is not expected unter the hydraulic boundary condition in this test. Thus, the thicknesses of 0.3 m and of 0.5 m are not considered. The thickness of 0.02 m could be too small for the active layer, because the

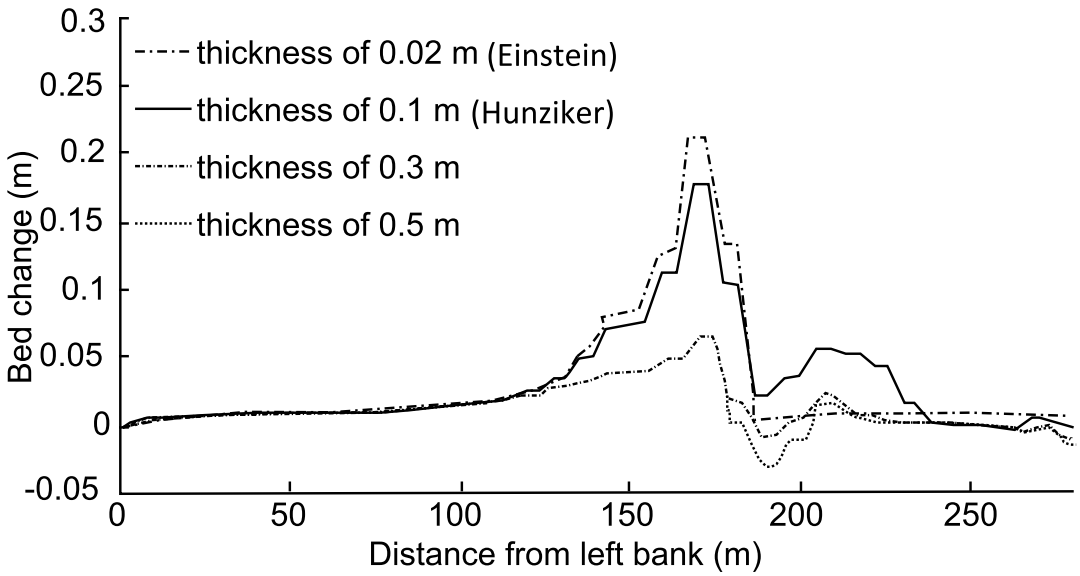

Figure 4.8: Bed change in the cross section of River Rhine-km 333.0 with different thicknesses of the active layer.

largest grain size used in the simulation is also 0.02 m. Additionally, the results turned out that the active layer thickness is a significant parameter when modeling fractional sediment transport processes. Analysis of the active layer indicates that the topography of the riverbed, which is strongly influenced by erosion and deposition, changes frequently in natural rivers. Thus, the thickness of the active layer is unique for each study area and this has to be considered as a calibration parameter to approach the correct solution (Zhang et al., 2015a). Moreover, it has to be noted that the choice of the thickness of the active layer depends on the time step.

After sensitivity analyses of the above mentioned parameters, a simulation under steady state conditions was carried out. A mesurement with a discharge of 1580 m^3/s and SSC of 32 mg/l was avaialble. Thereby, these were set as the model boundary conditions. The simulated velocity and concentration fields are presented in Figure 4.9. Before the bifurcation of the Rhine River, velocity and suspended sediment concentration reach their highest values in the inner curve. As a result of the division, a high amount of concentration follows the flow into the weir channel on the left side. Since the flow is retained in the weir channel, the velocity here is rather small in comparison to the middle branch leading to the turbines. Only a small part of the sediment concentration reaches the turbine channel on the left side of the branch. Nearly no sediment concentration and the lowest discharge values are found in the right branch. Induced by the ship lock there is almost no discharge in the ship lock channel in the model.

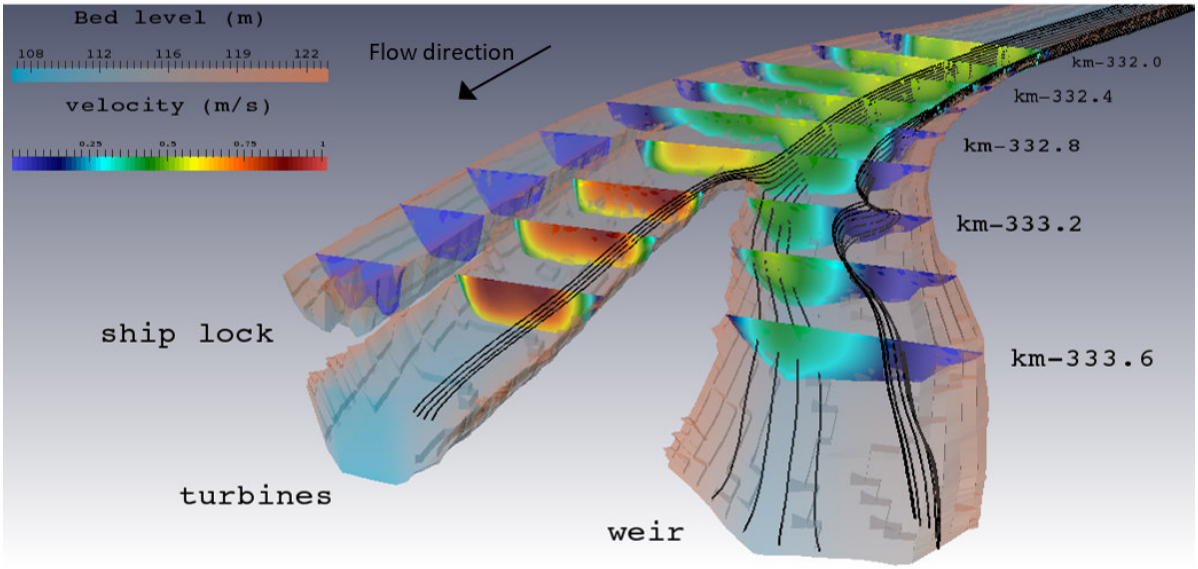

(a) Velocity profile.

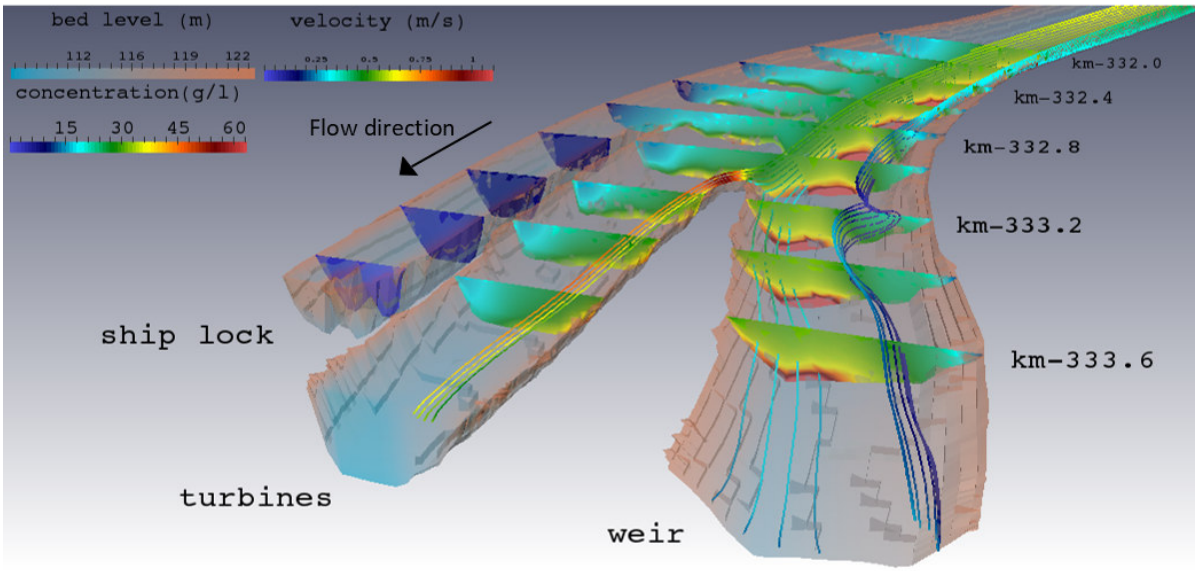

(b) Concentration distribution.

Figure 4.9: Simulated results under steady state condition.

4.4.4 Initial grain size distribution in the riverbed

The definition of the initial spatial distribution of the grain size composition is a key challenge when dealing with river morphodynamic modelling. More precisely this means, that not only the exact grain size fractions but also the spatial distribution of the material within the model area have to be considered and investigated regarding the effect on the hydraulic roughness and the stability of the riverbed. However, the initial grain size distribution is generally not accurately known as a result of the lack of high-resolution measurements. Furthermore, the grain size distribution is subject to variations during the transport and is sensitive to the history of flow and sediment supply.

In Zhang et al. (2016a) several scenarios are performed to determine the sensitivity of the spatially varying grain size characteristics:

- S1: Simulation with a non-uniform grain size composition distributed uniformly over the whole domain: with a mean grain diameter d_{50} between 0.01 and 19 mm, corresponding to the d_{50} of the fine-grained weir channel fill and the initial riverbed before 1977 (see Figure 3.8).

- S2: Simulation with a variable bed composition: coarse sediments (gravel) from the entrance of the model to the hydropower channel and on the right side of the weir channel; fine sediments (silt and clay) dominate on the left side of the weir channel where the major deposition of fine sediments is observed (see Figure 4.11a); nine grain size fractions are linearly interpolated at the transition from coarse to fine grains.

- S3: Simulation outputs for the initial riverbed (see Figure 4.11c): grain size distribution of an earlier numerical simulation by Hillebrand et al. (2012a).

- S4: Long-term (18 years) numerical simulation considering original riverbed material (see Figure 4.11 e): The simulation is limited to a discharge between 1000 and 2000 m^3/s to avoid erosion during the simulation and to generate a weir channel fill that is solely based on deposition; initial bathymetry of this run was based on the Iffezheim reservoir directly after construction (i.e. without deposition) and a non-uniform grain size composition of the former channel bed (before the construction of the Iffezheim barrage) was used as initial condition (BfG, 2016).

Analyzing the results of all methods, it can be concluded that the bed change patterns are strongly sensitive to the initial riverbed composition. Homogeneous grain size distribution for the whole domain (S1) is not representative to model realistic deposition

Figure 4.10: Deposition and erosion patterns for non-uniform grain size composition with d_{50} = 19 mm (gravel = channel bed) and d_{50} = 0.01 mm (silt = weir channel fill) distributed uniformly in the whole study area.

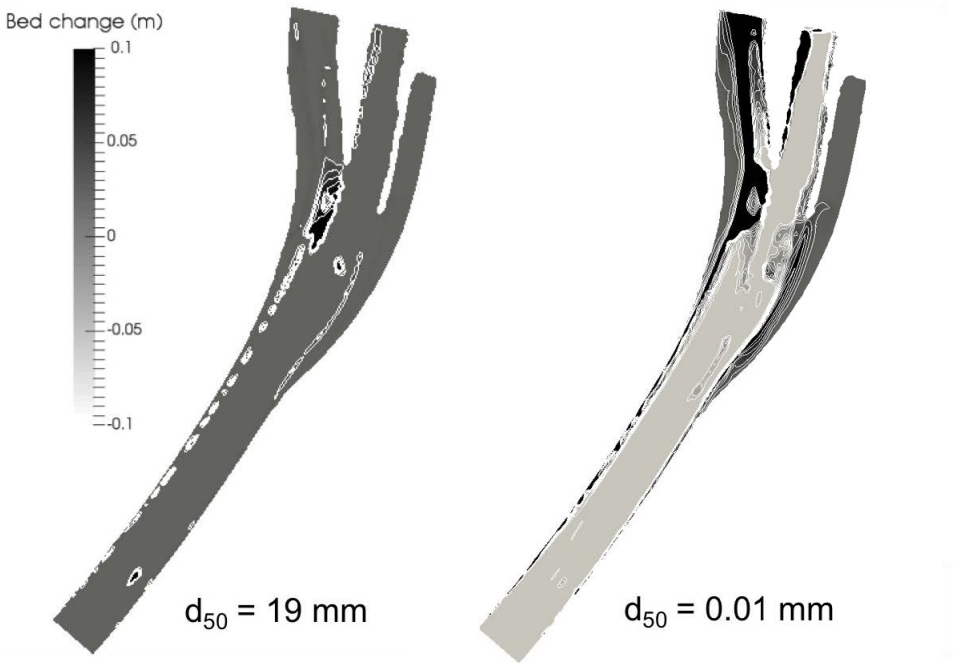

and erosion patterns (see Figure 4.10). In scenario S2 the initial grain size distribution is set directly based on measurements, while the grain size distributions are derived from numerical simulations in S3 and S4. In S2 and S3 the riverbed contains a larger percentage of cohesive sediments. Compared to the observed bed change volume, the predicted results in S2 and S3 are 13.6 % and 40.5 % higher, respectively, while in S4 the bed change is underestimated by 11.8 % (see Table 4.4). Both S3 and S4 are in good agreement with the observed deposition and erosion patterns. As a result, S4 can model the bed change evolution both quantitatively and qualitatively well for this event. Results demonstrate that the long-term numerical simulation can deliver grain size compositions, which are closer to natural river state. However, it should be noted that during long-term sediment simulations deviations of grain size characteristics may occur due to oversimplification of the natural processes. This deviation will influence the computed sediment deposition and erosion. Concerning the computational time, scenario S2 requires the least, because S3 and S4 require additional preparatory simulations. More detailed results are presented in Zhang et al. (2016a). S4 is further applied for the simulation.

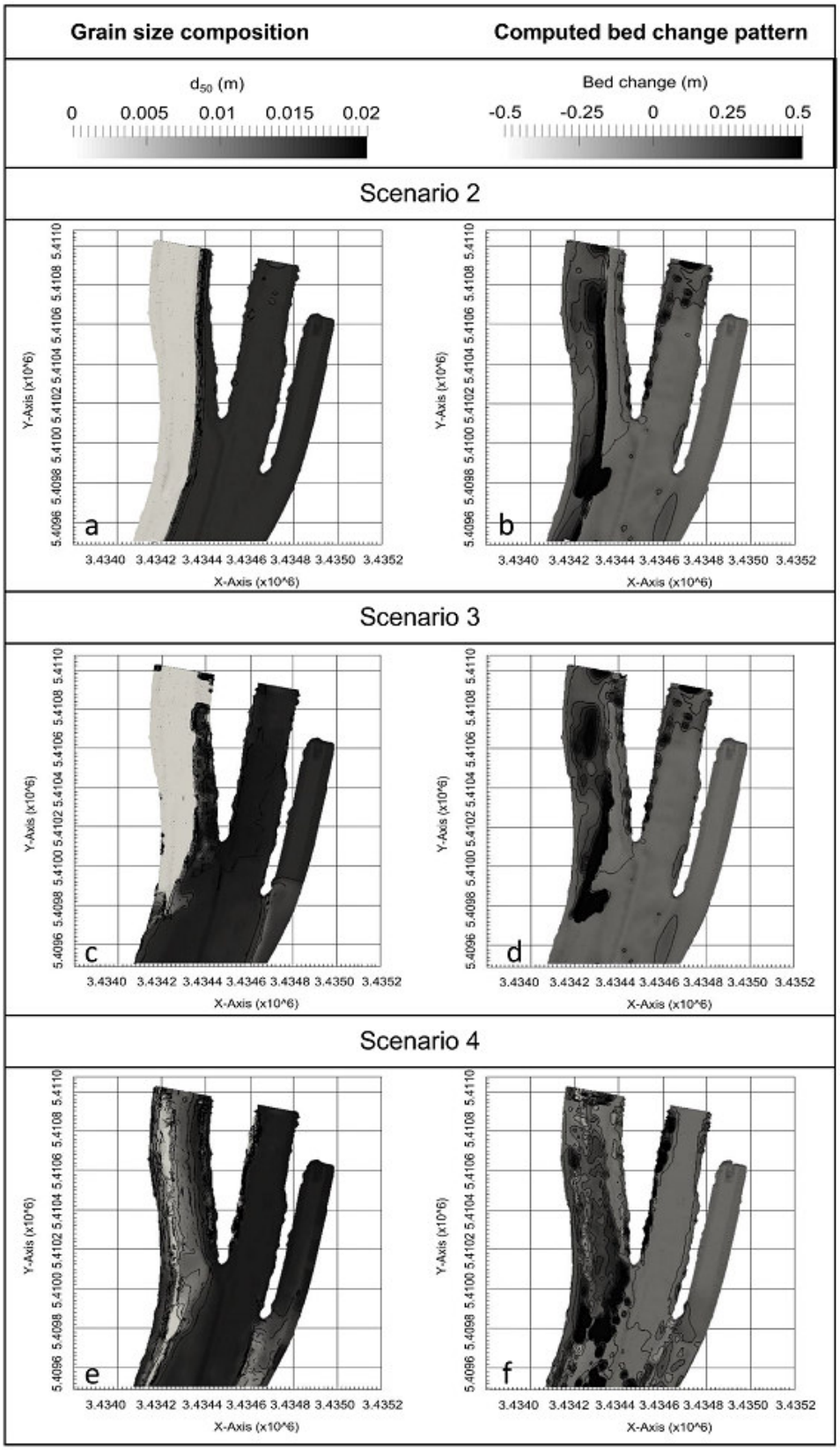

Figure 4.11: a, c, e: grain size composition corresponding to the mean grain diameter d_{50} as initial condition for scenario S2, S3 and S4, respectively. Light areas depict loamy and silty sediments, dark areas show gravel-sized fractions; b, d, f: simulate bed change patterns in the Iffezheim reservoir for scenario S2, S3 and S4, respectively. Light areas represent erosion and dark deposition (Zhang et al., 2016a).

Table 4.4: Simulated bed change depths and volumes for a period of 105 days.

	Bed change (m)		Bed change volume ($\times 10^3$ m^3)		
	Min	Max	Deposition	Erosion	Deviation
Measurement	-0.7	1.9	55.1	6.2	-
S2	-0.4	2.3	62.5	2.1	13.6 %
S3	-0.9	3.5	77.3	1.2	40.5 %
S4	-0.6	2.4	48.5	0.24	-11.8 %

4.5 Summary

The fully 3D numerical model SSIIM was introduced in this chapter. To compute the water flow, the SSIIM program solves the Reynolds averaged Navier-Stokes equations with the $k-\varepsilon$ turbulence model on unstructured grids. The suspended sediment transport is calculated by solving the transient convection-diffusion equation. A finite volume method was used for the discretization on a 3D unstructured grid. The active layer concept is integrated, which deals to tackle the problem with the sediment exchange between the flow and the riverbed.

SSIIM was applied to calculate the non-uniform multi-fractional sediment transport and bed evolution in the Iffezheim reservoir. The 3D high-resolution numerical model was set up with bathymetry and hydrological input data, upstream with measured discharge and downstream with water level boundary conditions, a generated mesh and several model parameters. The high-resolution grid has 301,478 cells in total. The established model was calibrated using a reference period from April to July 2007 lasting over 105 days.

A number of input parameters are investigated to determine optimized values for the Iffezheim model. For the solely hydrodynamic simulation, a time step of 200 sec with 30 iterations is recommended. For the morphodynamic simulation, a time step of 500 sec and 60 hydraulic iterations combined with the 10 iterations for sediment simulation is proposed. Zanke's equation was further used for the settling velocity and an active layer thickness of 0.1 m was set as constant value. More settings of the input parameters in SSIIM can be found in Table 4.1.

In addition, sensitivity studies showed that the resulting bed elevation changes are highly sensitive to the initial grain size distribution in the riverbed, sensitive to the settling velocity, the thickness of the active layer and the time steps for both hydrodynamic and morphological simulations and little sensitive to the number of iterations.

It can be concluded that the 3D SSIIM model enables the simulation and analysis of

morphodynamic problems. The model is sufficiently accurate to compute the complex flow field and sediment deposition in the Iffezheim reservoir. A computational time of 14.5 hours, using 24 cores of a 2.4 GHz reference computer, was needed to simulate a period of three months (reference period) based on the current grid resolution. This means that the simulation of morphodynamics of the fine sediment budget in the Iffezheim reservoir with this model is quite feasible for a relatively short-term period. Many simulation cases using the determined input parameters have been carried out in this thesis in the following.

Chapter 5

3D model reduction

5.1 Upscaling approach

In chapter 4, a high-resolution model was set up to investigate the river morphodynamic processes in the Iffezheim reservoir. The initial high-resolution model had 301,478 cells, i.e. 400 hexahedral cells in the streamwise direction, 90 cells in the lateral and 9 cells in the vertical direction, respectively, and it led to accurate results (Zhang et al., 2016b). In order to simulate a period of three months the model required a computation time of 14.5 hours using reference server.

The ultimate goal of this thesis is to develop methods for assessing the long-term morphodynamics of the fine sediment budget in the Upper Rhine, verified at the Iffezheim reservoir. The simulation period is here defined as 30 years or longer. That will necessarily require huge computational resources, which are difficult to obtain, e.g., 70 days is required for simulating a 30 years period using reference computer. Hence, rather than using the original grid for the long-term simulation, in this chapter, coarsened grids, reduced sediment fractions and optimised parameters are derived. Such an upscaling can be very helpful for saving resources, especially in the numerical simulation of cases with large spatial or temporal extents. The purpose of upscaling process is to optimize the computation time without significantly affecting the accuracy of the hydraulic and morphodynamic results.

The approach of this chapter is twofold. Firstly, a progressive coarsening of the spatial grid resolution was carried out. The grid coarsening was initially executed for horizontal and subsequently for the vertical direction. Afterwards, the sensitivity of the time step for the chosen grid was investigated. The computation time was recorded for each grid resolution. As second part of the upscaling, the number of grain size fractions, was reduced and its impact was investigated.

During the grid coarsening and time step optimization, only steady state simulations were carried out, while for the simulation of fraction reduction unsteady simulations were undertaken as well. For the steady state simulations, a period of 10 days was simulated. For the inflow boundary, a constant discharge of 1580 m^3/s and a suspended load concentration of 32 mg/l were used (based on field measurements in June 2010). The hydrodynamics and sediment concentrations were evaluated at three different cross-sections (see Figure 5.1); namely, section 1 at the upstream end close to the model boundary, section 2 upstream of the stream division at the weir channel and the turbine channel, and section 3 in the turbine channel upstream of the power station. For unsteady state simulations, the reference period of 105 days was simulated. The discharge hydrographs and the concentration of the suspended load, which were used as boundary conditions, are presented in Figure 4.3. The simulated volume of riverbed change and the deposition position were compared with the measurement at the end of the period (see Figure 4.3).

The analysis of the model reduction was based on the conformity of the new results with the results of the high-resolution model and the field measurements, in terms of accuracy and the CPU time. To evaluate, proportionality of the calculation time to the accuracy of results was determined. The baseline for the comparison of all ratio parameters was the equivalent value solved by the high-resolution model.

The detailed 3D model reduction is described in Speckter (2015) and Zhang et al. (2016b). In this chapter, the most important results are presented.

5.2 Spatial coarsening of grids and temporal coarsening

5.2.1 Coarsening of grid in horizontal direction

The spatial resolution of the grid was governed by the river section's topography in the first place. For the model reduction, the reference grid is first coarsened in horizontal direction. The impact of the horizontal coarsening on the hydrodynamics was assessed to find the best grid for further investigations. The total number of cells of the coarsest grid was 30 % less than of the reference grid. It was not possible to further coarsen the grid in order to represent the geometry of the Iffezheim reservoir in an adequate way. A time step of 60 sec was used for all simulations. Three resolutions for the grid in the horizontal direction were compared with the reference grid, their characteristics are shown in Table 5.1.

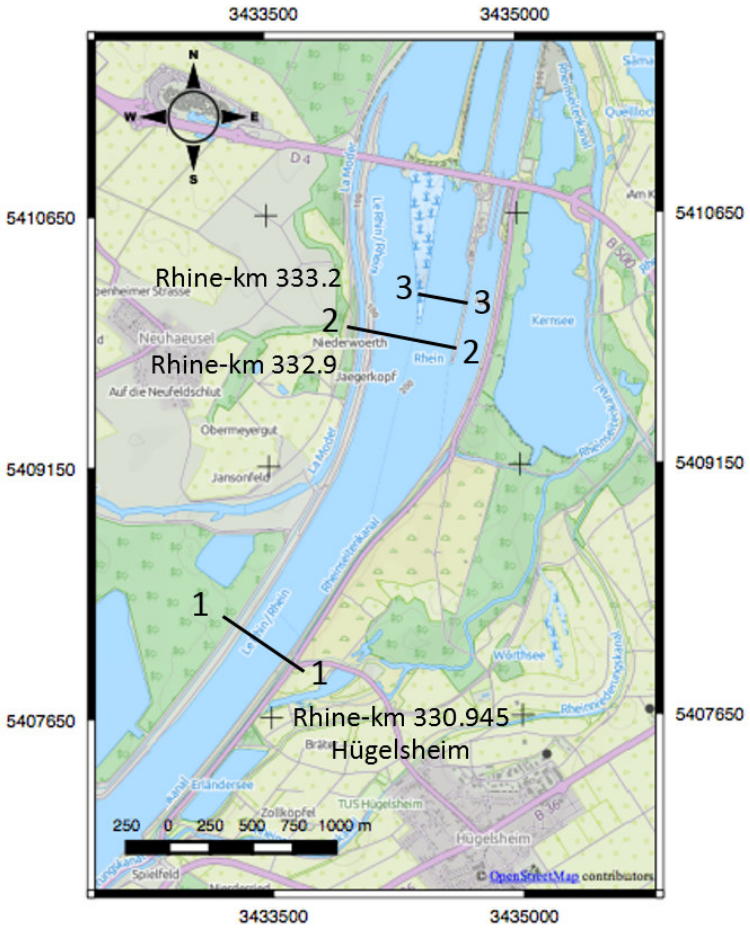

Figure 5.1: Computational domain and observation locations. Section 1-1: Rhine-km 330.945, Hügelsheim. Section 2-2: Rhine-km 332.9, weir channel with the channel of hydropower station. Section 3-3: Rhine-km 333.2, the channel of hydropower stations.

Table 5.1: Number of computational cells, number of cells in horizontal directions, approx. grid sizes Δx and Δy in the weir channel. Grid-0 is the high-resolution reference grid.

Grid	Computational cells	Number of cells in horizontal directions	Grid size Δx and Δy [m]
0 (finest)	301,478	90×400	10×10
1	197,731	75×325	12×14
2	144,275	65×275	15×18
3 (coarsest)	89,149	60×250	16×20

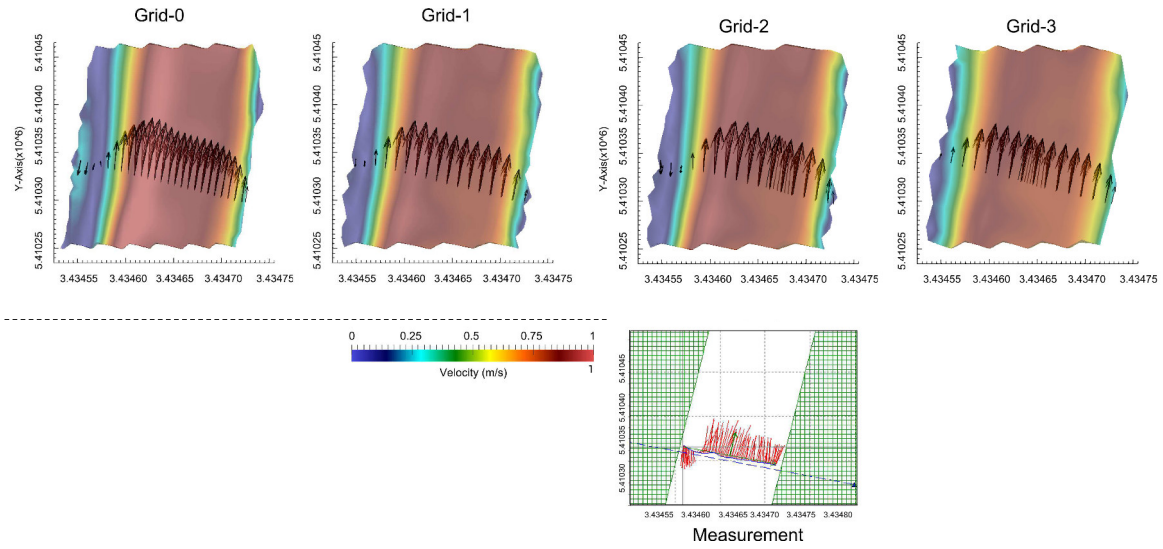

Figure 5.2: Velocity profile and velocity vectors of cross section 3-3 in turbine channel for grid-0, grid-1, grid-2, grid-3 and field measurements (Q = 1580 m^3/s).

Impact on hydrodynamics

The velocity and the secondary flow were firstly used as criteria for assessing the impact of coarsening the grid on the hydrodynamics. The results of cross section 3-3 are shown in Figure 5.2. Grid-1 and grid-2 achieved reasonable results when compared with the reference grid (grid-0). It can be seen that both grids were able to simulate the secondary flow. As in case of the reference grid, grid-1 and grid-2 clearly captured the recirculation zone close to the left bank in the turbine channel. The width of the recirculation zone of grid-1 and grid-2 was very similar to the one of the original grid and to the measurements. The coarsest grid (grid-3) was not able to simulate the secondary flow, as it could not sufficiently describe the topography of the riverbank. This caused a reduction in the effective width of the main stream and increased the velocity in this area. Therefore, grid-3 was excluded from further considerations.

100 points in the weir channel were randomly selected in order to check the result accuracy of grid-1 and grid-2. Deviations of average velocities from the reference grid are 4.1 % and 3.4 % for grid-1 and grid-2, respectively. The computation time is 35 % and 21 % of the reference case, for grid-1 and grid-2, respectively. Hence, grid-2 is superior in terms of accuracy and the computation time. Therefore, grid-2 was selected for the vertical coarsening.

In general,the resolution is limited by the topography and also by the hydrodynamic and morphology modelling capability within an acceptable data range.

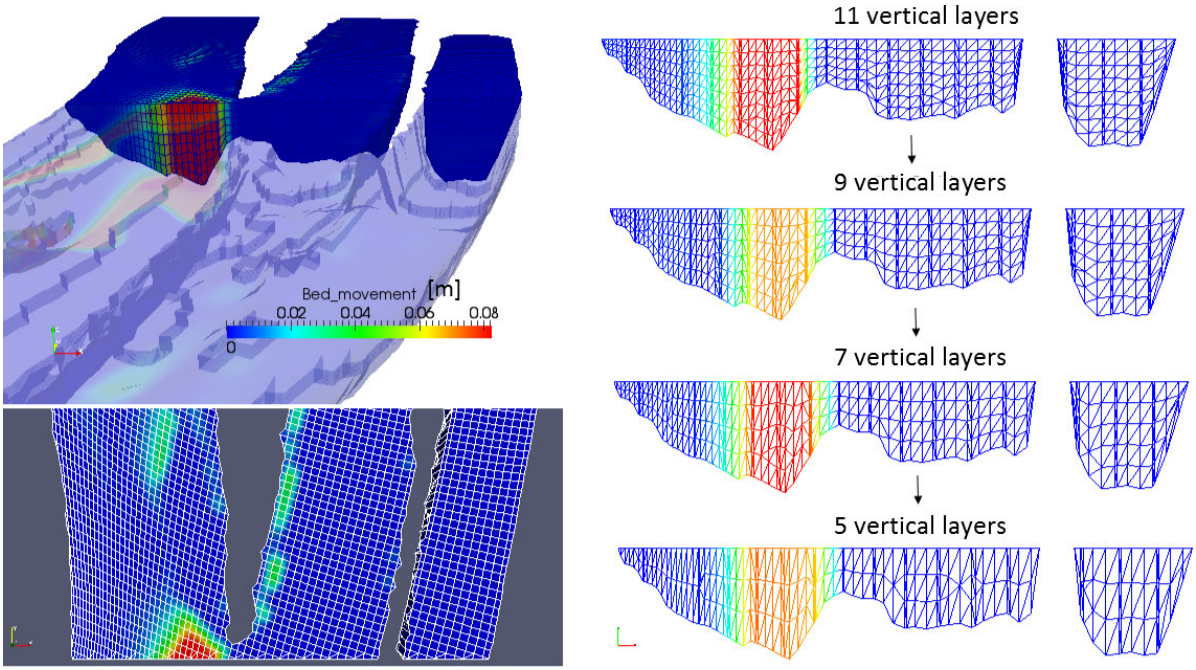

Figure 5.3: Coarsening of the spatial grid resolution (Speckter, 2015).

5.2.2 Coarsening of grid in vertical direction

Three vertical resolutions for grid-2 were analyzed, namely 9, 7 and 5 layers, in addition to 11 layers which were used in the reference grid (see Figure 5.3). The SSIIM model uses a varying number of grid cells in vertical direction. So the numbers give the maximum number of cells defined for each grid. The impacts on both the hydrodynamics and the sediment transport were assessed. The observed cross sections were projected into the two-dimensional plane. They were used to assess the simulated velocity and the sediment concentration profiles.

Impacts on hydrodynamics

Figure 5.4 shows the velocity profile and the average velocity values for all grids and field measurements in three cross sections. The flow velocity varies in the lateral and vertical directions. Comparing the numerical results to the measurements shows that the simulated velocity profiles in the three cross sections achieved a good agreement. Flow velocity is in general at the surface and towards the middle of the channel faster, and slower along the sides and the bottom of the channel because of friction. Low velocities at the left side of cross sections 2-2 and 3-3 appeared due to recirculation zones caused by flow separation at the inner bank of the river and the mole separating weir and turbine channel, respectively. The highest velocities occurred in the channel to the hydropower

station at cross section 3-3.

Mean velocities in all simulations are smaller than the measured values at all cross sections, especially at cross section 2-2, with a deviation of 11 %. However, the comparison of numerical results with measurements based only on average values ignores the variations throughout each cross section. So, average values are only one indicator to facilitate the comparison between the different grid resolutions, besides the variations are also considered in a qualitative way. By comparing the results of all grid resolutions in the vertical directions (see Figure 5.4), there is no significant difference with respect to velocity field between the different vertical resolutions.

Impacts on sediment transport

Figure 5.5 shows the sediment concentrations for all simulations and field measurements. Contrary to the velocity profiles, changing the vertical resolution clearly affects the sediment concentrations, especially when comparing the 11 layers grid with the other grid patterns. The 11 layers grid overestimated the sediment concentration in sections 1-1 and 3-3, while the other grids achieved better agreement with the measured data. However, average values can be misleading as uncertainties in suspended sediment concentration are high near the bottom, where the highest concentrations are observed. The bed change in the study area and the CPU time after 10 simulation days are listed in Table 5.2. The bed change signifies the change of the sediment volume in the study area at the end of the simulation. The bed change error is the ratio of the deviation between the bed change volume for each grid and the reference grid divided by the value of the reference grid. Likewise, the CPU time ratio is the ratio of the CPU time needed for each grid to the CPU time of the high-resolution grid.

Table 5.2 indicates that the net bed change volume in the study area decreases, similar to the decrease in suspended sediment concentration at the cross sections with reduced numbers of vertical layers. Moreover, the CPU time is reduced strongly as well. Using 5 layers achieves the minimum CPU time. However, the error in the bed change is higher than 10 %. Thus, with regard to the accuracy and the efficiency, the grid with 7 layers was chosen for all further investigations. In this case, the deviation in the net deposition is 6 % and only 30 % of the computation time of the reference grid is needed.

Following the spatial assessment, two grid variations are selected and subsequently assessed for varying time steps.

Besides of hydrodynamic time step size and iterations, tests on a grid with a resolution of 301,478 cells and a grid 4 times finer and another one 10 times coarser were

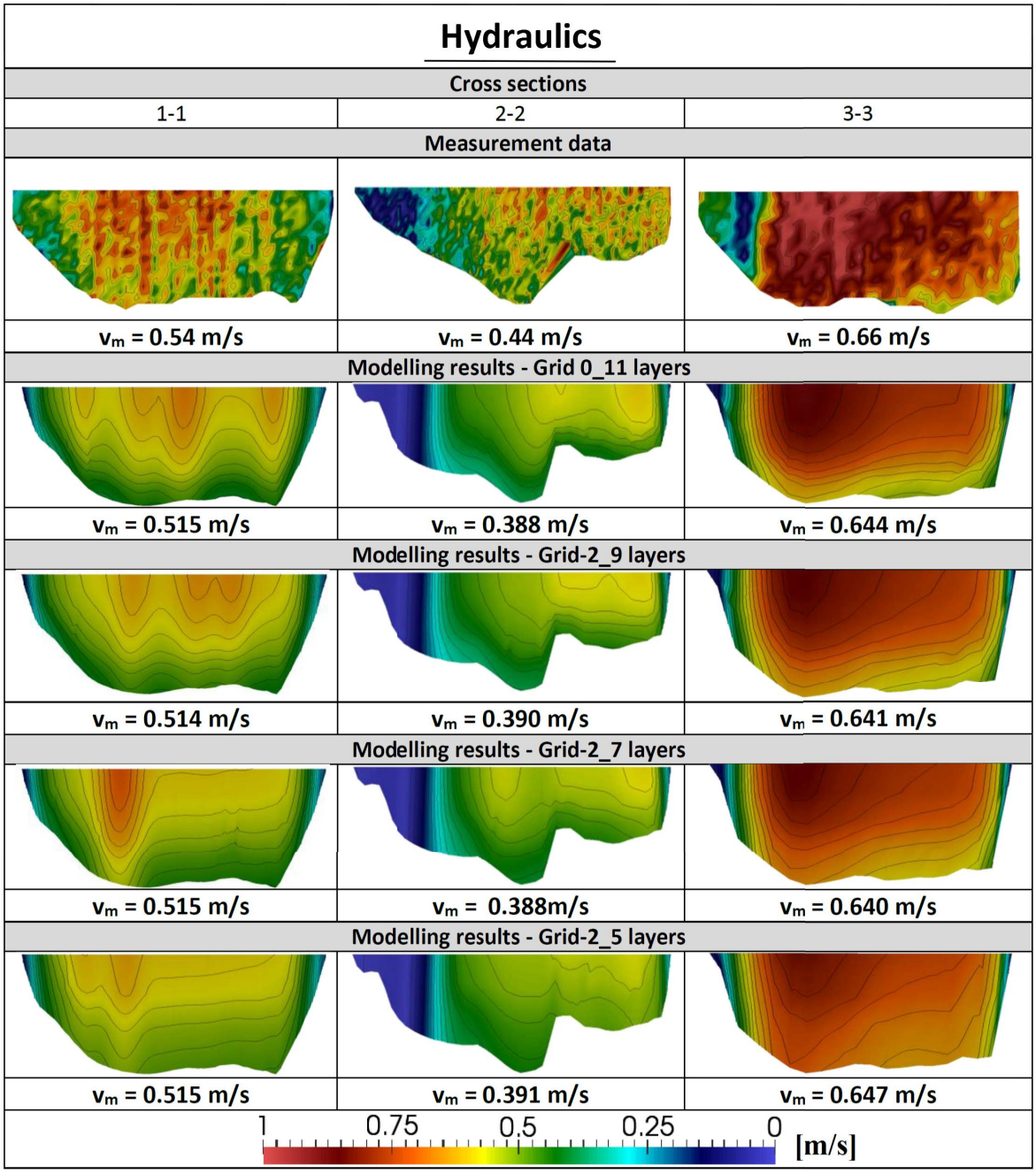

Figure 5.4: Velocity profiles for the field measurements and SSIIM results for 11 layers of reference grid, 9, 7 and 5 layers of coarsened grids for three different cross sections.

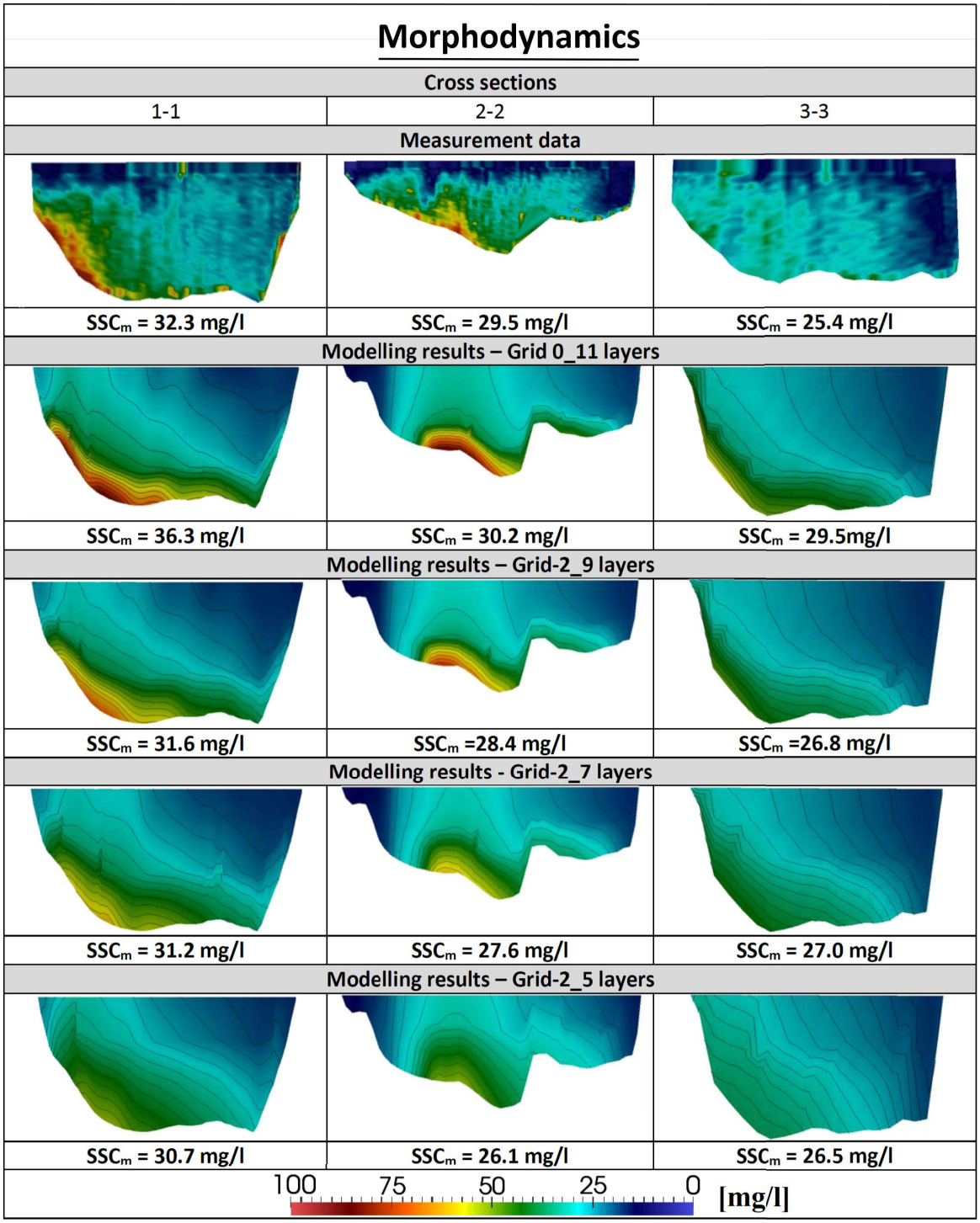

Figure 5.5: Sediment concentration profiles and mean concentrations at all cross sections for all simulations and field measurements.

Table 5.2: Deviation of bed change volume and CPU time expressed by error and ratio values.

Layer	Bed change error [-]	CPU time ratio [-]
11	-0.05	0.43
9	-0.07	0.36
7	-0.06	0.30
5	-0.13	0.23

carried out (Zhang et al., 2013). There are no significant differences in terms of the calculated flow field using a grid with 301,478 cells or a grid with 4 times finer resolution. The grid with a resolution of 301,478 cells is found as suitable for high-resolution simulations, because the secondary flow in the recirculation zone fits the best with the measured data. Moreover, the composition and quality of the grid affect the accuracy and the stability of the solution of the equations.

5.2.3 Temporal coarsening

Impact on hydrodynamics

The purpose of this section is to analyze the impact of the time step on the hydrodynamics and the sediment transport. Therefore, the time step for grid-2 with 7 layers was successively increased from 60 to 100 and then 200 sec. The hydrodynamic results show that the water flow was converging for all time steps. The accuracy was assessed in terms of deviation in the flow velocity. The deviation was calculated as the ratio between average velocity of grid-2 and grid-0. The average value was calculated as an average velocity of 100 random point velocity values in the weir channel (see Table 5.3). The deviation for grid-2 with a time step of 200 sec is 11 %, which is considered to be acceptable in this study, especially when the time saving for the calculation is of 97 %. Thus, a time step of 200 sec can be used instead of 60 sec for the hydrodynamic simulations.

Impact on sediment transport

A quasi-steady transient sediment computation was carried out with different time steps ranging from 60 sec up to 600 sec, whereby the water flow field was not recomputed after an update of the bed. Table 5.4 shows that the deviations of bed change was very small with respect to a varying time step, while the CPU time reduced significantly. For the

Table 5.3: Hydraulic computation: Velocity error and CPU time ratio for grid-0 and grid-2 with 7 layers for different time steps.

Time step [sec]	Grid-0		Grid-2_7	
	Velocity error [-]	CPU time ratio [-]	Velocity error [-]	CPU time ratio [-]
60	-	1.00	0.04	0.13
100	0.09	0.65	0.21	0.08
200	0.05	0.33	0.11	0.03

Table 5.4: Sediment transport computation: Bed change error and CPU time ratio of grid-0 and grid-2 with 7 layers for different time steps.

Time step [sec]	Grid-0		Grid-2_7	
	Bed change error [-]	CPU time ratio [-]	Bed change error [-]	CPU time ratio [-]
60	-	1.00	0.0610	0.30
100	0.0001	0.63	0.0610	0.16
200	0.0002	0.31	0.0610	0.09
300	0.0004	0.21	0.0611	0.07
400	0.0005	0.16	0.0611	0.05
600	0.0007	0.11	0.0613	0.04

coarsened grid-2 with 7 layers the deviation of bed change for a time step of 600 sec compared to the reference grid-0 is 6 %, whereas timesaving is up to 96 %.

It can be concluded that for a transient sediment computation with steady flow the time step can be increased significantly, e.g. to 600 sec.

5.3 Reduction of particle size fractions

The number of grain size fractions was reduced and analyzed using grid-2 with 7 layers. Its impact on the sediment concentration and the bed change volume was investigated. The number of fractions used for the suspended load and the initial riverbed composition (see Figure 5.6) were 9 (reference case), 7 and 5. The detailed classification is shown in Table 5.5. The size class limits were reconsidered and the characteristic sediment diameters for each fraction were calculated afterwards. The settling velocities were obtained using Zanke's equation (see Table 2.3 and subsection 4.4.2). A steady state simulation was carried out. Assuming only small changes in the bed change, an uncou-

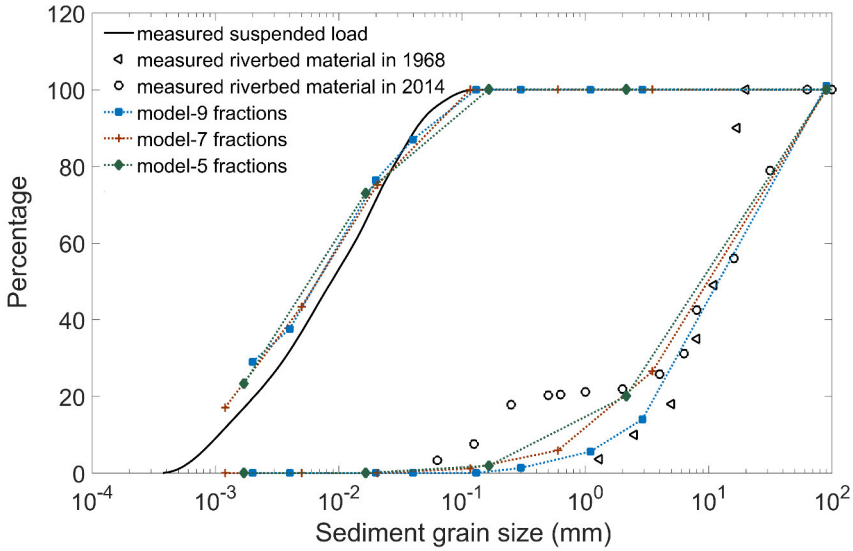

Figure 5.6: Grain size distribution measured for the suspension in 2010 and for the riverbed material in 1968 and 2014. The dashed lines with markers represent the different sediment fractions with the characteristic diameter used in model.

pled simulation of the sediment transport was carried out without recomputation of the hydrodynamics. The numerical results of sediment concentration profile for section 2 were compared with the measurements and the reference grid.

Figure 5.7 shows that the cross section profile with 7 fractions has the highest concentrations, while the concentration profile with 5 fractions has the lowest value. A tendency cannot be determined based on the simulation results. However, the computation with 5 fractions does not provide a good agreement with the measurements. The bed change in the weir channel between Rhine-km 332 to 333.8 is simulated, the numerical results are compared with the measurements. The bed change error, the ratio to the value of the reference grid-0 is applied. Table 5.6 shows that the sediment volume increases by 2 % and 5 % when using 9 and 7 fractions in comparison to the high-resolution model, whereas the computation times are reduced to 30 % and 24 %, respectively. The deviation of the bed change volume in case of 5 grain fractions is 28 %. Using 7 fractions instead of 9 achieved better agreement with the measurements in terms of the deposition pattern (see Figure 5.8), while 5 fractions could not describe the deposition pattern in the weir channel. Considering CPU time and an acceptable accuracy, simulations with 7 fractions can be applied for future studies.

A reduced number of fractions successfully simulates the bed change volume, as well as the sediment distribution in the weir channel.

Table 5.5: Grain size distribution in 9, 7 and 5 fractions.

Mean diameter (mm)	Suspension fractions (%)	Initial bed composition (%)	Settling velocity (cm/s) (Zanke, 1982)
Fraction 9			
0.002	29	0	2.6E-04
0.005	8.6	0	1.6E-03
0.02	38.8	0	2.5E-02
0.04	7.6	0	0.1
0.13	16	0	1
0.4	0	1.3	6.5
1.3	0	2.3	15.1
3	0	8.4	23.9
20	0	88	56.8
Fraction 7			
0.003	17.1	0	4.3E-04
0.005	26.3	0	2.2E-03
0.021	31.8	0	2.5E-02
0.1165	24.8	1.2	1.1
0.6	0	4.7	9.2
3.5	0	20.6	25.9
21	0	73.5	64
Fraction 5			
0.008	23.3	0	6.6E-04
0.0165	49.7	0	1.8E-02
0.165	27.1	1.9	2.1
2.15	0	18.2	20
20	0	80	56.8

Table 5.6: Bed change volume, bed change error and CPU time for stationary simulations.

		Bed change volume [m^3]	Bed change error [-]	CPU ratio time [-]
Measurement		55,050	-	-
Grid-0		59,600	-	-
Grid-2_7	9	60,470	0.02	0.30
	7	62,470	0.05	0.24
	5	42,930	-0.28	0.12

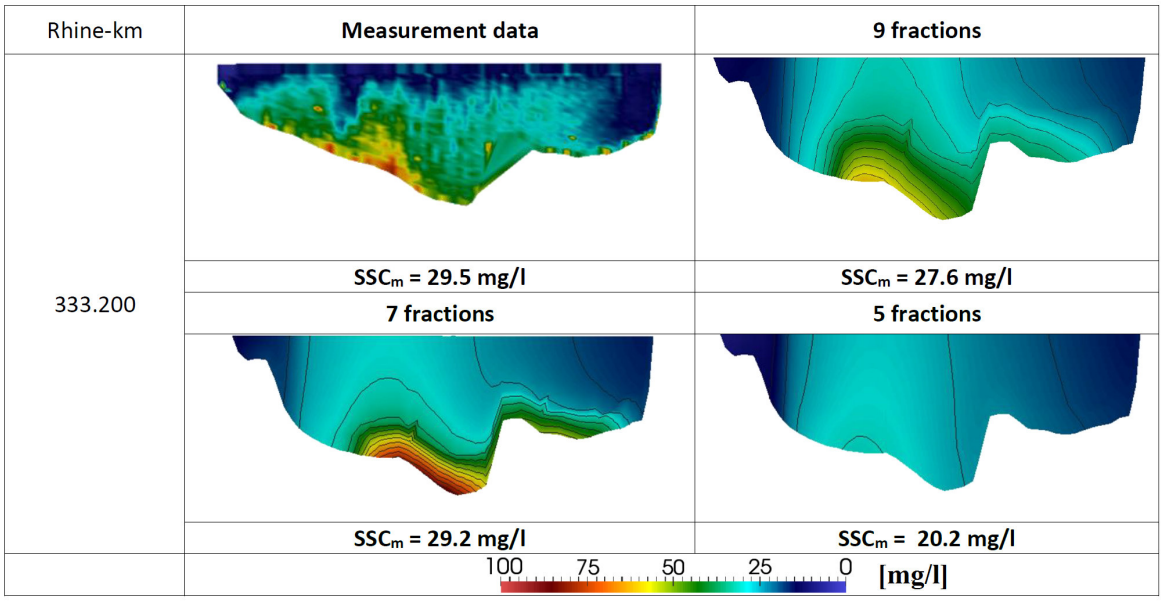

Figure 5.7: Concentration profiles and mean concentrations of cross section 2-2 for different sediment fractions.

It can also be concluded that the assignment of a wide grain size distribution in the case of the River Rhine (only 5 grain size fractions) is not sufficient for a good representation of the particle distribution curve, especially in the case where coarse and also very fine fractions dominate the grain size distribution. The smallest characteristic diameter is increased using the reduced grain size class. It results in an increasing settling velocity, whereby under the same hydraulic condition, more deposition occurs. The highest amount of deposition in case of only 5 size fractions occurs near the upstream boundary of the study area. The flow momentum is not sufficient to transport the sediment material into the weir channel. In the course of this study at least 7 fractions are therefore recommended.

The final assessment of the calculation with unsteady conditions for 105 days shows reasonable results for the two selected coarsened grids in comparison to the measured data. The sediment deposition distribution and the maximum depositions in the weir channel extensively agree with the measured data.

5.4 Summary

In order to assess the long-term morphodynamics of the fine sediment budget in the Iffezheim reservoir, an upscaling approach for a high-resolution numerical model was carried

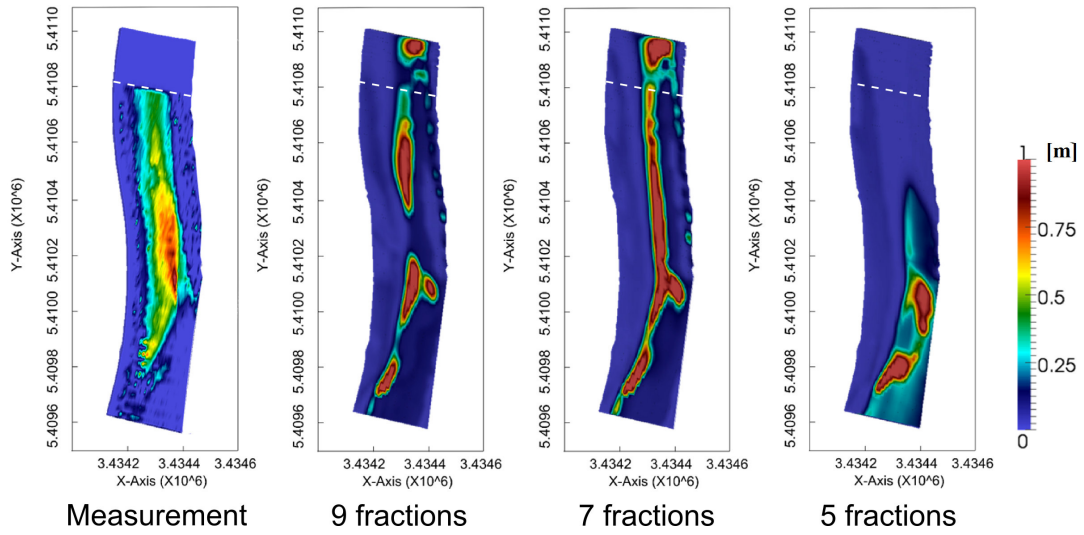

Figure 5.8: Deposition patterns in the weir channel using 9, 7 and 5 fractions, compared with the measurement. The dashed line is at Rhine-km 333.8. It limits the area where the bed change volume is evaluated in the weir channel.

out. The purpose was to optimize the computational time by a coarsened grid, an appropriate time step and a reduced number of fractions, without significantly affecting the results accuracy. The impact of each aspect on the hydrodynamic and morphodynamic processes was investigated.

The results show that considerable reductions of computational effort can be obtained by applying a combination of the coarsening of the grid resolution and the reduction of fractions. The study of the grid coarsening shows that the discretization of the vertical layers has little impact on the hydrodynamics as long as several vertical layers remain. Anyhow vertical grid coarsening has a significant impact on the sediment transport.

Table 5.7: Summarized analysis of the results for a sediment computation with unsteady flow.

	Original	Applied
Number of cells in horizontal directions	90×400	65×275
Vertical layer	11	7
Hydraulic time steps	60	200
Morphodynamic time step	60	200
Sediment fractions	9	7
Bed change error	-	0.05
CPU ratio time	-	0.24

The results is summarized in Table 5.7. A time step of 200 sec can be used for the hydrodynamic simulation and a time step of e.g. 600 sec can be used for a transient sediment computation under the steady state flow conditions. Reducing the number of fractions shows that using less than 7 fractions is not recommended for the simulation of the Iffezheim reservoir (Zhang et al., 2016b).

As a result, a coarse grid, with 40 % less cells than the high-resolution grid and 7 fractions for the sediment grain size distributions provide adequate results in a quarter of computation time when compared with the high-resolution grid (with the hardware used in this study 3:30 instead of 14:30 hours respectively) for 105 days simulation time.

Chapter 6

Classification of upstream boundary conditions

6.1 Introduction

Up to now, most research studies have calculated sediment transport using 3D models (Fischer-Antze et al., 2008; Haun et al., 2013; Jia et al., 2013), but only for relatively short-term periods, not using a fractional sediment transport approach or with just a small number of transport equations. For long-term studies of 3D models, using a fractional sediment transport approach we face limitations regarding computational power. Besides of the method of model reduction, described in chapter 5, upscaling of numerical models becomes urgently necessary.

In this chapter, a reduced complexity approach called "classification of boundary conditions of discharges and suspended sediment concentrations" was developed for a long-term numerical simulation. The purpose of this upscaling approach was to determine the long-term riverbed evolution in the Iffezheim reservoir much faster but with only small loss of accuracy compared to the conventional instationary simulations using 3D high-resolution model, which was set up in the Iffezheim reservoir for investigating sediment transport processes and the short-term volume change in the weir channel in the previous Chapter 4.

The field data relating to bathymetry, discharge and suspended sediment concentration between July 2000 and February 2011 are used in this research and have been presented in Figure 3.9 and in Table 3.4 in chapter 3 Field data and statistics. Discharge data during the period are illustrated by red lines in the hydrograph in Figure 3.9 and the concentration of suspended load is in black. The design capacity of the hydro-power plant up to 2013 was 1100 m^3/s. On average, the discharge is below this value for about

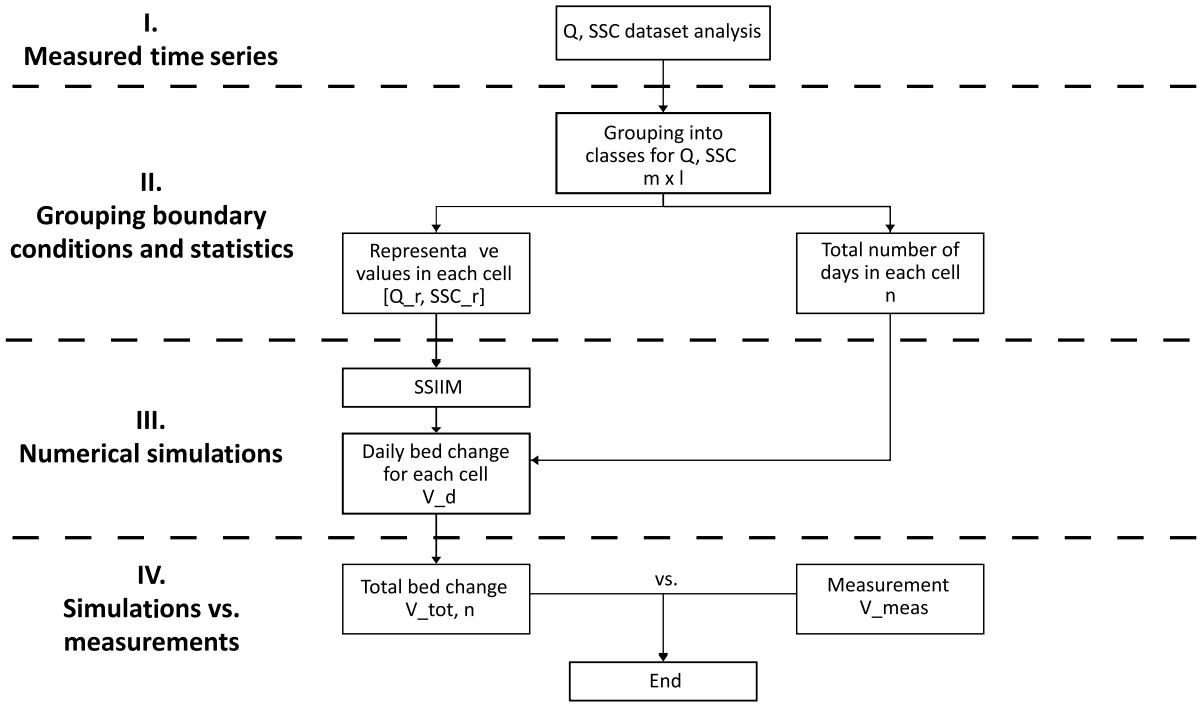

Figure 6.1: Flowchart of classification boundary conditions.

183 days per year, and there is no flow through the weir. For the period when the discharge exceeds this value the mean flow is about 1550 m^3/s. During the period under investigation, the maximum value of a flood discharge was 4170 m^3/s, which was measured on 10/08/2007. The sediment concentration data are shown as well. Thirty-seven sets of echo sounding data relating to 36 periods were used in this research. Each period is called a short-term period. Several short-term periods form a long-term period.

6.2 Concept

The basic idea of **upscaling approach** of this chapter is to replace instationary simulations of the riverbed volume change by a series of stationary ones. The flowchart in Figure 6.1 shows the concept of the upscaling approach based on classification of boundary conditions. This method consists of four steps described below.

Generally, the boundary conditions - measured water discharges and measured sediment concentrations - represent a very wide range of values. Thus, in the first step, the range of the values is considered and subdivided into classes of equal sizes for the discharges and the sediment concentrations resulting in a raster consisting of cells (see Figure 6.2).

In the second step, for each cell, the median values of Q and SSC are determined. These values are then used as representative values for that cell [Q_r, SSC_r] (see Equation 6.1 and Equation 6.2).

$$Q_r = \frac{\sum_{i=1}^{n} Q_i}{n} \tag{6.1}$$

$$SSC_r = \frac{\sum_{i=1}^{n} SSC_i}{n} \tag{6.2}$$

Q_i is the average daily discharge and SSC_i is the average daily suspended sediment concentration, n is the number of daily measurements for each cell.

In the third step, stationary simulations are performed applying the 3D high-resolution numerical model SSIIM using fractional sediment transport with 9 transport equations to simulate the daily volume change on the riverbed with the calculated representative values [Q_r, SSC_r] for each cell used as stationary boundary conditions. In order to prepare stable initial conditions, a calculation time of two days for water flow and five days for sediment transport simulations are carried out. The simulations with the stationary boundary conditions are running against quasi steady state. The simulated daily volume changes and the number of daily measurements for each cell are then multiplied to obtain the total volume change contributing from that cell. The total volume change for a certain period is then obtained by summing up the simulated values of all the cells.

In the fourth step, the simulated results are compared to the measurements.

Procedure and data preparation

In this section, the application of the upscaling approach based on the field data in case of Iffezheim reservoir is described.

The approach is applied to 10 short-term and 2 long-term periods. The investigated periods are selected between two echo sounding periods without dredging events. This is done because the bathymetry changes after dredging. This in turn changes the hydraulic conditions and potentially affects the deposition rate in the reservoir. The short-term periods are chosen between two successive echo sounding measurements to investigate the average flow conditions. Thus, short-term periods with strong flood events, i.e. with high erosion and high deposition rates, were excluded, as our approach is a too strong simplification for extreme events. The short-term periods 3, 4, 5, 6, 7, 8, 22, 23, 24, 29 met these criteria (see Table 3.4).

Figure 6.2 gives an example of the application of the approach for the longest time period (19-36). Figure 6.2a shows the distribution of the discharge and concentration

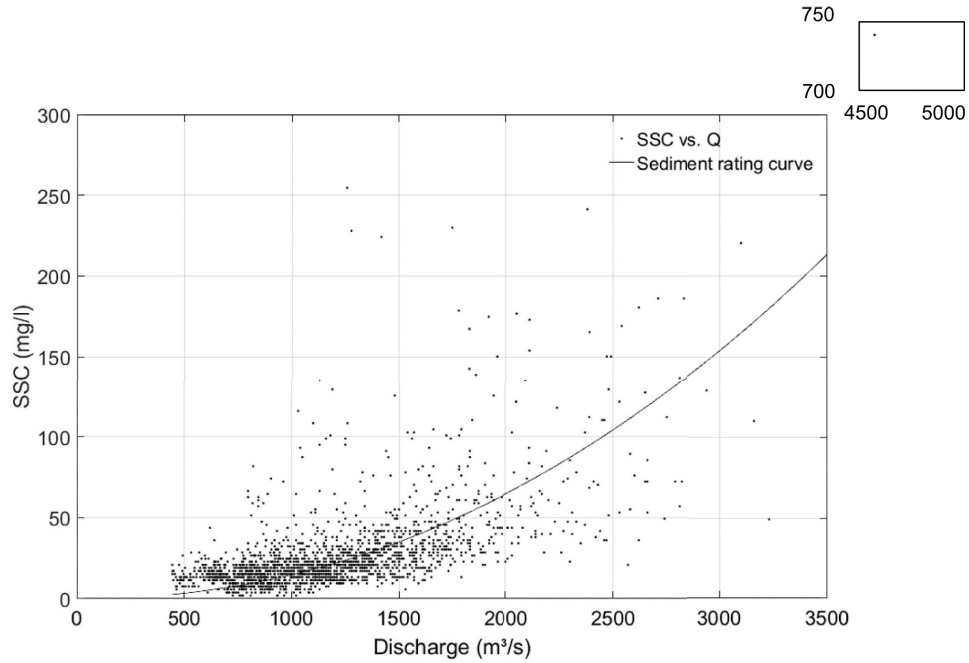

(a) Q, SSC data set analysis and determination of class sizes.

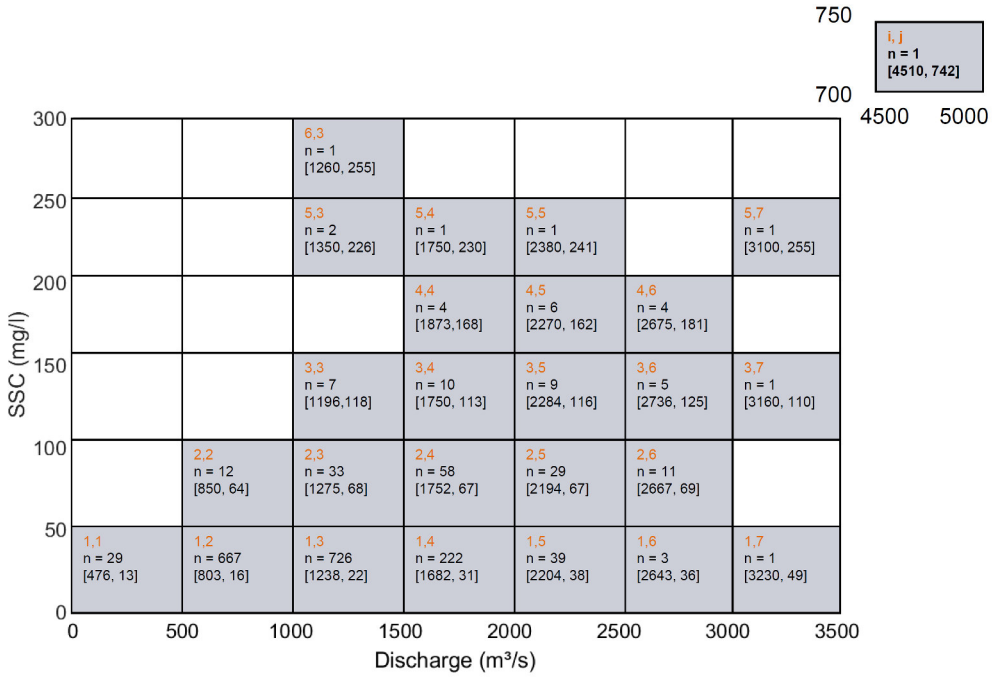

(b) Boundary conditions classification and representative Q and SSC calculation. i, j, index of cell, n: total number of days in this cell, bracket left: Q_r, bracket right: SSC_r.

Figure 6.2: Field data of boundary conditions of Iffezheim model from December 2005 to February 2011, accordingly the long-term period 19-36 (see Table 3.4). An extreme value is shown separately.

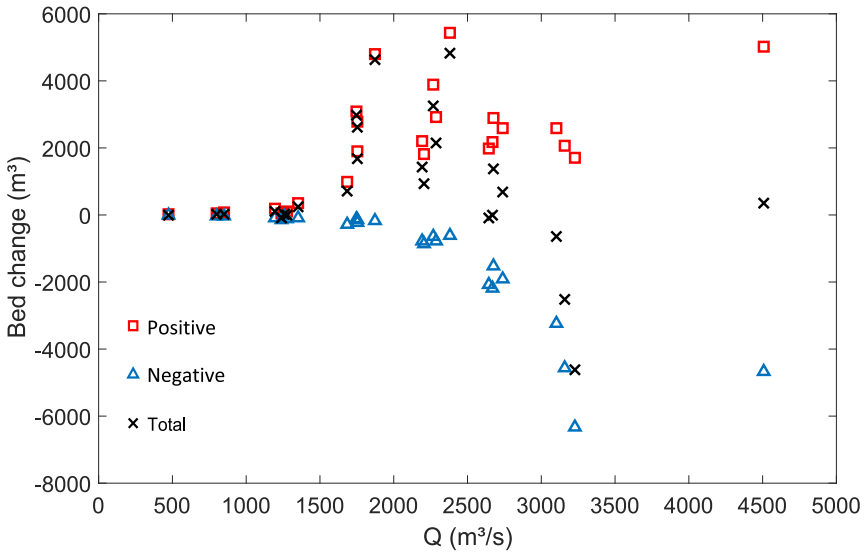

Figure 6.3: Discharge-sediment volume change with all the calculated boundary conditions of Figure 6.2.

values. The class sizes for the discharge and SSC was chosen as ΔQ = 500 m^3/s and ΔSSC = 50 mg/l (see Figure 6.2a). An extreme value of flooding event was detected far outside the specified class. The choice of the class sizes is important to make sure that the computation time stays within practical limits. In Figure 6.2, all values are classified into cells, which are marked with grey area. A representative discharge Q_r and a representative concentration SSC_r were calculated for each cell, with which the stationary simulation was carried out to obtain the daily volume change. Our approach covers much more combinations of Q and SSC when compared to using the sediment rating curve (see Figure 6.2).

6.3 Application to short-term and long-term time periods

6.3.1 Application to the longest time period

The simulated volume change deviations with their respective boundary conditions discharge and concentration for this time period (19-36) are shown in Figure 6.4. The Figures 6.4a to 6.4e show the relationship between discharge and sediment volume change in the riverbed for different concentration ranges up to 250 mg/l during the period of investigation. The concentration ranges are divided into 50 mg/l steps. In Figure 6.4f, a

Table 6.1: Comparison of simulated daily total volume changes with the measurements for short and long-term period.

	short-term									
Period	3	4	5	6	7	8	22	23	24	29
Deviation	+1 %	+285 %	-101 %	-37 %	-27 %	-27 %	+9 %	-110 %	-37 %	-5 %
	long-term									
Period	3-8	19-36								
Deviation	-3 %	+20 %								

higher concentration value between 251-300 mg/l and the extreme value are presented.

An overview of all the simulation results is given in Figure 6.3. It emphasizes that the volume change firstly increases with a growing discharge till it reaches its maximum at approximately 2000 m^3/s and then decreases again. With the extreme value a rather average volume change of 360 m^3 per day was calculated. This flood event brought a high sediment input, but almost as much sediment had been removed by the large flow rate. The highest volume change in this longest time period is located at 5500 m^3 per day with the boundary conditions Q = 2300 m^3/s and SSC = 241 mg/l (see Figure 6.4e).

6.3.2 Application to all time periods

Figure 6.5 and Table 6.1 show a comparison of the simulated daily total volume changes with the measurements for all applied short- and long-term periods described in subsection 6.2. The results for the daily volume change for the short-term period show large variations; they are between +1 % (period 3) and +285 % (period 4). In comparison, the daily volume change of the two longer periods show only small deviations compared to the measurements. The deviations are +3 % (period 3-8) and +20 % (period 19-36). The simulation results for the long-term periods show much less deviations from the measurements than the shorter ones. This is explained by the circumstance that long-term periods include some averaging behavior regarding extreme events.

Additionally, the comparison of simulated positive, negative and total volume changes with the measurements is presented in Figure 6.6. The abscissa represents the length of the time period in days, whereas the ordinate indicates the proportional variation between the measurements and simulation results. The figure indicates that the simulated positive volume changes have a very good agreement with the measurements. Although the simulated negative bed changes tended to differ a lot from measurements, no large deviations between the simulated and the measured total volume changes occurred be-

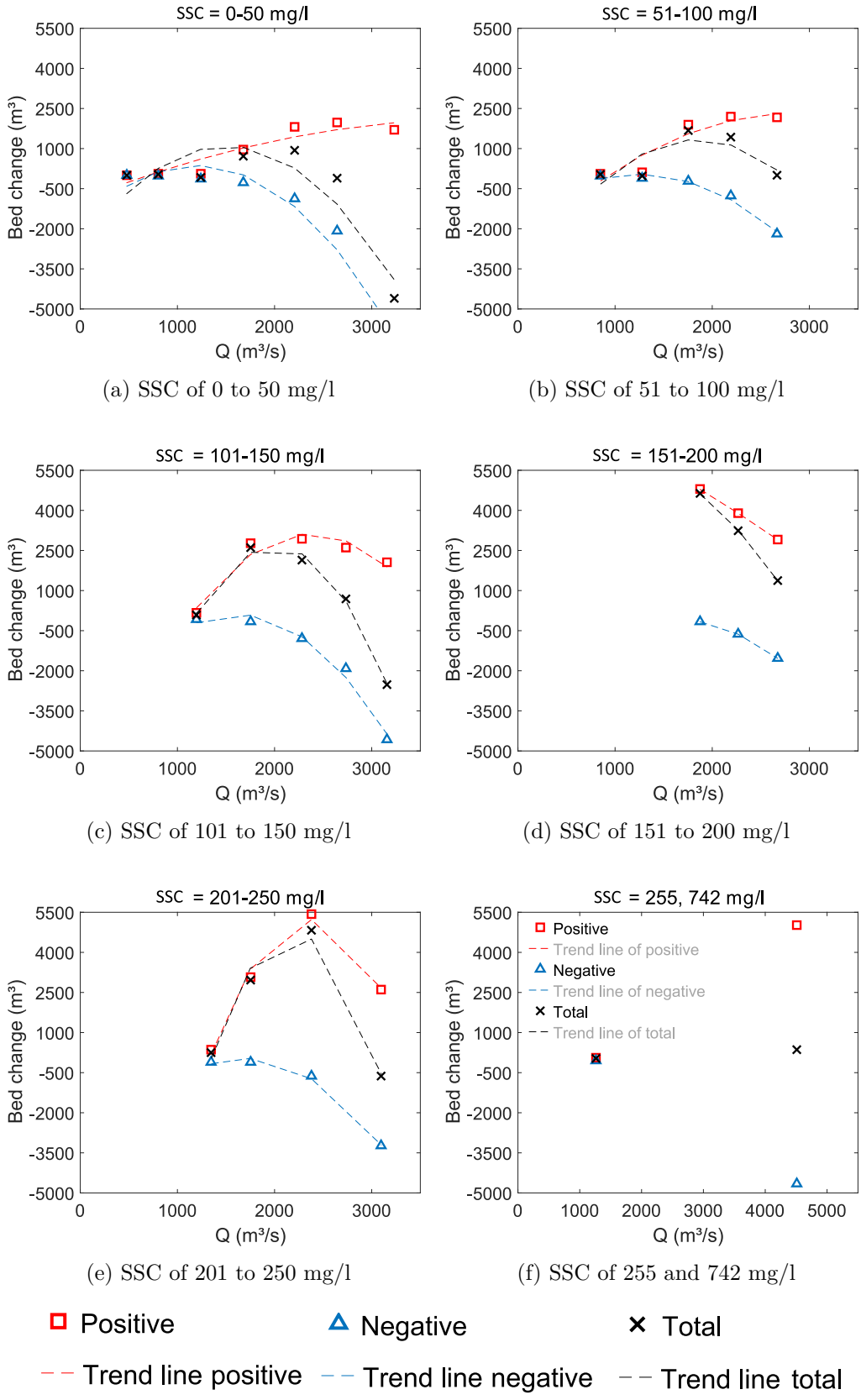

(a) SSC of 0 to 50 mg/l

(b) SSC of 51 to 100 mg/l

(c) SSC of 101 to 150 mg/l

(d) SSC of 151 to 200 mg/l

(e) SSC of 201 to 250 mg/l

(f) SSC of 255 and 742 mg/l

Figure 6.4: Discharge - bed volume change for different concentration bandwidths (see Figure 6.2).

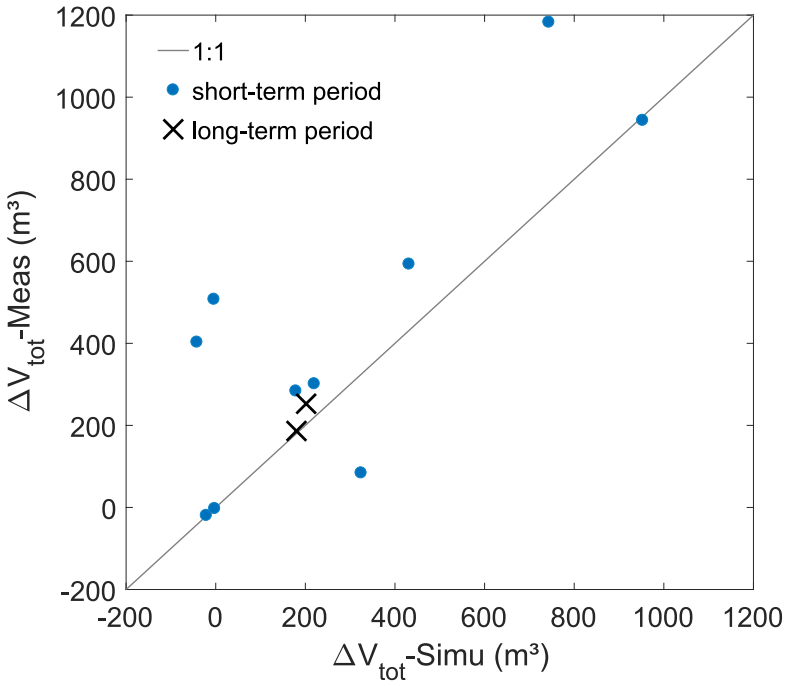

Figure 6.5: Comparison of simulated averaged daily total volume changes with the measurements for short- and long-term periods.

cause the absolute volume changes of the positive (deposition) were much bigger than the negative ones (erosion).

Finally, this simplified method showed clear savings in computational time, running 97 % faster than the instationary simulations. In this case only three hours of computation time were needed for a five-year simulation period using the reference computer mentioned before, while the instationary sediment transport calculation would require approx. 85 hours of computational time. Therefore, the developed approach is very suitable for a long-term simulation of riverbed evolution in the Iffezheim reservoir.

6.4 Impact of applying error coefficients

If large deviations are found during the comparison between the simulated results and the measurements, as presented in the fourth step of the concept (see Figure 6.1), various methods for estimating an error correction factor can be applied, e.g. linear distribution, weighted least-squares and unweighted least-squares methods. In this chapter, the weighted linear distribution is used. The error coefficient $coef_{i,j}$ in each cell (i, j) is obtained by a weighted function to fit the deviation of simulated amount of all cells and

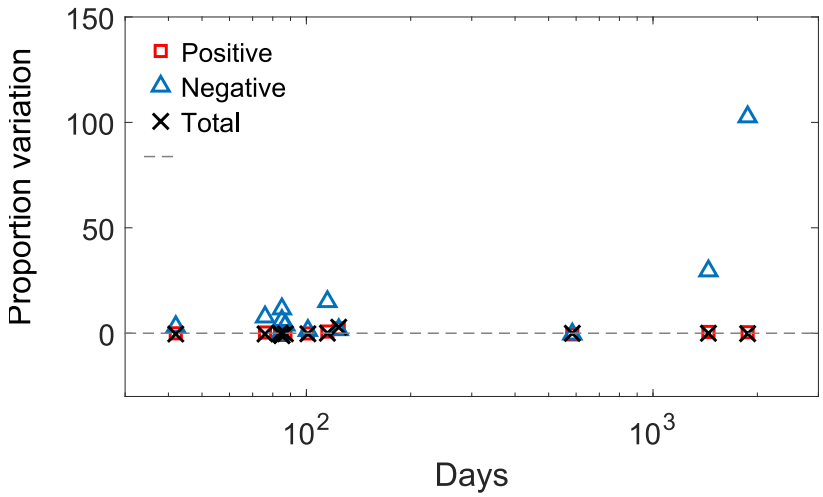

Figure 6.6: Comparison of the simulated results of deposition, erosion and total volume change with the measurements.

the measurement (see equations 6.3, 6.4 and 6.5).

$$coef_{i,j} = \frac{e_{i,j}}{v_{sd,i,j} + e_{i,j}} \tag{6.3}$$

$$e_{i,j} = \frac{w_{i,j} \cdot n_{i,j}}{\sum_{i=1,j=1}^{i=m,j=l} w_{ij} \cdot n_{ij}} \cdot (v_{sp} - v_{mp}) \tag{6.4}$$

$$w_{i,j} = \frac{Q_{r,i,j} \cdot SSC_{r,ij}}{\sum_{i=1,j=1}^{i=m,j=l} Q_{r,i,j} \cdot SSC_{r,i,j}} \tag{6.5}$$

with i and j are indexes of the cell (see Figure 6.2). $e_{i,j}$ is the corrected volume change of each cell. $v_{sd,i,j}$ is the simulated daily volume change of each cell. v_{sp} is the amount of simulated volume change in the investigation period, while v_{mp} is the measured volume change. m, l are maximum indexes of the cell in horizontal and vertical axis (see Figure 6.1), n_{ij} is the total number of days in each cell.

In order to cover a large bandwidth of the existing data for determination of error correction factors, the longest possible time period should be applied. The obtained error correction factors can be transferred to other time periods. In this chapter, error correction factors of each cell are calculated based on the total volume change within the longest time period (19-36) (see Figure 6.2). In Figure 6.7 results of all periods are compared with and without error correction. The abscissa shows the simulated total

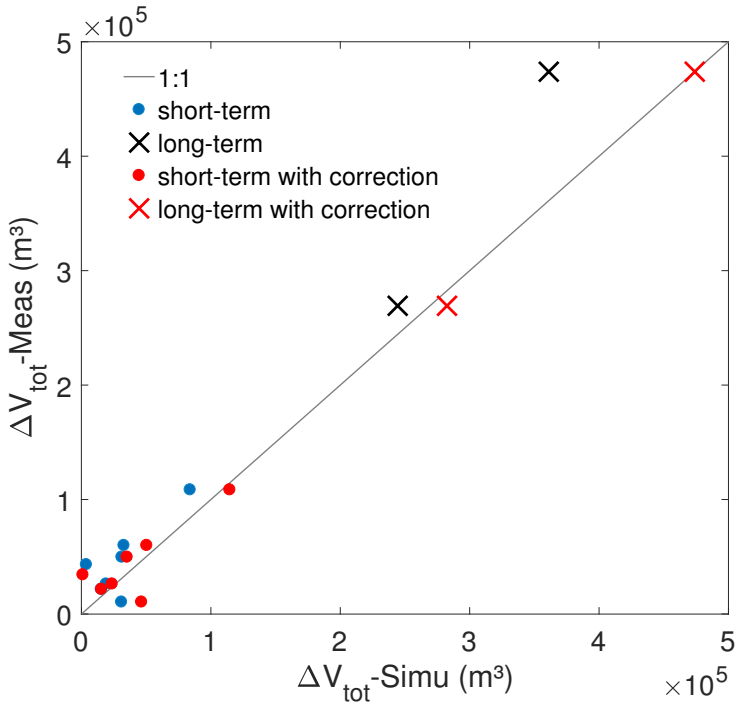

Figure 6.7: Comparison of simulation results with measured data, with and without error coefficients for all time periods.

volume change, and the measurements are plotted on the ordinate. The results with the error coefficient are displayed in red. By using the error coefficients, the calculated volume changes are always magnified, so that the simulation results are only shifted in one direction. Therefore, the error coefficients have an increasing influence, because the simulated changes in volume become smaller than the measurement data. In the case of the Iffezheim reservoir, the application of the error coefficients did not bring a significant improvement, since there was no clear trend in the simulation results of the different time periods, i.e. the simulation results provided sometimes larger and sometimes smaller volume changes compared to the measurements. Therefore, they were not further considered. Other error correction methods (e.g. based on least squares) also did not improve the results.

6.5 Summary

In this chapter, an upscaling approach based on classification of boundary conditions for discharges and suspended sediment concentrations was developed for a long-term numerical simulation. The basic idea of the approach was to replace instationary si-

mulations for modelling the volume change in the riverbed by precalculated series of simulations with stationary boundary conditions. The numerical simulation was carried out using the 3D SSIIM model based on a high spatial-resolution model for the Iffezheim reservoir. The measured time series of discharge and suspended sediment concentration at the gauge station Plittersdorf and the echo sounding bathymetry data in the weir channel of the Iffezheim reservoir for the period between July 2000 and January 2011 are the basis of the study.

This approach was applied to 10 short-term periods, each between two successive echo sounding measurements, and two longer ones, which included several short-term periods. Short-term periods were from one to three months, whereas long-term periods were two and five years. The simulation results showed an acceptable agreement with the measurements for the long-term periods with +3 % and +20 % deviations, while for the short-term periods the deviations were between +1 % and +285 %. The application of the error coefficients did not lead to a significant improvement of the results in the case of the Iffezheim reservoir.

Additionally, this upscaling approach exhibited clear savings in computational time compared to the instationary simulations (of 97 %). The results are promising, suggesting that the developed approach is very suitable for a long-term simulations of riverbed evolution in the Iffezheim reservoir. Future work in chapter 9 will deal with applying the developed approach till the year 2100.

Chapter 7

Time-series analysis and synthesis

7.1 Long-term forecasting using time-series analysis and synthesis

In order to predict the long-term evolution of fine sediment budget in the Iffezheim reservoir, the methods for direct target, i.e., the total volume change and intermediate objectives, e.g. the boundary conditions of numerical model - discharge and suspended sediment concentration, are employed in this investigation. Using the numerical model comprehensively introduced in chapter 5, the quantity of riverbed volume changes and positions of riverbed changes can be simulated for a short-term period. Using the approach described in chapter 6, the riverbed changes, primarily the quantity, can be determined for long-term periods. For both of the above mentioned methods, boundary conditions are required. Some examples of these conditions include daily values of discharges and suspended sediment concentrations. In the case that information regarding long-term boundary condition is unavailable, e.g. when the daily discharges from a KLIWAS project would not be available, stochastic forecasting models based on time-series analysis and synthesis may be applied in order to compute the boundary conditions.

In time series analysis it is assumed that the data consist of a systematic pattern and random noise. The systematic pattern can be described in terms of two basic classes of components: trend and seasonality. The trend represents a general systematic linear or non-linear component that is most often applied. The non-linear component changes over time. The seasonality may have a similar nature, but it repeats itself in systematic intervals over time, e.g. year cycle, season cycle (Janhabi and Ramakar, 2013; Yousif et al., 2016). The trend and seasonality are filtered out from the historical time series. The remaining time series is used to generate synthetic time series for a desired

length. The first step in this generation is the statistical evaluation of measurements by determining the mean value, the standard deviation and the skewness. Depending on the chosen model, different statistical parameters are computed. The noise is described by a statistical function or random component. To establish the synthetic time series, the observed values are used in the calibration phase as well as in the validation phase. At the phase of assessing the validation, it is notable that the result of each simulation merely represents one possible future scenario.

However, it should be noticed that in the application of many of those models, a great number of model parameters is a typical difficulty, e.g., for calculating the monthly flow, the calculation formula of the Fiering model considers the mean value, produces a relation to the previous month and includes a random component. The number of those model parameters should be kept low so that the sum of used parameters does not exceed an experience value (Maniak, 1997). For this reason this approach is rarely used for short time steps, e.g. daily. Therefore, in this study, the time series analysis and synthesis is applied only for monthly values.

The development of time series analysis techniques for prediction of monthly discharge began in the 1960th by introducing auto-regression (AR) modeling (Thomas and Fiering, 1962). AR models are applied under the assumption of a linear relation between the discharge within the regarded time and the past time. Thereby, the linear regression coefficient is the parameter of the AR model. Such a linear model, which also includes the annual periodicity, is the Fiering model. The memory of this model can be prolonged during a auto-regressive model around a term of moving average (MA). The resulting model is an ARMA model, consisting of AR and MA model. The primary difference between AR and MA model is the correlation between time series objects at different points of time. The AR model has a lasting effect of a shock while in MA model, shock quickly vanishes with time. A series which has to be made stationary by differencing is an "integrated" (I) series. This model is called Auto-Regressive Integrated Moving Average (ARIMA) model.

Due to the fact that most natural phenomena occurring in environmental systems seem to behave in random or probabilistic ways, different cases may need a different forecast method and even a unique treatment to improve the forecast accuracy. The present chapter exclusively deals with a time series forecasting model and aims to determine an appropriate model for forecasting monthly inflow to the Iffezheim reservoir. Fiering model, multivariate non-linear model and ARIMA model are investigated. These monthly discharge data can be used for assessing the monthly volume change in the reservoir.

The past discharge records with equally spaced time intervals between 1946-2013

from continuous records were used as inputs. The monthly values are calculated from average daily flows, which are derived from continuous measurements recorded every 15 minutes. The calibration period is 1946-2008, while the validation period is 2009-2013.

7.2 Methods

7.2.1 Fiering model

Fiering model is a linear model and allows for the non-stationary processes[1], e.g. measured monthly discharge values. The model is capable to consider the periodic processes, only the trend should be eliminated from the time series. The remaining time series and the residual in the time series can be then simulated. Afterwards, the simulated values are converted by including the trend. The formula describing the monthly discharges is as follows:

$$q_{i,j} = \bar{q_j} + \frac{r_j s_j}{s_{j-1}}(q_{i,j-1} - \overline{q_{j-1}}) + t_{i,j} \cdot s_j \sqrt{(1 - r_j^2)}^{1/2} \tag{7.1}$$

where

- $q_{i,\,j}$ is the discharge for months j in the year i,
- $\overline{q_j}$ is observed mean variable for months j,
- r_j is observed correlation coefficient between q_j and q_{j-1},
- s_j is observed standard deviation of flow for month j,
- $b_j = \frac{r_j s_j}{s_{j-1}}$ is observed regression coefficient,
- $t_{i,\,j}$ is a random value in year i and month j, with $\bar{t} = 0$ and $s_t = 1$.

The calculation formula considers mean value, produces a relation to the previous month and includes a random part. The Fiering model is hardly used for shorter time steps, since a large number of parameters should be estimated. If the time step is too short, standard deviation (s), variance (s^2), and the skewness (c_s) for the current time step may be extremely large, which would lead to an inaccuracy in the next time step. In addition, the creation of the model has to contain a sufficient amount of data. Maniak (1997) suggested a criterion: $m \leq N/20$, where N is the number of measurements and

[1] As opposed to stationary, a non-stationary process is one whose statistical properties change over time.

m is the number of coefficients, so that the prediction of monthly discharge should at least utilize 60 years of historical data.

7.2.2 Multivariate non-linear regression model

Non-linear regression techniques often use time series analysis methods. The assumption of multivariate non-linear regression (MNLR) models is that the relationship between the dependent variable y and the regression x is non-linear. The periodic processes, e.g. monthly discharge, can theoretically be approximated using a sum of a sine wave function and a Fourier transform function. In this study, both methods are investigated and compared in their ability to give a better fit for the monthly discharge data.

Sum of sine wave function:

$$y = \sum_{i=1}^{n} a_i sin(b_i x + c_i) \tag{7.2}$$

where a_i, b_i are regression coefficients and c_i is constant value, i=1, ..., n is the order of function.

Fourier transform function:

$$y = a_0 + \sum_{i=1}^{n} (a_i cos(i \cdot x \cdot w)) + b_i sin(i \cdot x \cdot w)) \tag{7.3}$$

where a_0 and w are constant values. a_i, b_i are regression coefficients and i=1, ..., n is the order of function.

7.2.3 ARIMA model

The ARIMA model is an important forecasting tool and it is sometimes called Box-Jenkins model. The basic idea in modeling time series using ARIMA is the identification of a simple model with the lowest possible number of model parameters in order to provide a good statistical fit to the data.

An iterative four-stage process, i.e. identification, parameter estimation, diagnostic checking and forecasting, is required to determine the adequacy of the proposed model. First, in the identification step, data transformation has to make the time series stationary, which implicates that the mean value and the variance of the series are constant and an auto-covariance should not depend on time. To check the stationary of the time series, Dickey-Fuller test (Dickey, 1976), Brockwell and Davis (Brockwell and Davis, 1987) and Maximum entropy method (Burg, 1967) are commonly used. For

stationarizing a time series, methods, e.g. detrending, differencing, seasonality and power transforming etc., can be applied. Secondly, after specifying a model, estimating the model parameters is straightforward. Box and Jenkins proposed to use the autocorrelation function and the partial autocorrelation function of the data sample as the basic tools to determine whether lags of the stationarized series or lags of the forecast errors should be included in the forecasting equation, and to find optimal parameters and identify the optimal order of the ARIMA model. The parameters are estimated such that an overall measure of errors is minimized. This can be done with a non-linear optimization procedure (Zhang, 2003), such as the Akaike information criterion (AIC), which is utilized to enhance this flexible approach to set up the model. Thirdly, the diagnostic checking is applied to test whether the model assumptions about the errors, ε_t, are satisfied. Bayesian information criterion is used here to examine the goodness of fit of the predicted data to the historical data. In case of inadequate performance, a new tentative model should be identified. The above mentioned three-stage process is typically repeated several times until a satisfactory model is found. Finally, this can be used for prediction purposes (Zhang et al., 2017).

The seasonal autoregressive integrated moving average $(p,\, d,\, q) \times (P,\, D,\, Q)_s$ model is expressed as follows:

$$\begin{aligned}(1 - \Phi_1 B^s - \Phi_2 B^{2s} - ... - \Phi_p B^{Ps})(1 - \varphi_1 B - \varphi_2 B^2 - ... - \varphi_p B^p)(1 - B^s)^D (1 - B)^d Z_t \\ = (1 - \Theta_1 B^s - \Theta_2 B^{2s} - ... - \Theta_Q B^{Qs})(1 - \theta_1 B - \theta_2 B^2 - ... - \theta_q B^q)\varepsilon_t \quad (7.4)\end{aligned}$$

where ε_t is the random variable, s denotes the seasonal period (12 month in this study), B is the difference operator as $B(Z_t) = Z_{t-1}$, Z_t is the stationary time series. $(1 - B^s)^D$ is the D^{th} seasonal difference measure s, $d = (1 - B)^d$ is the d^{th} non-seasonal difference, p and q are integers and referred to the orders of non-seasonal autoregressive and moving average terms, respectively. P and Q are the seasonal autoregressive and moving average terms, respectively. d and D are the order of differencing for the regular and seasonal part; Φ is the parameter of seasonal autoregressive model, φ is the parameter of non-seasonal autoregressive model, Θ is the seasonal moving average model, and θ is the parameter of non-seasonal moving average model (Karamouz and Araghineja, 2012; Valipour et al., 2013).

The number of ARIMA model parameters are determined by performing Auto Correlation Function (ACF) and Partial Auto Correlation Function (PACF) curves (Aljoumani et al., 2012; Valipour et al., 2013).

7.2.4 Evaluation of models

Many performance evaluations can be applied to assess the accuracy of the developed model, such as root mean square error (RMSE), correlation coefficient (R), sum of square error, mean bias error (MBE) and coefficient of determination (DC), which is also called R^2 or Nash Sutcliffe coefficient. Legates and McCabe Jr. (1999) found out that correlation coefficient is unsuitable for evaluation of statistical models. Hence, the RMSE, MBE and DC were used here.

$$RMSE = \sqrt{\frac{\sum_{i=1}^{N}(O_{obs_i} - O_{com_i})^2}{N}} \tag{7.5}$$

$$R = \frac{\sum_{i=1}^{N}(O_{com_i} - \overline{O_{com}}) \cdot (O_{obs_i} - \overline{O_{obs}})}{\sqrt{\sum_{i=1}^{N}(O_{com_i} - \overline{O_{com}})^2 \sum_{i=1}^{N}(O_{obs_i} - \overline{O_{obs}})^2}} \tag{7.6}$$

$$MBE = \frac{\sum_{i=1}^{N}(O_{obs_i} - O_{com_i})}{N} \tag{7.7}$$

$$DC = 1 - \frac{\sum_{i=1}^{N}(O_{obs_i} - O_{com_i})^2}{\sum_{i=1}^{N}(O_{obs_i} - \overline{O_{obs}})^2} \tag{7.8}$$

where N, O_{obs}, O_{com} and $\overline{O_{obs}}$ are number of observations, observed data, computed values and mean of observed data, respectively.

RMSE, MBE and DC provide different types of information about the predictive capabilities of the model. RMSE is utilized to measure forecast exactness, which gives a positive value by squaring the errors. The RMSE value decreases from large positive values for poor performance to zero for perfect forecasts. MBE yields a more balanced perspective of the goodness of fit at moderate values (Karunanithi et al., 1994). The DC introduced by Nash and Sutcliffe (1970) measures the agreement between the observed and forecast data using regression line. This indicates how close the points are to the bisector in the scatter plot of two variables. The DC value has a range of minus infinity to 1, declaring perfect agreement. DC could only be negative when the chosen model does not follow the trend of the data. Small values for RMSE and MBE and high values for DC (up to one) show a high model efficiency.

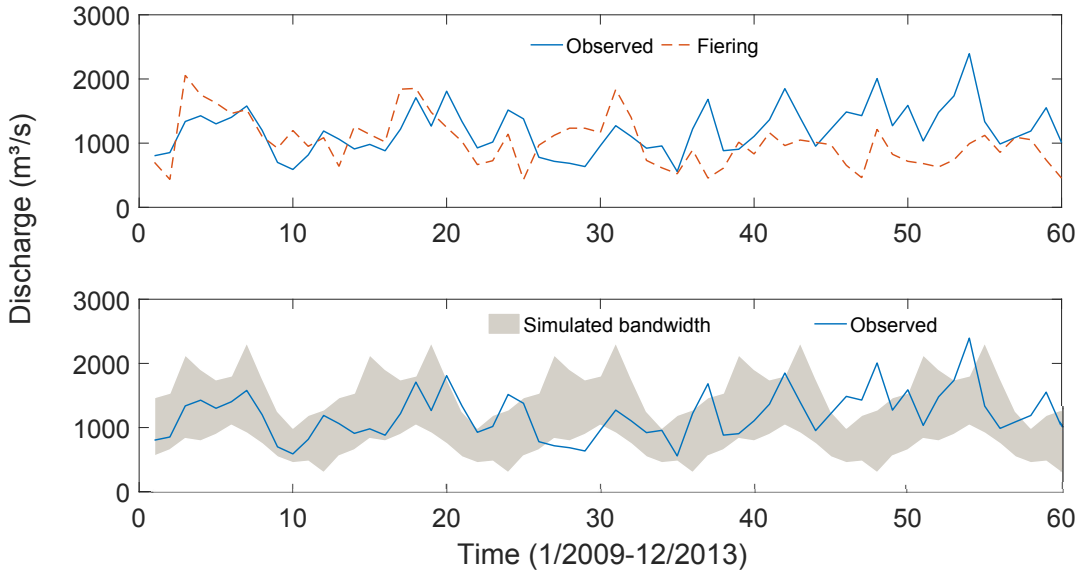

Figure 7.1: Results obtained from Fiering model and bandwidth of a range of predicted discharge between maximum and minimum values.

7.3 Results of long-term forecasting and discussion

7.3.1 Monthly discharge using Fiering, MNLR and ARIMA models

Fiering model

A linear falling trend is eliminated from the observed time series. After filtering, the time series is analyzed by the Fiering model. The predicted results are presented in Figure. 7.1.

The results obtained are based on measured values from the calibration period (1946-2008). In the validation period (2009-2013), the simulated bandwidth indicates a range of simulated monthly discharge maxima and minima. The mean value of the discharge time series shows a good agreement between simulations and measurements, with a deviation of 3.7 %. The simulation records 1224 m^3/s, where the measurement is 1269 m^3/s, respectively. Within the 5-years prediction, 75 % of the observed data are located in the simulated bandwidth. The absolute average variation between the Fiering model simulated and observed value is 34 %. The results show that the Fiering model generates synthetic time series, i.e. time series with the same statistical properties, but other sequences of discharges. Therefore, it is a suitable method for long-term forecasting, e.g. 100 years.

Table 7.1: Coefficient of MNLR model.

Sine wave 8								
	1	**2**	**3**	**4**	**5**	**6**	**7**	**8**
a	3292.0	4791.0	276.7	2702.0	106.4	102.5	104.8	95.8
b	0.006	0.009	0.524	0.010	1.049	0.076	0.215	0.049
c	-0.693	1.171	-1.711	3.784	0.449	1.193	0.815	1.655
Fourier 8								
a	-12.5	-6.0	-24.0	250.2	32.2	52.6	-26.9	114.7
b	55.3	-41.5	5.75	-89.6	9.2	-7.4	-16.0	-14.3
c	1179							
w	28.62							

MNLR model

During the calibration period, the sine wave function and Fourier time series with order i = 8 are chosen assuming the best goodness of fit. Table 7.1 shows the coefficients of the sine wave function and Fourier time series for the MNLR that are selected in this analysis. The evaluation criteria are calculated for both calibration and validation period and depicted in Table 7.2. The sine wave function shows better results with R^2 = 0.34, and smaller RMSE value compared to Fourier time series. Because the calibrated Fourier time series shows periodic time series around the mean value, the MBE of Fourier model is relatively small (MBE = 0.9).

During the validation phase, the periodical behavior of observed discharge time series can be simulated well with both models (see Figure 7.2). The Fourier model can simulate the frequency of peaks well, however, partly not with the same value, which is underestimated for the high value, as well as overestimated for the low value. This latter behavior is also appearing by using the sum of sine wave functions. The sine wave functions describe the period with a larger frequency. Looking into all evaluation criteria, the Fourier performs better than sine wave function. For the long-term prediction, Fourier model may predict a possible trend in time series. A better long-term prediction requires the Fourier time series in combination with a model assessing extreme events.

ARIMA model

The nonparametric regression technique is used to evaluate the trend of a time series. Figure 7.3 presents the observed data set (X_t), which is a part of the calibration period, and its trend (T_t), seasonal (s) and random (ε_t) components. A seasonal decomposition of the observed time series is performed by determining the trend using “locally weighted

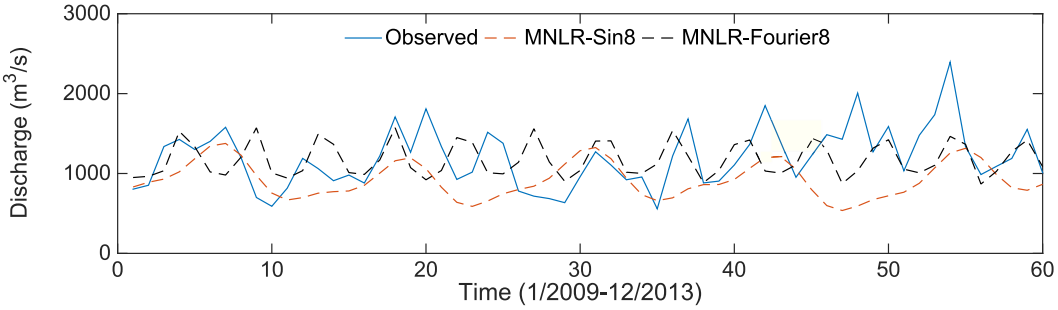

Figure 7.2: Results obtained from MNLR model for predicting monthly discharge during validation period.

scatterplot smoothing (LOESS)" regression (a algorithms in programming language R) and then calculating the seasonal component and the residuals from the differences $X_t - T_T$. Here, the recurring period s is 12 month.

The next parameter that should be determined is d, which is defined for ARIMA models. In this case after first order of differencing the time series became stationary. Therefore, d=D=1 is set. After the time series is stationary, the number of ARIMA model parameters is determined by performing ACF and PACF curves. These curves are depicted in Figure 7.4. The horizontal axis shows the delay time and the vertical axis indicates the amounts of ACF and PACF, respectively. The ACF time series presented a negative spike at lag 4 and at lag 12, whereas the PACF shows a more gradual decay pattern in the vicinity of both these lags. So a pure MA model is determined, choosing up to 4 moving average parameters for non-seasonal and 12 parameters for seasonal.

The purpose of AIC criterion is to select the parsimony model[2] with less number of parameters, therefore ARIMA $(0,1,4)(0,1,1)_{12}$ is chosen as the parsimony model. The RMSE, MBE and DC values are calculated between the predicted and observed data for the last 5 years (2009-2014) and shown in Table 7.2 and the predicted time series is presented in Figure 7.5. The results show that the majority of the observed values are located in the confidence area of simulated results. The predicted discharges through ARIMA procedure is closer to the observed time series. The benchmark error index $RMSE/\overline{Q_{obs}}$ for the forecasting model ARIMA $(0,1,4)(0,1,1)_{12}$ data is equal to 0.3.

[2]Parsimonious models are simple models with great explanatory predictive power. They explain data with a minimum number of parameters, or predictor variables (Andale, 2016).

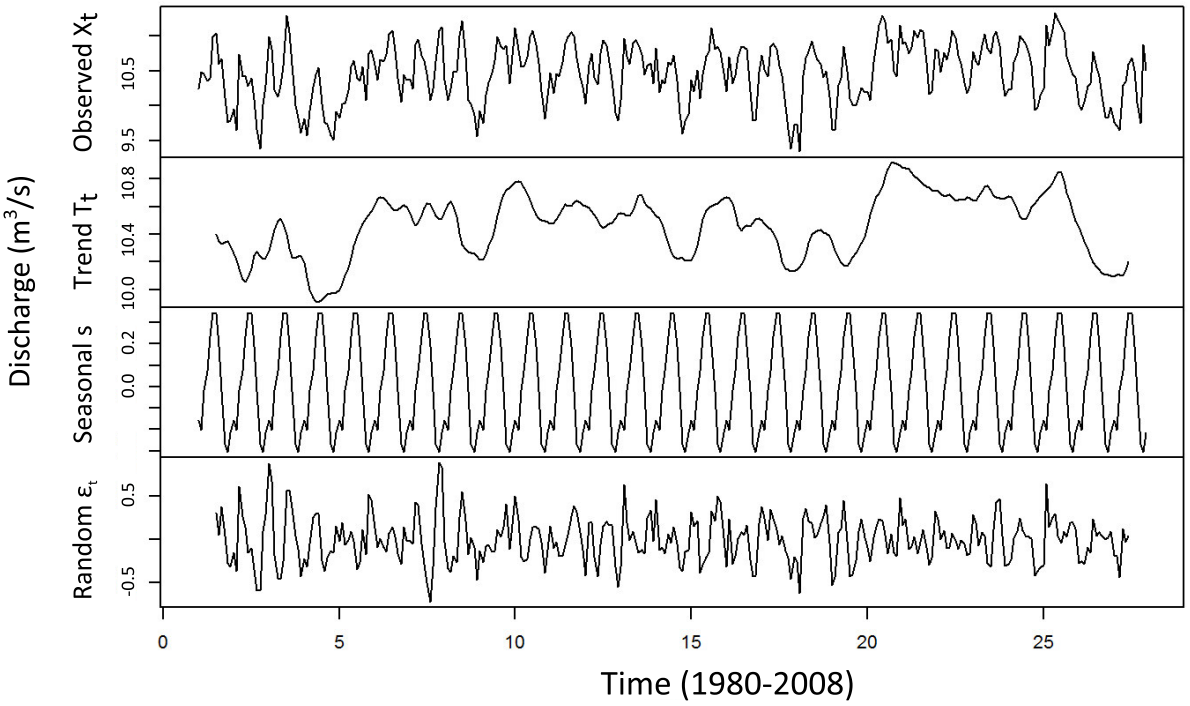

Figure 7.3: Decomposition of additive discharge time series from 1980-2008.

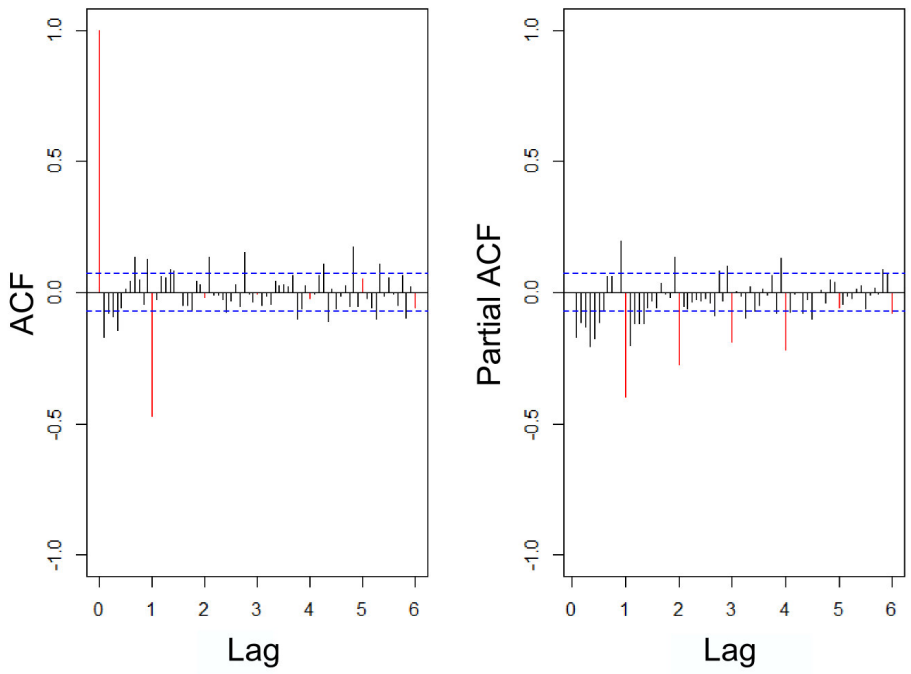

Figure 7.4: ACF and PACF diagram based on inflow to the Iffezheim reservoir.

Table 7.2: Comparison of Fiering model, MNLR and ARIMA using monthly discharge from 1946 to 2008. The results of MNLR are shown for 95 % confidence level.

Model	Calibration			Validation		
	RMSE (m^3/s)	MBE (m^3/s)	DC	RMSE (m^3/s)	MBE (m^3/s)	DC
Fiering	-	-	-	373.3	177.2	0.11
MNLR_sin 8	348.3	31.6	0.34	473.3	277.2	0.05
MNLR_Fourier 8	487.4	0.9	0.04	397.5	24.3	0.19
ARIMA	108.2	10.2	0.68	153.1	18.2	0.61

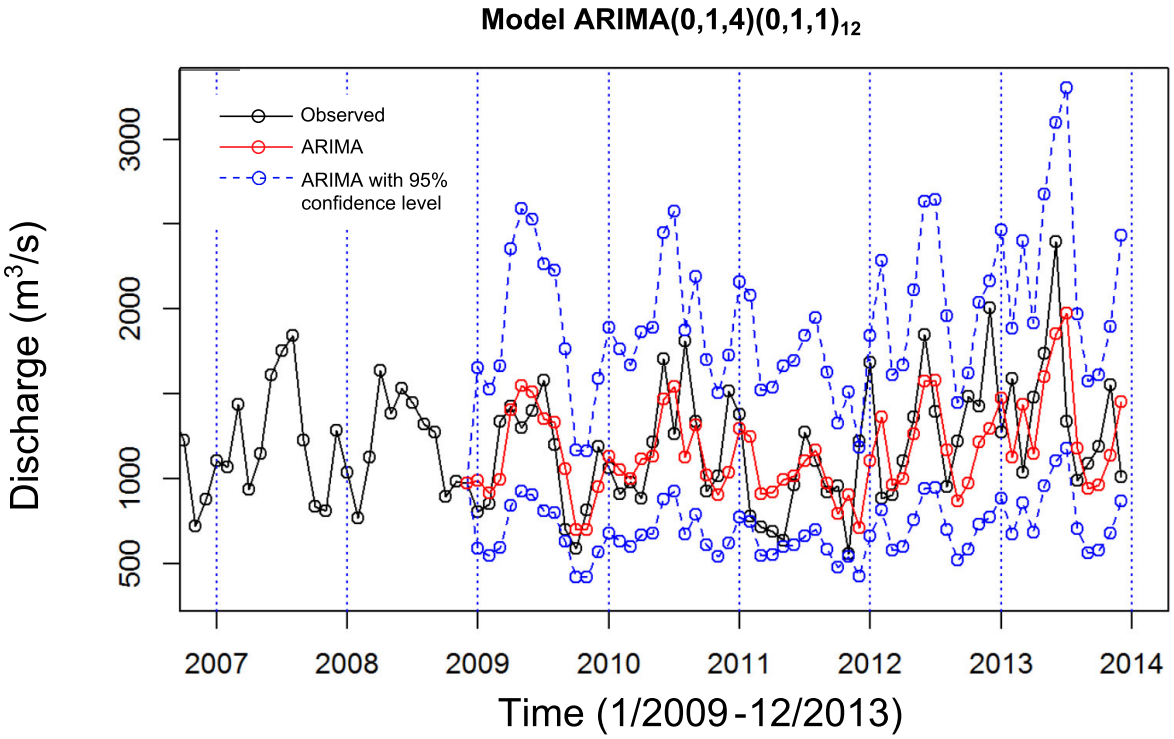

Figure 7.5: Results obtained from ARIMA model for prediction of monthly flow during validation period (Aljoumani et al., 2017, with permission).

7.3.2 Ability of used models in inflow forecasting

Table 7.2 shows training and forecasting RMSE, MBE and DC used for models. The comparison of the Fiering model, MNLR and ARIMA model revealed that ARIMA model could provide better outcomes during validation period than Fiering and MNLR. All used models had problems in forecasting peak flows. The Fiering model is most efficient, but the effort in calibration the ARIMA model is much larger than other models.

7.4 Summary

In this chapter, the time series analysis and synthesis is used to predict the discharge boundary condition for the Iffezheim reservoir. The ability of the Fiering model, MNLR and ARIMA models were investigated. The evaluation criteria RMSE (root mean square error), MBE (mean bias error) and DC (coefficient of determination) were used to compare the observed and predicted data.

The results showed that the Fiering model generates synthetic time series, i.e. time series with the same statistical properties, but other sequences of discharges. The Fiering model is the most efficient model among three models. However, the data set should be of sufficient length. MNLR is merely able to predict the periodicity. Both models deliver just basic correctness for short-term prognoses and suffer from the expectations of stationary states. In other words, these models can only deliver effective results for stationary non-linear time series data. Nevertheless, the Fiering model can provide statistically possible time series and bandwidths of discharges to be expected.

In contrast to aforementioned models, the ARIMA model performs the non-linear dynamics of time series well, as the predicted and observed values show reasonably good agreements for short-term prognoses. By investigating the abilities of these models, the ARIMA model is most suitable for forecasting appropriate monthly inflows for the 5 years validation period. Moreover, it should be noted that the effort for the calibration of the ARIMA model is higher than for other models.

Chapter 8

Artificial neural networks

8.1 Introduction

The purpose of this chapter is to determine an appropriate model for forecasting long-term daily suspended sediment concentrations (SSC), which serves as boundary conditions for numerical model of the Iffezheim reservoir. The projected daily discharges till the year 2100 obtained from KLIWAS program will be applied in the investigation.

Because the sediment behaviour is complex, dynamic and non-stationary as well as not uniformly related to the stream flow behaviour, no mathematical relation between the two parameters can be detected, hence simulation of SSC is rather difficult. To reduce the complexities of the simulation of SSC, in terms of developing practical techniques, the classical models such as Sediment Rating Curve (SRC) is widely used. SRC is used to get a quick first impression of the relation and behaviour between flow and suspended sediment concentration due to the fact that the SRC can be determined quickly. However, such curves have a limited ability to capture non-stationary processes considering streamflow and other hydrologic processes, as well as non-linear relationships between these variables (Melesse et al., 2011b; Rajaee, 2011; Rajaee et al., 2009). For complex hydrological systems or non-linear model applications, Artificial Intelligence (AI) based methods have proven to be useful. They are a kind of data-driven models and offer an effective way to handle some amount of non-uniform data from dynamic and non-linear systems (Nourani et al., 2014). Additionally, data-driven models are can be used as alternative tools in certain applications where the physically-based equations are not as accurate (Wieprecht et al., 2013).

Various researchers predicted sediment concentrations using several data-driven models and compared their ability of accurate performances. A review is summarized in Table 8.1. Nagy et al. (2002) developed an ANN model to estimate SSC in rivers. The

ANN model was compared to several commonly used sediment discharge formulas using 80 data observations. They concluded that ANN achieved better results than the other tested discharge formulas. In the study of Rajaee et al. (2009), ANNs, neuro-fuzzy (NF), multi-linear regression (MLR) and conventional SRC models were considered for time series modeling of SSC in two different rivers. Obtained results showed that ANN and NF models were in better agreement with the observed SSC values than MLR and SRC methods. Melesse et al. (2011a) used ANNs, ARIMA, MNLR and MLR models to estimate the daily suspended sediment load (SSL) for three major rivers (Mississippi, Missouri and Rio Grande) in USA. The results revealed that ANN predictions for most simulations were better when compared with the ones using MLR, MNLR and ARIMA. Rajaee (2011) proposed a Wavelet-ANN (WANN) model for the prediction of the daily SSL in Yadkin River in the USA. The comparison of prediction accuracy from WANN to the ones of MLR and SRC models illustrated that the WANN was the most accurate model to predict daily SSL. Additionally, the WANN model could satisfactorily simulate hysteresis phenomenon. Liu et al. (2013) came up with the same conclusion, where they found that the WANN model predicts the highly non-linear and non-stationary SSC time series one day in advance better than ANN or SRC. Zounemat-Kermani et al. (2016) estimated the daily SSC using eight-year data series from hydro-metric stations located in Arkansas, Delaware and Idaho in USA using ANN models. The results confirmed the superiority of ANN models with Broyden-Fletcher-Goldfarb-Shanno (BFGS) training algorithm. It was recommended as a useful option for simulating hydrological phenomena. Joshi et al. (2016) used ANN to simulate stage discharge suspended sediment relationship for the ablation season (May-September) for melt runoff released from the Himalayan Gangotri glacier. The study revealed the suitability of ANN approach to simulate and estimate daily SSC in glacier melt runoff.

Until now, many researchers proved the superior prediction performance of AI models in predicting daily SSC (Cigizoglu and Alp, 2006; Cigizoglu and Kisi, 2006; Kumar et al., 2016; Liu et al., 2013). However, many studies investigated only the competence of models based on the daily SSC time series, which first prepare the input combinations using the entire data series and later divide them into calibration and validation data sets to setup the models, that send some amount of future information into the processes. As a consequence, the resulted input used to forecast the value of a particular moment is computed using information from future values, which are not available at that particular moment in the forecasting process (Zhang et al., 2015b). Therefore, this is not a real forecast but a historical re-forecast. The historical re-forecast modeling can be used to compare the abilities of models or the one-step advance prediction. However, it is not

Table 8.1: Literatur research of AI research parameters and algorithms.

Year	Authors	Input variables	Predicted variable	Data set	AI methods	Best performance	AI learning algorithm
2002	Cigizoglu	Q, SSC	SSC	10-1994/11-1997	ANN, SRC	ANN	
2006	Cigizoglu & Kisi	Q, SSL	SSL	10-1952/09-1981	RDNN, ANN, LR	RDNN	LM
2006	Lee et al.	Rainfall, Q	SSL	1991/2000	ANN, HSPF	ANN	
2007	Alp & Cigizoglu	Rainfall, SSL	SSL	01-1983/06-1989	FFBP, RBF, MLR	FFBP, RBF	LM
2008	Kisi	Q, SSC	SSC	10-1993/09-1995	ANN	ANN	LM, CG, GD
2008	Paratal & Cigizoglu	Q, SSL	SSL	10-1952/09-1981	WANN, ANN, SRC	WANN	
2009	Cobaner et al.	Rainfall, Q, SSC	SSC	1971/1973	SRC, GRNN, RBNN, MLP, ANFIS	ANFIS	
2009	Rajaee et al.	Q, SSC	SSC	10-1980/ 10-1984; 10-1984/ 10-1988	ANN, NF, MLR, SRC	NF	LM
2009	Kisi et al.	Q, SSC	SSC	10-1993/09-1995	EFM, NF, NN, SRC	EFM	
2010	Mirbagheri et al.	Q, SSC	SSC	10-1988/ 09-1993	WNF, ANN, NF, SRC	WNF	LM
2010	Kisi	Q, SSC	SSC	10-1993/ 10-1995	ANN, SRC, NF, NDF	NDF, NF	
2011	Rajaee	Q,SSL	SSL	10-1958/09-1982	WANN, MLR, SRC	WANN	
2011	Melesse et al.	Rainfall, Q, SSL	SSL	1971/1975; 1977/1981	ANN, ARIMA, MNLR, MLR	ANN	
2012	Mustafa et al.	Q	SSL	01-1993/10-1998	MLP, FFNN	ANN (LM)	LM, GDM, SCG, GD
2012	Kisi & Shiri	Rainfall, Q, SSC	SSC	(11 years)	ANN, ANIF,GEP	GEP (GD)	LM, CG, GD
2013	Haddadchi et al.	SSL	SSL		ANN	ANN	LM
2013	Liu et al.	Q,SSC	SSC	1967/1972	WANN, BPNN, SRC	WANN	
2015	Nourani et al.	Q, SSL	SSL	1982/2002	WANN, ANN, WLSSVR, LSSVR	WLSSVR	
2016	Zounemat-Kermani et al.	Q,SSC	SSC	(10 years)	ANN, SVR, MLR, SRC	ANN (BFGS), SVR (RBF)	LM, BFGS, GD, CG
2016	Kumar et al.	Rainfall, Q, SSC	SSC	01-2003/ 12-2010	ANN, RBFNN, LS-SVR, MLR, CART	ANN	LM, newrb

LM: Levenberg Marquardt
CG: Conjugate gradient
GD: Gradient descent
RDNN: Range dependent NN
RBNN: Radial basis NN
ANFIS: Adaptive neuro-fuzzy inference system
EFM: Evolutionary fuzzy models
WNF: Wavelet neuro-fuzzy model
GEP: Gene expression programming

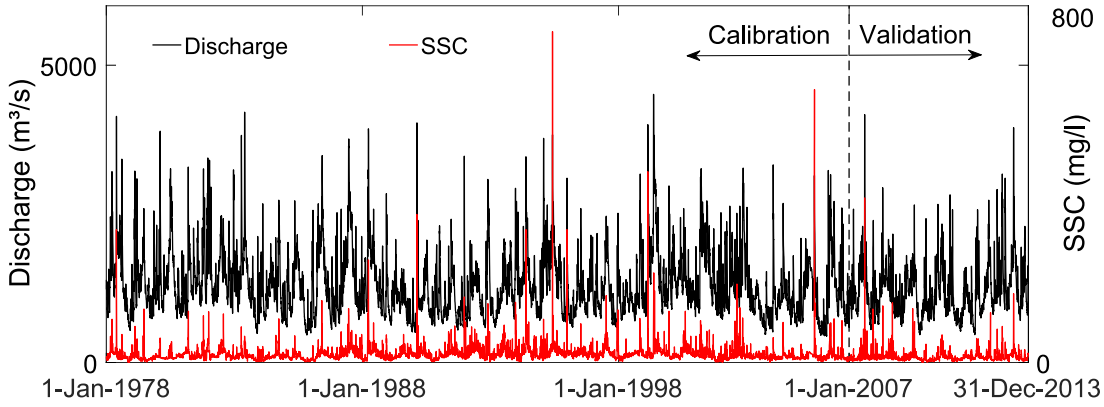

Figure 8.1: River discharge and SSC time series at the Plittersdorf station from 1978 to 2013 (36 years).

suitable for long-term predictions, as the information from future values, SSC in this case, is not available.

To overcome the above mentioned drawback in the previous work, in this study the ANN and appropriate WANN models are used to predict long-term daily SSC without involving the future SSC value in the process.

8.2 Data set and statistical analysis of the data

For the calibration and the validation of the models, the data from January 1, 1978 to December 31, 2006 (29 years; 81 % of the whole data set) and the data from January 1, 2007 to December 31, 2013 (7 years; 19 % of the whole data set) were selected, respectively (see Figure 8.1). For the prediction of the sediment concentrations, the predicted values of the discharges from January 1, 2014 to December 31, 2100 (87 years) were applied.

The statistical analysis of training and testing data sets including the mean, minimum, maximum, standard deviation (SD), skewness coefficient (Csx) and kurtosis are listed in Table 8.2. It should be noted that like all empirical models, ANN models perform better when they do not extrapolate beyond the range of the data used for model training (Tokar and Johnson, 1999), and consequently, the extreme values of the available data should be included in the training data set.

The analysis of the historical data sets showed that the Q and SSC exhibit highly peaked values (discharge higher than 4000 m^3/s) in May 1978, May 1983, February 1990, May 1999 and August 2007. The highest discharge occurred in May 1999, it was about

Table 8.2: Statistical analysis for all historical data sets, calibration, validation and projected time series, respectively.

Statistical parameters	All historical data (1978-2013)		Calibration (1978-2007)		Validation (2008-2013)		Prediction (2014-2100)
	Q (m^3/s)	SSC (mg/l)	Q (m^3/s)	SSC (mg/l)	Q (m^3/s)	SSC (mg/l)	Q (m^3/s)
Mean	1297.4	18.39	1297.0	19.4	1206.7	14.4	1269.3
Max	4510	742	4510.0	742.	4170.0	369.0	7552.4
Min	444	1	444.0	1	467.0	1	408.6
SD	516.6	20.0	531.4	20.9	443.1	14.9	554.5
	Q	SSC	Q	SSC	Q	SSC	Q
COV (-)	0.40	1.08	0.41	1.08	0.37	1.03	0.43
Csx (-)	1.34	12.42	1.31	12.68	1.38	8.2	1.64
Kurtosis (-)	5.65	303.16	5.41	303.25	6.48	143.5	8.18

4510 m^3/s (SSC = 121 mg/l). The largest value of SSC was in August 2007, it was about 369 mg/l (Q = 4170 m^3/s). The range of Q and SSC in the validation period was included in the calibration period. The statistical analysis showed also that the standard deviation values for both Q and SSC in the calibration period were higher than the ones in the validation period.

The coefficient of variation (COV), i.e., ratio of SD to the mean, for both parameters (Q and SSC) in the calibration period was low. This is suitable for the simulation, because higher COV causes poor learning performance in the ANN model leading to convergence problems (Melesse et al., 2011b).

Kurtosis values indicate the relative flatness and peakedness in the distribution. A positive value indicates the possibility of a leptokurtic distribution (too thin and too tall) and a negative value indicates the possibility of a platykurtic distribution (too platy and too low) (Melesse et al., 2011b; Taylor, 2016). SSC-values, especially highly peaked ones, indicate high variability and non-normal distributions in the whole data set.

The statistical analysis of the prediction data set showed that the mean value of discharge is in the same range of the one of the historical data, however, maximum and minimum discharge values in the projected data set were beyond the range of the historical data sets. The maximum discharge reached about 7552 m^3/s. It corresponds to the highest SD, extremely high COV, and lightly high Csx and kurtosis. Therefore, it is supposed that in the prediction period the extreme values of SSC would be underestimated.

Table 8.3: Correlation and distribution of historical data.

	Q_t	Q_{t-1}	Q_{t-2}	Q_{t-3}	Q_{t-4}	Q_{t-5}
Corr.	0.52	0.48	0.41	0.35	0.3	0.22
vs.		SSC_{t-1}	SSC_{t-2}	SSC_{t-3}	SSC_{t-4}	SSC_{t-5}
SSC		0.76	0.53	0.4	0.35	0.3

Correlation coefficients (R) in Table 8.3 were used to get a better understanding of the correlation between the inputs (flow, antecedent flow and antecedent sediment concentration) and the output (current sediment concentration). The correlation between suspended sediment SSC and discharge Q_t, antecedent flow Q_{t-1} and antecedent sediment SSC_{t-1} werer 0.52, 0.48 and 0.76, respectively. The correlation decreased the longer away the antecedent flows are (R was 0.22 for five antecedent flow Q_{t-5}). In this work, antecedent flows and suspended sediment concentrations up to 5 days as inputs were due to the low correlation ignored.

8.3 Methods

8.3.1 Artificial neural networks

Artificial neural networks (ANN) were inspired originally by the human brain and nervous system (Muller et al., 1995). The first fundamental concepts related to neural computing were developed by McCulloch and Pitts (1943). Afterwards many ANN activities have been centered on its extensions (Salas et al., 2000). In the last two decades, ANN methods have gained significant attention to efficiently address hydrological applications, such as flood forecasting, precipitation and evaporation estimation, water quality modeling, prediction of discharge and prediction of sediment concentration (Adamowski and Chan, 2011; Aksoy and Dahamsheh, 2009; Baareh et al., 2006; Cannas et al., 2005; Chen et al., 2016; Cigizoglu, 2003; Çimen, 2016; Dahamsheh and Aksoy, 2013; Dogan et al., 2007; Farajzadeh et al., 2014; Kisi, 2011; Krishna et al., 2011; Melesse et al., 2011b; Nilsson et al., 2006; Nourani et al., 2014; Partal and Cigizoglu, 2008; Schreider et al., 2002; Tayyab et al., 2016; Wei et al., 2013).

ANN is an effective approach to handle non-linear data and to identify underlying relationships between input and output data sets, especially in situations where the relationships between physical processes are not fully understood (Tayyab et al., 2016). Within many paradigms, the most common and widely-used engineering application is the feed-forward backpropagation (FFBP) neural network (Melesse et al., 2011b), which

was firstly mentioned in Rumelhart et al. (1986). A network with three-layers has been proven to be satisfactory for forecasting and simulating in the water science (ASCE, 2000), and it is therefore used in this study. FFBP neural network consists of three layers, namely the input layer, the hidden layer and the output layer.

A set of inputs or signals (x_i) are forwarded from the input layer to artificial neurons in the hidden layers, a weighted sum (z_i) is calculated using a summation function, weights (w_i) and a bias (θ_i), where:

$$z_i = \sum_{i=1}^{n} x_i w_i + \theta_i \tag{8.1}$$

z_i is then passed through an activation function (f) in the output layer, in this study the sigmoid logistic non-linear function was used, where:

$$f(z) = \frac{1}{(1 + e^{-z})} \tag{8.2}$$

The objective of training the model is to find the set of weights between neurons that determine the global minimum of an error function. The training process is carried out by randomly assigning the initial weights and applying different activation functions for hidden and output layers. During the training process, errors are permanently calculated and propagated backwards, the weights and biases between neurons are iteratively adjusted using gradient descent (Lohani et al., 2011) and optimized after multiple runs.

The backpropagation algorithm is used to minimize the error. Several trials are performed to receive best training stage of the model; the training is stopped as soon as a validation error rate starts to increase (Araghinejad, 2014).

Normally one or two hidden layers are sufficient to solve any non-linear complex problem (Karsoliya, 2012). One can adopt the solution of a third hidden layer, but this will increase overall complexity of the neural network and the total training time will be increased. Moreover, unreasonable increment of layers may lead to overfitting of the problem.

Additionally, determining the numbers of neurons in the hidden layer is the fundamental task in building the network. Many researchers developed approaches to estimate the number of neurons and hidden layers requirement for a neural network, but the approximation also gets dependable on the type of the database samples for which the network is designed (Karsoliya, 2012).

Since there is no specific algorithm to specify how many neurons are required in the hidden layer, a thumb-rule was applied in this work. The number of hidden neurons was investigated using 0.7 to 2 multiplied with the number of input parameters. The

network architecture that reached the best result in terms of the model performance was chosen as the optimized structure. The neural network from Matlab® is used here (Beale et al., 2016).

8.3.2 Wavelet-artificial neural network

A wavelet is a waveform of effectively limited duration with an average value of zero. The wavelet analysis is suitable for non-stationary data, where the mean and autocorrelation of the signal are not constant over time. The wavelet has the ability to elucidate the signal simultaneously in both time and frequency.

There are two main wavelet transformation methods: continuous wavelet transformation (CWT) and discrete wavelet transformation (DWT). The CWT calculation requires a significant high amount of computation time and resources. Conversely, DWT calculates the wavelet coefficients using a simple and very efficient way (Cannas et al., 2005). The advantage of using the DWT is that it allows for the implementation of digital filtering effects. The wavelet transformation can be constructed using downsampling into an approximation coefficient at level n through a low pass filter and detail coefficients at different levels through a high pass filter (see Figure 8.2). DWT was used in this study to analyze the suspended load concentration. This chapter will not delve into the theory behind wavelet transformation and only the main concepts of the discrete wavelet transform are briefly presented, more information is found in Mallat (1989) and Labat (2005).

The DWT decomposes the signal into a group of functions, which are usually expressed by:

$$\psi_{j,k}(t) = a_0^{-j/2}\psi(\frac{t - ka_0^j\tau_0}{a_0^j}) \tag{8.3}$$

where $\psi_{j,k}(t)$ is produced from a mother wavelet $\psi(t)$, which has to satisfy the condition:

$$\int \psi(x)dx = 0 \tag{8.4}$$

j and k are integers. a_0 and τ_0 are a fixed dilation step and a translation factor, respectively, the most common choice is $a_0 = 2$, $\tau_0 = 1$, and then the DWT becomes binary and is called dyadic scales and positions (Wei et al., 2013).

In the WANN model, the decomposed SSC and Q time series are linked to the ANN method for prediction of SSC firstly for one day ahead. Afterwards, the simulated SSC

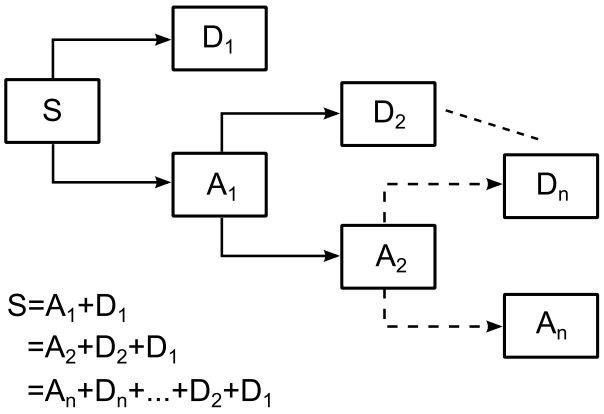

Figure 8.2: Wavelet decomposition and reconstruction processes in n levels.

is decomposed by discrete wavelet transformation (Mallat, 1989). When conducting wavelet analysis, the most important steps are selecting an appropriate wavelet function and choosing the optimal number of decomposition levels. To investigate the effects of the employed wavelet type as well as the decomposition level on the WANN model efficiency, Nourani and Andalib (2015) have applied the 5 mother wavelets model and investigated the mother wavelet and decomposition level impacts on daily suspended sediment load predictions. They found out that the mother wavelet and levels alterations did not have impressive upshot. Therefore, in this study only the most used and so called best mother wavelet models Daubechies wavelet 5 (db5) was used to predict the suspended sediment concentration. To select the number of decomposition levels, Equation 8.5 was used (Daubechies, 1992; Nourani et al., 2009; Wang and Ding, 2003):

$$j = int(log(N)) \tag{8.5}$$

where L and N are number of decomposition levels and daily time series length.

8.3.3 Sediment rating curve

Q_w is the instantaneous river discharge, which is taken from a stage-discharge curve of the gauging station every 15 minutes. Q_w in this study describes the mean daily value in m^3/s. SSC is the instantaneous suspended sediment concentration in mg/l. The suspended sediment concentration was measured by analysis of water samples. The sediment rating curve is used to assess the sediment discharge corresponding to the measured flow discharge. Generally, the functional relationship between sediment concentration and discharge form a power equation (see Figure 6.2a):

$$SSC = aQ_w^b + c \tag{8.6}$$

8.4 Model applications

8.4.1 Application of ANN and WANN models

The calculation process with the ANN and the WANN models was utilized to determine the future SSC values based on the projected Q values (obtained from the KLIWAS program, described in section 3.1). The ANN and WANN models should be first setup using the measured values of Q and SSC in the calibration process. The input layer should be arranged in a way that should include all pertinent information on the target data. Based on statistic analysis in section 8.2, the input layer was optimized with only the most important time memories. In this regard, input combinations of discharge time series up to four lag time steps, and of both Q and SSC time series up to five lag time steps were used here.

The input combinations are listed in Table 8.4, where t is the current time step. In the first combination, the input layer consisted of the flow only at day Q_t. In the second to fifth scenario, one to four previous days were employed. In the sixth scenario, the SSC at day $t-1$ (SSC_{t-1}) and the discharge Q_{t-1} together with Q_t were incorporated into the input layer. In seventh to tenth scenario, the SSC and Q for two to five previous days together with current discharge were used.

The calculation process with the ANN, as shown in Figure 8.3, started with the calibration phase in which the observed Q and SSC (according to the aforementioned scenarios) were applied as input to train the ANN model. The output layer comprised only one variable, i.e. suspended sediment concentration at the current time step SSC_t. The input and output parameters are linked via neurons in the hidden layer. The number of nodes in the hidden layer was determined depending on the number of input parameters. The appropriate number of nodes in the hidden layer was found by trial and error. During training, the weights within the network were changed until the ANN reached the global minimum of the error function, which means that the ANN has learned the optimal relationship between input and output parameters. The Levenberg-Marquardt algorithm based on the feed-forward backpropagation method was employed to train ANN models in this study. Several trials were performed to get best training stage of the model. The Tansig (Schmitz et al., 2006) and Purelin functions were utilized as transfer functions in hidden and output layers. They prevent the ANN model from

Table 8.4: Input combinations.

Combinations	Input parameters
Comb. 1	Q_t
Comb. 2	Q_t, Q_{t-1}
Comb. 3	Q_t, Q_{t-1}, Q_{t-2}
Comb. 4	Q_t, Q_{t-1}, Q_{t-2}, Q_{t-3}
Comb. 5	Q_t, Q_{t-1}, Q_{t-2}, Q_{t-3}, Q_{t-4}
Comb. 6	Q_t, Q_{t-1}, S_{t-1}
Comb. 7	Q_t, Q_{t-1}, Q_{t-2}, S_{t-1}, S_{t-2}
Comb. 8	Q_t, Q_{t-1}, Q_{t-2}, Q_{t-3}, S_{t-1}, S_{t-2}, S_{t-3}
Comb. 9	Q_t, Q_{t-1}, Q_{t-2}, Q_{t-3}, Q_{t-4}, S_{t-1}, S_{t-2}, S_{t-3}, S_{t-4}
Comb. 10	Q_t, Q_{t-1}, Q_{t-2}, Q_{t-3}, Q_{t-4}, Q_{t-5}, S_{t-1}, S_{t-2}, S_{t-3}, S_{t-4}, S_{t-5}

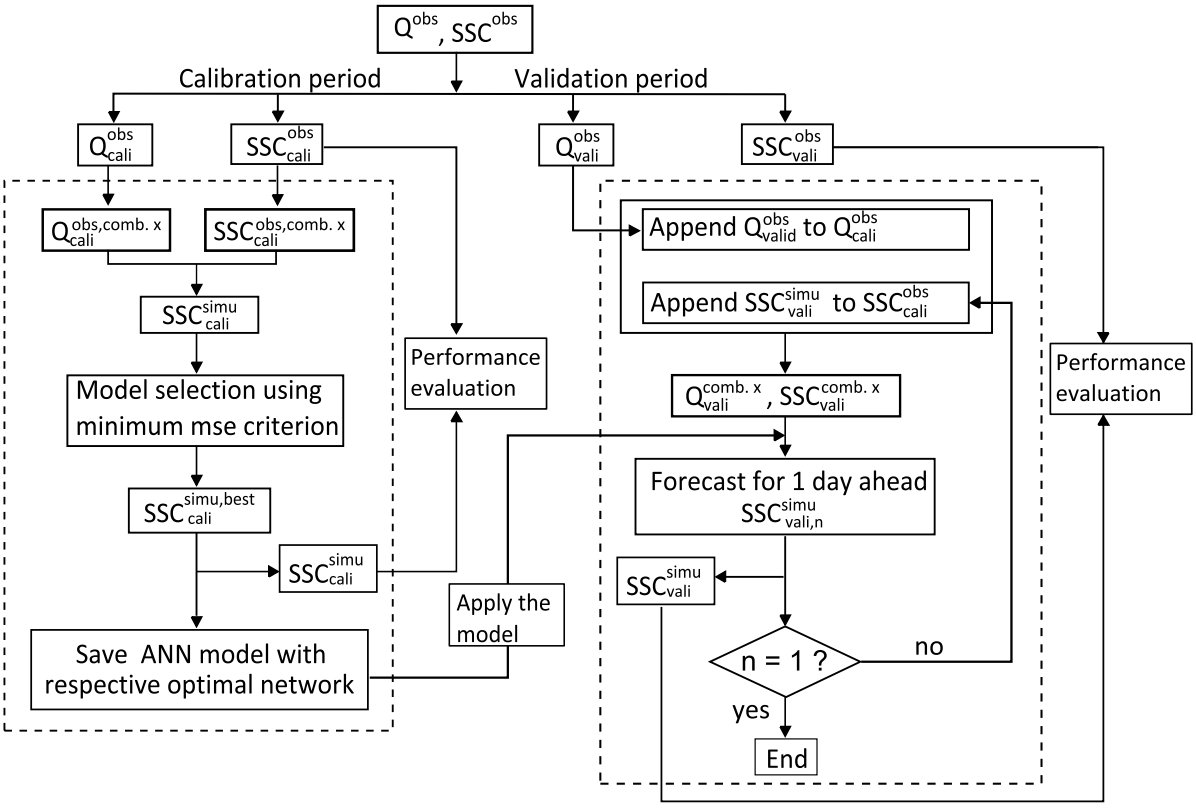

Figure 8.3: A graphical structure of neural network model in case of long-term forecasting.

being overtrained. It was found that 500 epochs achieve a training network considering 10^{-6} as goal performance. The simulated output SSC values in the calibration period were compared with the observed ones in terms of model evaluation criteria (RMSE, MBE and DC) (see subsection 7.2.4). The best ANN architecture was then used to validate the model.

During the validation phase, the measured Q and SSC values were used as input parameters in the first run, here only SSC values of the previous days were required and used for the simulation. Then a series of runs were carried out, in each the simulated SSC value of the previous run was used as input for the current one to calculate the value of the subsequent day. Finally, the simulated SSC values were compared to the observed values, taking the model evaluation criteria into account.

For the WANN model, only the entire data series of Q and SSC during the calibration phase were decomposed into components. Only these components were used to establish the model, to avoid the phenomen that the formulation sends an amount of future information into the model. According to the time series length (10592 values) of the observed data, the maximum calculated decomposition using equation 8.5 was 5, thus, the observed Q and SSC series were decomposed at five levels (2-4-8-16-32 days) (see Figure 8.4). The WANN model was then used to compute the 1-day advance forecast across all the calibration components. The best model was then chosen to compute the corresponding 1-day ahead forecasts. Afterwards, the first projected value was appended to calibrate data series. Using db5 L4 the whole data were divided again into 5 components. The next forecast value of the validation data set was calculated by WANN. This process was repeated until the 1-day ahead validation forecast SSC_{vali}^{simu} was obtained.

8.4.2 Application of SRC method

The SRC method was employed to simulate the relationship between the input variables and the SSC. The regression equations were referred as trained models. The predictive ability of the models were tested with the same data sets used for testing the ANN models. Hence, the results are comparable.

Applying the SRC model, the relationship between measured discharge and SSC with 95 % confidence level was as follows:

$$SSC = 1.683 \cdot 10^{-14} Q^{3.03} + 11.99$$

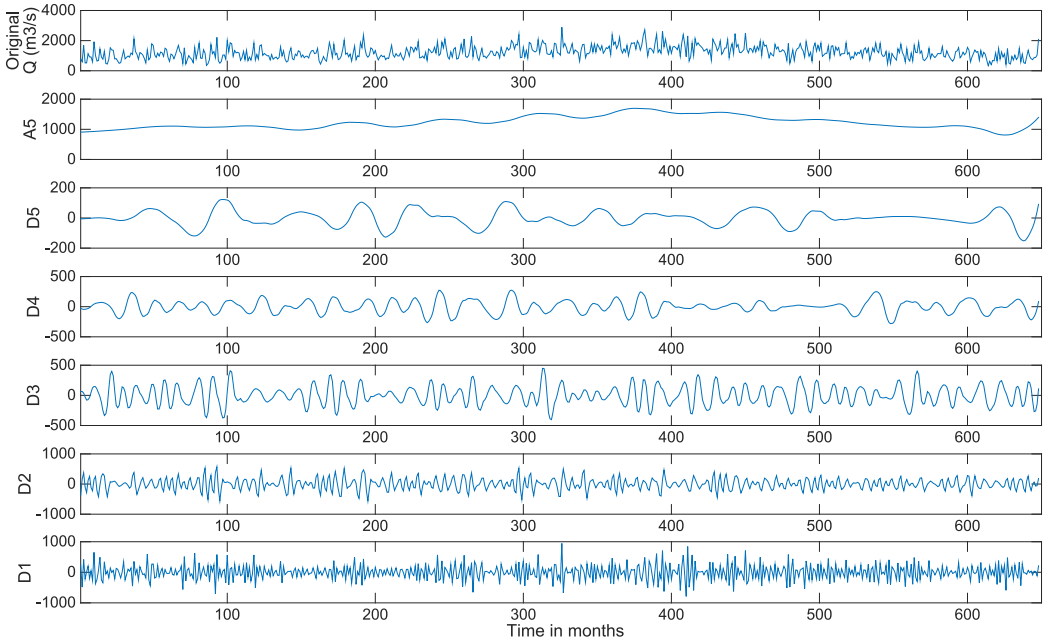

Figure 8.4: The original and decomposed SSC time series at Plittersdorf station using Daubechies wavelet 5.

8.5 Results and discussion

8.5.1 Prediction of SSC using ANN and WANN

Table 8.5 and Figure 8.6 present the values of the performance in the calibration and validation phases for each input scenario. There the third column describes the optimized structure of the combinations, e.g., in comb.1 the optimized ANN structure is (1,2,1) representing 1 input neuron, 2 neurons in the hidden layer, and 1 output neuron for predicting the SSC in the subsequent day. The optimized structures were chosen by altering the number of neurons during the validation phase to achieve the best performance.

According to the results in Table 8.5, the quality of the ANN results were not dependent on the number of the antecedent Q and SSC values, i.e., more input data did not lead to more accurate results. The SSC dependent combinations 6 to 10 achieved better performance than the independent combinations 1 to 5 according to the RMSE and DC values. A clear improvement of the performance was started in combination 6, in which the current SSC value was simulated using the value of the previous day. In the validation phase, the RMSE and DC values were quite similar in all scenarios, so they could not be used to identify the best scenario. However the best scenario in this phase

Table 8.5: Performance of the ANN model for different input combinations.

Comb.	Optimized ANN structure	Calibration (training)			Validation (testing)		
		RMSE (mg/l)	MBE (mg/l)	DC	RMSE (mg/l)	MBE (mg/l)	DC
Comb. 1	1,2,1	15.230	-0.085	0.38	10.920	-3.14	0.46
Comb. 2	2,2,1	15.712	-0.135	0.37	10.854	-3.188	0.47
Comb. 3	3,3,1	14.217	-0.022	0.43	10.612	-3.175	0.49
Comb. 4	4,7,1	15.505	-0.042	0.40	10.628	-3.223	0.49
Comb. 5	5,8,1	17.409	2.788	0.37	10.587	-0.722	0.50
Comb. 6	**3,4,1**	**11.515**	**-0.678**	**0.71**	**10.517**	**-1.305**	**0.51**
Comb. 7	5,7,1	10.529	0.284	0.72	10.929	-1.595	0.46
Comb. 8	7,10,1	10.546	0.083	0.77	10.896	-2.458	0.47
Comb. 9	9,5,1	9.183	0.927	0.77	10.363	-1.665	0.52
Comb. 10	11,5,1	9.602	-0.054	0.78	10.922	-3.585	0.46

Table 8.6: Performance of the WANN model for different input combinations.

Comb.	Optimized WANN structure	Calibration (training)			Validation (testing)		
		RMSE (mg/l)	MBE (mg/l)	DC	RMSE (mg/l)	MBE (mg/l)	DC
Comb. 1	**5,2,1**	**16.950**	**-3.231**	**0.33**	**10.723**	**-0.313**	**0.49**
Comb. 2	10,7,1	16.075	0.170	0.37	10.470	-0.825	0.48
Comb. 3	15,6,1	16.329	-2.820	0.36	11.190	-3.337	0.44
Comb. 4	20,8,1	17.890	0.325	0.34	11.658	-3.750	0.42
Comb. 5	25,5,1	17.640	0.020	0.33	11.329	-3.210	0.44
Comb. 6	15,7,1	13.966	4.741	0.70	13.178	-2.321	0.22
Comb. 7	25,15,1	4.424	-0.204	0.95	12.689	-1.634	0.28
Comb. 8	35,7,1	6.683	0.459	0.88	12.842	-4.237	0.26
Comb. 9	45,11,1	3.277	0.047	0.97	14.879	-2.323	0.01
Comb. 10	55,8,1	3.197	-0.056	0.98	14.123	1.131	0.10

was chosen based on the MBE values. In this case comb. 6, which has the minimum number of input parameters, the lowest MBE value of -1.305 mg/l was obtained.

Comparing the results of WANN (see Table 8.6) with those of ANN (see Table 8.5) showed that the combinations 1 to 5 accomplished only minor improvements in case of WANN. Likewise, the number of Q and SSC values is as well irrelevant for the quality of the results. For the input dependent combinations 6 to 10, there was a clear improvement in the calibration phase compared to the ANN models. However, that was not the case in the validation phase. The more values of the SSC were chosen as input parameters, the worse the results became. One reason could be the order of the input data sets. The decomposed input nodes should be ordered in the same way in the validation phase as in the calibration phase, which means that high weights should be applied to the high level of the time series.

Also by comparing the results between ANN and WANN, the ANN configurations with the current day discharge, the previous discharge and SSC (Comb. 6) achieved the best efficiency among all the other combinations, i.e best fitting with the observed data.

8.5.2 Analysis of WANN models

As mentioned earlier, in the traditional procedures for applying WANN, the predicted 1-day ahead value of SSC should be involved again in the original data set to create the updated data base. The whole data set is then discretized again to be used as new input for the input layer in WANN. The variations of the data boundary during the discretion could lead to large deviations of the outcomes. This behavior was analyzed by feeding the WANN with the 5 components shown in Figure 8.5, after appending the first predicted SSC across all the calibration time series. At the end of the data, part of it begins to "spill over" the edge. That is due to the fact that the wavelet analysis of the signal is based on the convolution of the signal with the filters, which leads to border distortions when performed on finite-length signals (Addison, 2002; Zhang et al., 2015b). The boundary effect hurt the modeling quality as well as the overall prediction performance. To restrain the boundary effect the signal should be extended. However, it is impossible to extend the data set with unknown future information. Therefore, it can be concluded that the traditional procedure for applying the WANN model is not suitable for real forecasting of daily SSC. Hence, in this study it was suggested to decompose only the current discharge instead of imposing the past days values as inputs. Accordingly, the SSC independent combination 1 is the best here.

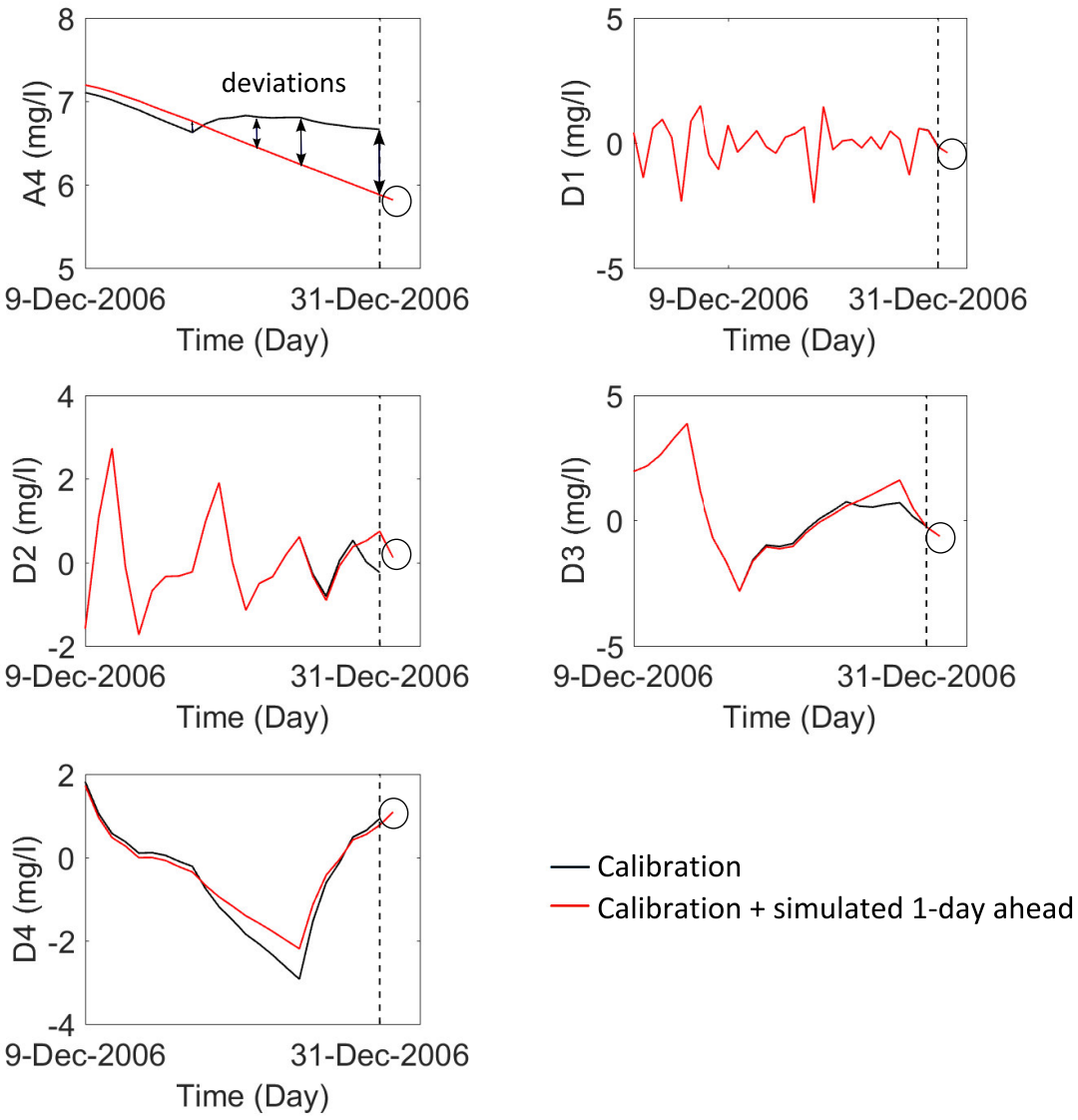

Figure 8.5: Resulted deviations after appending a simulated SSC in each component. A simulated 1-day ahead value is marked with circle. The resulted deviations are, for example, presented in component A4.

8.5.3 Comparison with SRC method

Prediction of SSC using SRC was performed with the same data set, to be comparable with the results of the ANN and WANN models.

In Figure 8.6 the estimated SSC using SRC method versus the observed data is

Table 8.7: Performance of SRC model in predicting SSC during calibration and validation phases.

Model	Optimized structure	Calibration			Validation		
		RMSE (mg/l)	MBE (mg/l)	DC	RMSE (mg/l)	MBE (mg/l)	DC
ANN	**5,8,1**	**11.515**	**-0.678**	**0.71**	**10.517**	**-1.305**	**0.52**
WANN	5,2,1	16.950	-3.231	0.33	10.723	-0.313	0.49
SRC	-	17.011	0.0258	0.34	10.983	-3.021	0.46

shown. There, the observed sediment values are presented in form of sediment hydrographs and scatter plots. The scatter plots exhibited deviations from observed values with RMSE = 10.983 m^3/s, MBE = -3.021 m^3/s and DC = 0.46.

The results of SRC showed that it tends to underestimate peak values and either under- or overestimate the smaller values of SSC. That is due to the inherent highly non-linear behavior of discharge and sediment suspension. The average SSC estimated by SRC method was about 17 mg/l whereas the averaged observed SSC was 14 mg/l.

A comparison between the performance of SRC method and other developed ANN models is summarized in Table 8.7. It was found that the RMSE did not vary too much among the three models. On the other hand, WANN and ANN were better than SRC in terms of MBE. The small absolute value of MBE means that the deviations between simulations and observations oscillated around the zero value, which is an indication of high simulation accuracy. In terms of DC, the ANN achieved the best results when compared to the other two models.

Considering all performance measures, it can be concluded that ANN showed the best results. Figure 8.6 shows the observed and computed time series via ANN, WANN and SRC models in daily time scales. It was found that the general behavior of sediment dynamics was captured by all methods except at few points. It was also noticed that although the accuracy in calculating the extreme values of sediment concentration was relatively low, the accuracy with respect to the lower values, was high by the developed ANN model. The sediment hydrograph in Figure 8.6 illustrates that most of the observed values of sediment concentration were simulated with significant high degree of accuracy, where a considerably good value of DC (0.52) for a real prediction was achieved. Finally, it could be pointed out that ANN performed better than the other models.

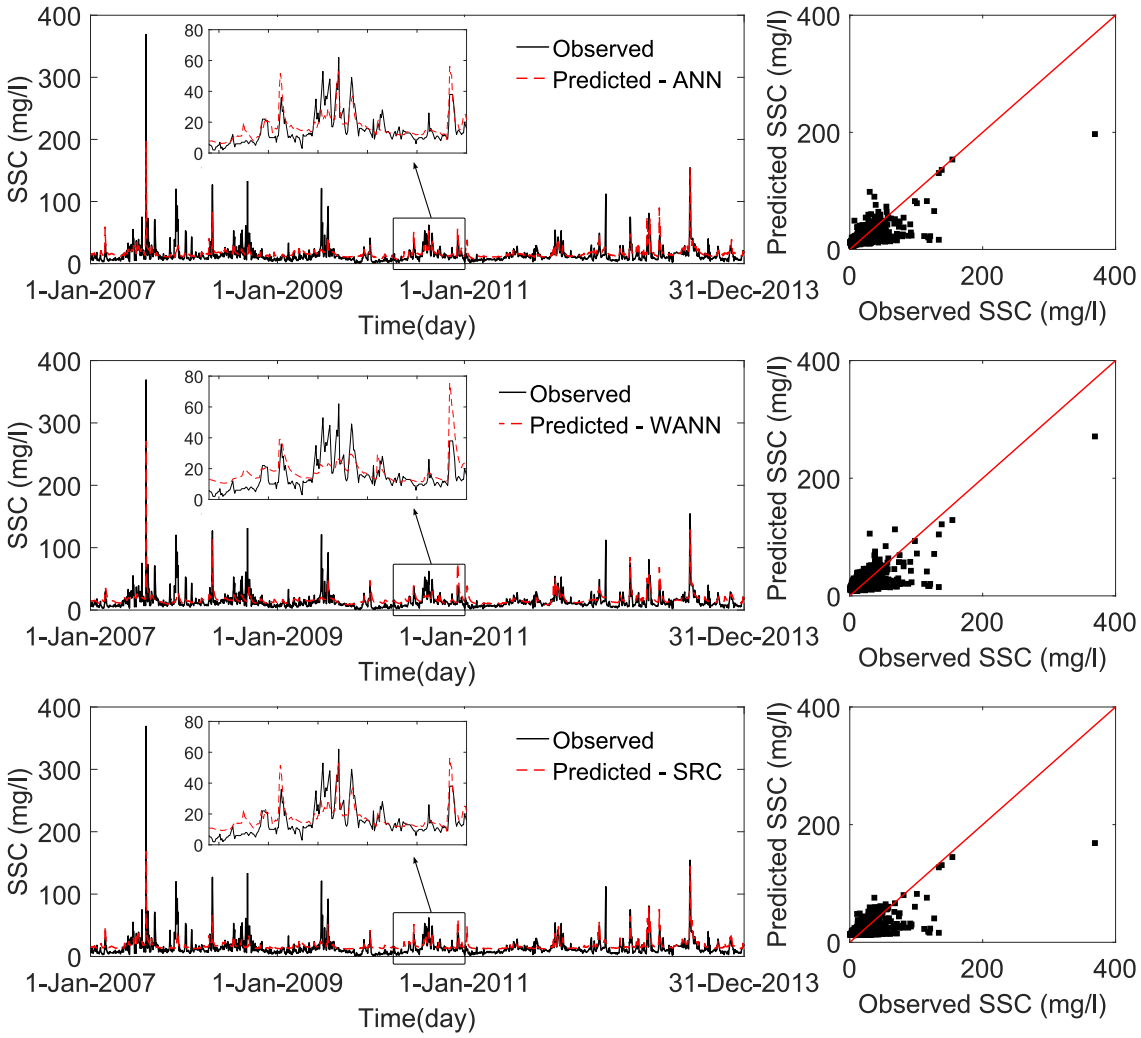

Figure 8.6: Comparison between the measured and the predicted SSC values during the validation phase.

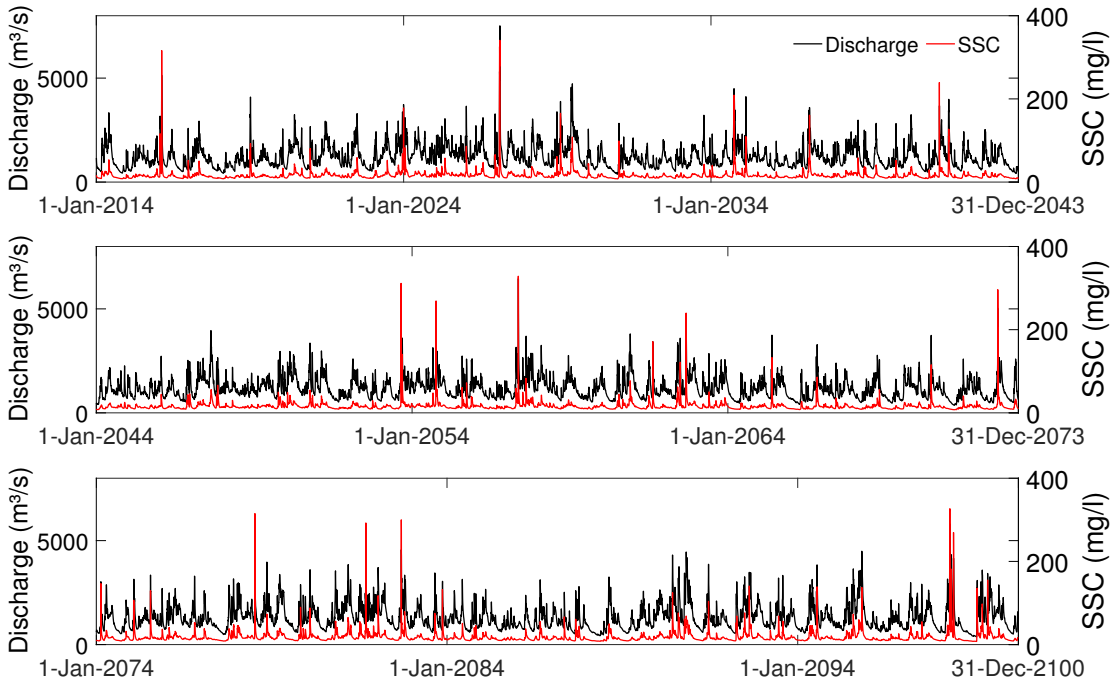

Figure 8.7: Long-term projected SSC till the year 2100 based on the projected discharge from KLIWAS program.

8.5.4 Long-term forecasting using the best model

By applying the best structure of ANN model and using the simulated discharge from KLIWAS program, long-term suspended sediment concentration at the Iffezheim reservoir was projected up to 2100. The results are shown in Figure 8.7. According to the results, the SSC matched well with the behavior of the discharge. The averaged projected SSC at the Plitterdorf station was 9 % less than the historical data, whereas the averaged projected discharge was only 2 % less. The maximum projected SSC was 340.74 mg/l (see Table 8.8), which is smaller than the maximum value of 742 mg/l of the historical data set (see Table 8.2). It should be noted that the application of ANN was bounded by some conditions. Accurate estimation of the sediment concentration for data which are out of the range of the learning pattern data was not possible. However, this problem was addressed by feeding the models with wide data range.

Table 8.8: Statistics of the long-term projected SSC values (till the year 2100) and historical data sets from 1978 to 2013.

	Mean (mg/l)	Max (mg/l)	Min (mg/l)	SD (mg/l)	COV (-)	Csx (-)	Kurtosis (-)
SSC_{his}	18.39	742	1	20.00	1.08	12.42	303.16
SSC_{pre}	16.70	340.74	1	13.12	0.78	10.95	197.93

8.6 Summary

The prediction of the amount of sediment that might be deposited in a reservoir is necessary for better management. Here the long-term sediment concentration of the Iffezheim reservoir in the Upper Rhine in Germany was predicted. Three models were applied for simulating the SSC; namely ANN, a WANN and SRC models. The expected discharge by 2100 was obtained from the KLIWAS program from the Federal Institute of Hydrology in Germany. The prediction performance of the models were evaluated using root mean square error, mean bias error and coefficient of determination. Dislike the traditional procedures (historical re-forecast) for applying AI, in this research the real forecast model of ANN and WANN were setup without involving any future SSC data. Comparing the results of three models indicated that the ANN model can predict the complex SSC time series more precisely and provides a realistic stream-sediment concentration behavior. The input combination with one day ahead SSC, one day ahead Q and current Q showed the best agreement with the observations. It was found that the WANN model has a limited accuracy due to the boundary effect. The SRC could capture the general behavior, though, lower and high values were less accurately projected. It can be concluded that ANN model is suitable for long-term prediction of suspended sediment. The projected SSC values will subsequently be used for estimation of long-term sediment budget in the Iffezheim reservoir till the year 2100.

Chapter 9

Evaluation of approaches and development of a simplified coupled concept

9.1 Evaluation of approaches

In the framework of the project "Assessment of long-term fine sediment budget in the Upper Rhine", four approaches were developed and applied to the study area of the Iffezheim barrage to examine their practical applicability. These were model reduction (see chapter 5), upscaling approach based on grouping boundary conditions (see chapter 6), time series analysis and synthesis (see chapter 7), and artificial neural networks (see chapter 8). All methods have advantages and limitations for their particular application and in this chapter, these aspects, previous unexpected results and future perspectives about the four approaches are discussed.

Using numerical models, sediment transport processes, erosion and deposition within river environments can be effectively simulated. The prerequisite for this is a precise record of the prevailing hydraulic behaviour, which characterizes the fluvial system. The non-linear behaviour of the sediment transport can thereby be represented and the unsteady flow can be taken into account. Some natural effects such as delay, attenuation, amplification and externally impacting factor (e.g. dredging management) etc. can be modelled. Using these models, it is possible to simulate and visualize the sections of the river where erosion and deposition occur in three dimensions. Thus, a high-resolution 3D model was initially set up for the study area. It was possible to estimate how well the model could represent the real world. For example, the curved channel with helical flow

in the reservoir could be simulated. Afterwards, in order to ensure running the 3D model over a long period, the high-resolution model was coarsened both spatially, temporally, and number of sediment fractions was reduced only minor affecting the quality of the results. In this way, the reduced 3D model contributed to large savings of computation time. However, even only the method of model reduction was not sufficient to simulate a long-term period, e.g. 100 years, in practicable computation time.

A further possibility for reducing the computational effort is upscaling approach based on the classification of boundary conditions. In this approach, the time-consuming instationary simulations was replaced by precalculated series of simulations with stationary boundary conditions. The measured discharge and sediment concentration values are divided into classes of equal size. For each of these classes, a representative discharge and concentration value was determined, so that several events are represented by one computational run. This upscaling approach is especially applicable for the long-term when compared to short-term periods, since long-term periods include some averaging behaviour.

Also, the time series analysis is a suitable tool for producing the model boundary condition - discharge and can also be used for computing morphodynamic evolution. In time series analysis, mathematical methods are used to first eliminate a trend, jump, periodicity of available observations, e.g., discharge time series. Then in conjunction with a auto-correlative and pure random components, synthetic time series were generated, which provided statistically possible time series. Applying a time series analysis is not complicated, but the predictions of future daily volume change required a large number of measurements. Moreover, non-unique relationship from the measured data sets could not be captured by the time-series analysis, e.g., SSC vs. discharge, SSC vs. volume change rate. A time series analysis of the sediment budget would therefore only provide valid predictions in case that the boundary conditions remain in similar ranges, but this can not be expected. Hence, the time series analysis are used here to improve the prediction of the temporal development of boundary conditions, e.g., discharge time series. These values can then be used as input parameters for other models, to finally calculate the sediment budget. Additionally, it should be noticed that the number of model parameters in the application should be kept low so that the sum of used model parameters does not exceed an experience value, as described in Maniak (1997). Short time steps, e.g., days are rarely chosen, commonly months are applied.

Artificial neural network (ANN) is a method that is capable of recognizing any functional relationships such as the relationship between discharge and SSC in data. However, the construction of an ANN model is much more complicated than the application of

a time series analysis. The ANN is a black-box model that consists of neurons which are interconnected and represent the relationship between input and output parameters. To construct a suitable ANN model, the number of neurons and neuron layers has to be determined. Additionally, the type and number of input neurons have to be tested so that an optimal result can be achieved. For the training phase, which serves to determine the weighting between the neurons, a smaller number of measured values is sufficient in order to achieve as good results as those of time series analysis. The ANN is a robust and flexible data-driven model that is capable of recognizing patterns, learning and mapping them. Similar to time series analysis, the ANN can only properly reproduce relationships that are known from the learning process, i.e. from the available measurements. Therefore, the quality of the measured data is of great importance. Additionally, "over-fitting" and "under-fitting effect" can occur during ANN modelling, i.e., the simulated values could lead to unrealistic high or low values.

In the following section, the discussed methods will be combined to use their advantages.

9.2 Coupled simplified concept

9.2.1 Concept

Diagram flowchart of the developed coupled concept is shown in Fig. 9.1. The aim is to achieve a quantitatively and qualitatively good result with low computation time.

The prediction of the future riverbed changes ΔV is, of course, only possible by using predicted discharge (Q_{pred}) and sediment concentration values (SSC_{pred}), which can be simulated based on the past values. In this study, the time series of daily discharges from 1923-2013 and suspended sediment concentrations from 1978-2013 are available. Time-series analysis and synthesis is carried out to forecast future discharge values (AP3). The ARIMA model proved to be suitable to simulate monthly discharge values (see chapter 7). In addition, artificial neural network (AP4) could also be applied for this purpose. In this work, however, the daily discharge values from the KLIWAS program were available. These values are subject to a much more differentiated consideration and are therefore used for the calculation. The daily suspended sediment concentration values associated with the discharge values are determined by the artificial neural network.

In the next step, the simulated input parameters are grouped using the upscaling approach based on classification of boundary conditions. In order to determine the daily volume change of representative discharge and concentration values, the reduced

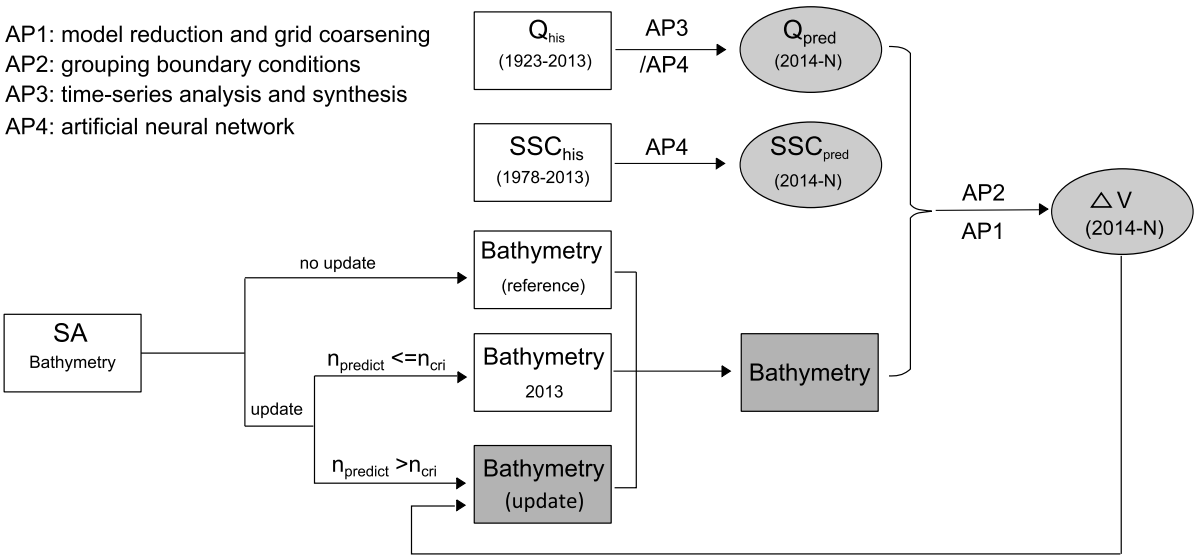

Figure 9.1: Flowchart of workflow for estimating evolution of fine sediment budget in the Iffezheim reservoir; grey marked: predicted future values; AP: approach process; SA: sensitivity analysis; n_{crit}: chosen critical time period; $n_{predict}$: predicted time period.

model (AP1) is applied instead of high-resolution model for saving computation time. By summing up the simulated values of daily volume changes, the total volume change for a certain period is obtained.

The basic idea of the developed concept (AP2) was to replace instationary long-term simulations by a precalculated series of simulations with stationary boundary conditions. However, while simulating over a long period, the elevation of the riverbed has changed. It could affect the hydraulic conditions in the channel and in turn potentially affect the riverbed volume change. Therefore, the question arise: Do the changes in morphology affect the volume change in the weir channel, how great is the influence of the altered riverbed bathymetry and is an updating of bathymetry required?

In order to answer these questions, a sensitivity analysis of various bathymetries on the simulated volume changes in the riverbed was carried out. An example is demonstrated in subsection 9.2.2. If the change of the bathymetry should also be considered, an updating becomes necessary using different criteria. In the diagram, n_{crit} stands for the critical time period for which the riverbed evolution is calculated under the assumption of a constant riverbed bathymetry. If the simulation time is shorter than critical time period, bathymetry of the year 2013 is used here for the future assessment. If the simulation time is longer, the bathymetry should be recalculated and updated for the next time period. It is, however, also possible to use the change in the water depth at a certain position or the change rate of the total volume in the weir channel as a further

criterion. If the bathymetry change is not sensitive to the simulated volume change, a reference bathymetry can be chosen for the further prediction.

9.2.2 Sensitivity analysis of bathymetry

9.2.2.1 Impacts on short-term volume changes

In order to determine the impact of bathymetry changes on the short-term[1] riverbed volume changes, three studies are carried out. The longest possible time period from 2006-2010 was **first** investigated. To record the influence of the bathymetry as accurately as possible, comparisons were performed using a simulation of an entire year.

Discharges between 1000 m^3/s and 2800 m^3/s with 200 m^3/s steps were chosen and the concentration values corresponding to discharge values were taken from the sediment rating curve (see Figure 9.2a), which was computed based on the historical data sets between 1927 and 2003. Similar to the boundary conditions, the observed bathymetry data at the respective beginning of the year were chosen. The results of daily volume changes are presented in Figure 9.2c. Discharge values smaller than 1400 m^3/s only have a small influence on the riverbed change. For higher discharges than this, a clear increase of the riverbed volume is shown, which reaches its maximum between 1800-2000 m^3/s for different bathymetries. Different values for volume changes at various bathymetries were only observed for discharge values of 1800 m^3/s and higher. All volume change values, except for 2006, reduced to a negative value. The reason for this exception in discharge values in 2006 was a period of extensive dredging in 2005. In the dredged areas, the channel cross-section was more increased so that the flow velocity was reduced, thereby resulting in higher deposition of sediment in the weir channel. For periods following the dredging event, the changes of channel cross-section always reduced with time, so that the volume change rate decreased as well.

In order to illustrate the influence of the individual discharge on the volume changes in the riverbed, the daily volume changes were multiplied with the frequency of the respective discharge values (see Figure 9.2b). Figure 9.2 demonstrates that a discharge, of 1600 m^3/s had a greater significance on the volume change than a discharge of 2000 m^3/s. Since the discharges of 1200 m^3/s were the most frequent, the maximum value from Figure 9.2 d) shifts to left in comparison with Figure 9.2c. The largest values are now between 1600-1800 m^3/s. In the long-term, therefore, these discharge values decisively determine the volume change in the riverbed. Figure 9.2 indicates that a large part of the simulated riverbed change was calculated almost independent of the bathymetry.

[1] different as defined in Chapter 6. It means here, shorter than 10 years.

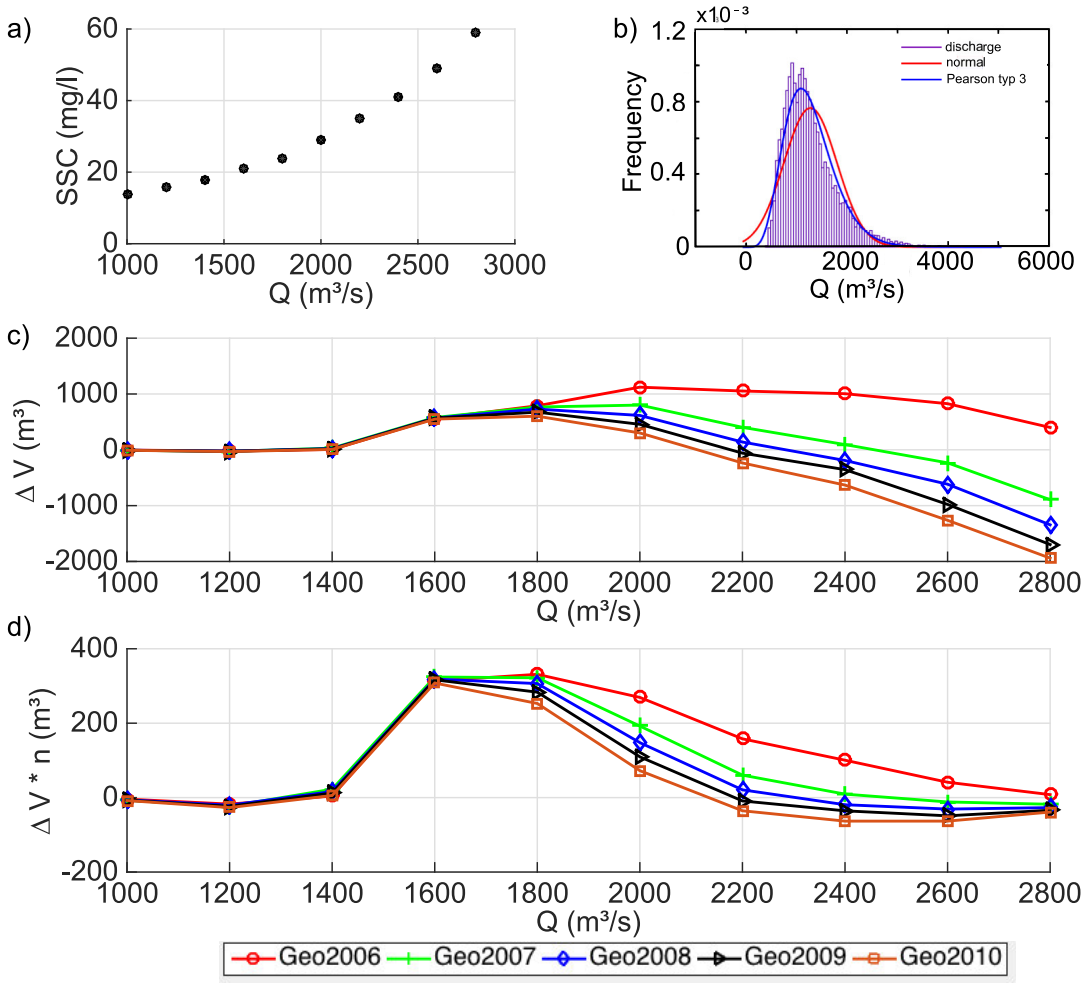

Figure 9.2: a) Discharge - suspended load concentration relationship as boundary condition; b) Frequency of discharge from 1927-2003; c) Riverbed volume change - discharge diagram for different bathymetries; d) Product of volume change and frequency of discharge, discharge diagram for different bathymetries.

Therefore, an update of the bathymetry for the long-term simulation was not necessary according to the results of this investigation.

Second, we assume that the riverbed bathymetry should be considered in this study area. The bathymetry was updated annually for the longest possible time period of 5 years. The results with and without updating the bathymetry of the riverbed are shown in Table 9.1. The results show that an annual adjustment of the channel bed simulates lower volume changes. The deviations of the total volume change are -48 % with annually updating and -24 % without updating during 5 years. The deviation is the difference between simulated and the measured total volume change related to the measurements. It can be observed that updating the bathymetry did not lead to any improvement in results in this case.

Table 9.1: Comparison of the calculated total volume changes for the longest time period with and without annually updating of bathymetry to measurements. The sums of results of long-term period are shown in bold.

Updating	Period	Duration (days)	$Meas_{total}$ (m^3)	$Simu_{total}$ (m^3)	Deviation (%)
With	2006	390	191199	91324	-52
	2007	365	135308	62053	-54
	2008	363	82322	34540	-58
	2009	382	78447	30028	-62
	2010	373	71149	26138	-63
	2006-2010	**1873**	**558425**	**244083**	**-48**
Without	**2006-2010**	**1873**	**473821**	**361122**	**-24**

Third, an investigation of daily riverbed volume changes with varied bathymetries in relation to dredging events was carried out. Three dredging events occurring in 2000, 2004 and 2005 were chosen (see Table 3.3). The simulations were performed with the bathymetry before and after dredging event under steady state conditions with an average discharge of 1500 m^3/s and a high discharge of 2600 m^3/s, respectively. The results of both simulations show that altered riverbed bathymetry has only minor influence on the daily volume changes (see Figure 9.3).

In all, the original cross-section shape of the river will be maintained through regular dredging. An intervention in the flow profile with a decisive effect on the volume change cannot be seen. In addition, the computational effort is reduced if the bathymetry updates were omitted.

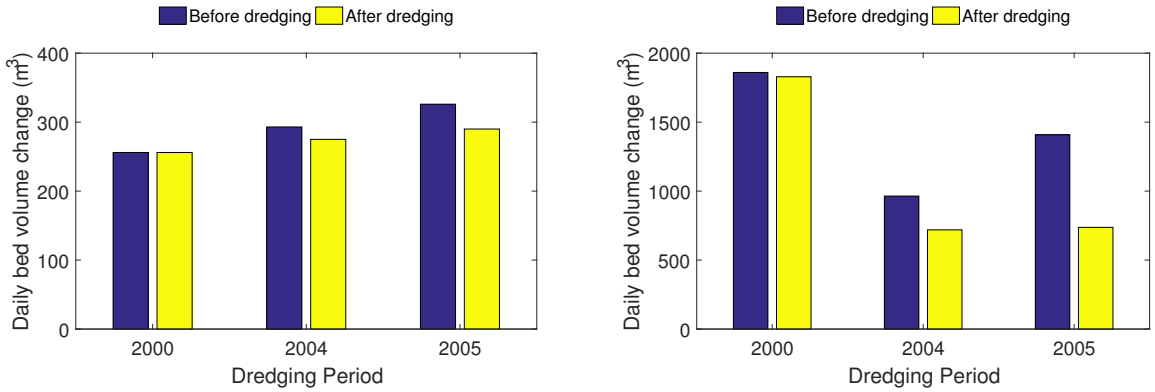

(a) Q = 1500 m³/s (b) Q = 2600 m³/s

Figure 9.3: Investigating of daily bed volume change with varied bathymetries in related to dredging events.

9.2.2.2 Impacts on long-term volume changes

In order to investigate the impact of bathymetry on the long-term[2] riverbed volume change, a sensitivity analysis of bathymetry of the year 2006, directly after a dredging event, and bathymetry of the year 2010, a long period without dredging, was carried out. Thereby, three time slices, each 30 years long, were chosen. The future periods, including the near future from January 2020 to December 2049 and the far future from January 2070 to December 2099 were investigated using on the KLWAS research results. The reference time slice was chosen from January 1980 to December 2009. 20 model results for predicting discharges till the year 2100 are available from the KLWAS program (Nilson et al., 2014). Among all the results, a time series with the most frequent discharges, between 1600-1800 m³/s, is chosen to investigate the range for which the highst deposition over a long-term period was expected (see Figure 9.2). Additionally, another criterion to choose this time series was the highest 75 % probability (upper quantile)[3] value. According to the statistical analysis, the time series with MAXA_C20-A1B_HCQ0_RE-BFG_ls_EPW_HBV-134 fulfilled both criteria, and thus was used for the simulation. The discharges above 1800 m³/s have a proportion of 13 %, 18 % and 22 % for the reference, near and far future periods.

The results are given in Table 9.2. They indicate that the discharge in the future shows an increasing trend. For the chosen series the discharges increase by 12 % for the

[2]longer than 10 years

[3]The upper quantiles of a set of values divides them so that 75 % of the values lie below and 25 % of the values lie above.

Table 9.2: Sensitivity analysis of riverbed bathymetry on the long-term riverbed volume change; * Assumption: No erosion occurred, if discharges less than 2600 m³/s; Devi: deviation to reference time slice.

Initial bathymetry	Reference (1980-2009)		Near future (2020-2049)				Far future (2070-2099)			
	Q_{mean} (m³/s)	$\triangle V_{total}$ (10^6 m³)	Q_{mean} (m³/s)	Devi (%)	$\triangle V_{total}$ (10^6 m³)	Devi (%)	Q_{mean} (m³/s)	Devi (%)	$\triangle V_{total}$ (10^6 m³)	Devi (%)
2006	1264	1.86	1401	11	2.08	12	1435	14	2.05	10
2010		0.49			-0.36	-173			-0.59	-220
* Assumption										
2006	1264	2.77	1401	11	3.10	12	1435	14	3.06	11
2010		1.73			1.04	-40			0.87	-49

near future and by 14 % for the far future. The total simulated riverbed change for the 30 year reference time slice using the bathymetry of the year 2006 was $1.86 \cdot 10^6$ m³. In the near and far future, the volume of the riverbed change increases by 12 % and 10 %, respectively, due to the increasing discharge. The total simulated riverbed changes using the bathymetry of the year 2010 have a volume of $0.49 \cdot 10^6$ m³ for the 30 year reference time slice. The riverbed shows much higher erosion with increasing discharge in the future. The total riverbed change were $-0.36 \cdot 10^6$ m³ and $-0.59 \cdot 10^6$ m³. This can be explained using Figure 9.2c. The bathymetry of 2006 provided only the positive daily volume changes till the discharge of 2800 m³. For bathymetry of the year 2100, the simulated daily volume changes have a peak at a discharge of 1800 m³/s and turned to negative values from 2100 m³/s onward. Moreover, the negative daily volume changes occurred due to the increasing discharges which have a much larger effect on the erosion volume than on the deposition.

In these three time slices the discharges above 1800 m³/s have a proportion of 13 %, 18 % and 22 % for the reference, near and far future. However, according to the research of Hillebrand et al. (2015), the critical discharge for the occurrence of erosion in the weir channel is 1500 m³/s, which means that the discharge at the boundary condition is 2600 m³/s[4]. Hence, we assume that the erosion could not occur, if the model inflow is less than 2600 m³/s. The results under this assumption are also listed in Table 9.2. Moreover, these results indicate that this assumption has a high impact on the bathymetry during the year 2010. The predicted volume changes in the Iffezheim reservoir for three time slices are $1.73 \cdot 10^6$ m³, $1.04 \cdot 10^6$ m³, $0.87 \cdot 10^6$ m³, respectively.

Comparing the results using bathymetries of the years 2006 and 2010, it can be

[4]In case of operation of 4 turbines, discharge with a constant value of 1100 m³/s flow to the hydropower station.

concluded that the long-term riverbed volume change is very sensitive to the bathymetry. For the future simulations, neither the bathymetry directly after the dredging (i.e. 2006) nor the bathymetry after deposition over some years (i.e. 2010) are suitable. Thus, a bathymetry of year 2007, which provided an average value, could be used as the reference riverbed.

9.2.2.3 Summary of updating bathymetries

The investigation of bathymetry updating suggested firstly that much riverbed volume change occurs almost independently of the bathymetry (see subsecion 9.2.2.1). Secondly, considering the computational efficiency of long-term simulation, the updating of bathymetry is not necessary here (see subsecion 9.2.2.2). Therefore, a bathymetry update for the long-term simulation will not be considered in the next study. For the long-term simulation, e.g., estimating volume changes till 2100, a reference bathymetry should be chosen. The simulated average annual volume change arising from this reference bathymetry should be similar to the average annual volume change measurement from e.g. 2000-2011. From a practical point of the view, bathymetry of 2007 is recommended to be used for predicting the evolution of fine sediment in the reservoir.

9.2.3 Assessment of long-term riverbed evolution concerning deposition and erosion quantity till the year 2100

With the aid of the concept presented in section 9.2.1 and the reference bathymetry of the year 2007, a long-term projection of riverbed evolution till the year 2100 was carried out. The projection was simulated under a couple of assumptions: First, one projection of the discharge from the KLIWAS program was selected as an example, because the discharge would possibly increase due to the global warming. A projection was accordingly selected that a maximum effect could be expected. The corresponding suspended sediment concentrations were determined by the ANN model. Second, it was assumed that the riverbed would be almost perfectly maintained. Third, all other boundary conditions remained the same (e.g. operation of the hydropower or weir control). The presented results did not consider the operation of the 5^{th} turbine at the hydropower station. Due to the reduced inflow to the weir channel, if the 5^{th} turbine is operating, less accumulations are expected.

Table 9.3 lists the simulation results, which are divided into five time slices. The reference time period is between the years 1980 and 2009. Two future time slices are considered; these can be distinguished as near future (2020-2049) and far future (2070-

Table 9.3: Prediction of long-term riverbed volume change using reference bathymetry (2007) till the year 2100; *: Deviation compared to reference period; BTS stands for Between Time Slice; Propn. of domi. Q states for proportion of dominant Q, which has the value between 1600-1800 m^3/s.

		Reference (1980-2009)	BTS 1 (2010-2019)	Near future (2020-2049)	BTS 2 (2050-2069)	Far future (2070-2099)
ΔV	Sum (10^6 m^3)	2.107	0.661	2.786	1.886	3.409
	Annual (10^6 m^3)	0.070	0.073	0.093	0.094	0.114
	Deviation* (-)	1	1.045	1.328	1.342	1.629
	Scaled annual (10^6 m^3)	0.118	0.123	0.156	0.158	0.191
	Sum of all periods (10^6 m^3)			10.849		
Q	Qmean (m^3/s)	1264	1045	1401	1162	1435
	Deviation (-)	1	0.83	1.11	0.91	1.15
	Propn. of domi. Q (%)	6.634	4.570	6.890	6.910	6.361
	Propn. of Q > 1800 m^3/s (%)	11.389	9.940	13.178	11.840	16.137

2099) periods. The interim periods BTS 1 (2010-2019) and BTS 2 (2050-2069) are also included for completeness. BTS stands for Between Time Slice. The sums of total volume changes for each period are shown in Table 9.3, e.g., a total volume change of $2.107 \cdot 10^6$ m^3 is simulated for the reference period. In addition, average annual volume changes are calculated in order to observe a trend in the results. The results show that the sediment deposition increases in the near future by approx. 33 %, whereas in the far future up to 63 % higher sediment deposition compared to the reference time slice are expected.

In the reference period, an annual volume change of 70,000 m^3 is simulated, whereas the measured volume change is 118,000 m^3 (see Table 3.5). In order to obtain appropriate prospective volume changes, the simulated volume change for each period is scaled towards the measured amount. This value is shown by scaled annual in the table. After all, the riverbed volume change till the year 2100 can be assessed by adding up the volume changes in each period and it is $10.849 \cdot 10^6$ m^3 in total.

The results indicate that a clear increased volume changes are projected in the future. Under the above mentioned assumptions more extensive dredging management will be necessary in the future in order to ensure operability of the weir channel. Moreover, it is also clear that the volume change is not linearly related to the discharge.

Chapter 10

Conclusions and recommendations

Conclusions

In this thesis a concept to predict the long-term fine sediment budget for the Iffezheim reservoir with reasonable accuracy and an acceptable calculation time is presented. This concept links advantages of several methods, which are described in chapters 5 to 8. Using this concept, it should be possible to forecast the long-term sediment budget, even for the far future (up to 2100).

The first focus of this thesis is the application of a high-resolution 3D model to assess the riverbed evolution, to capture multi-dimensional flow effects in front of a barrage as accurately as possible and to represent the local erosion and sedimentation in a realistic manner. Thus, it was possible to determine the influence of the different discharges on the riverbed in the weir channel of the Iffezheim reservoir. In order to estimate the sediment management (e.g. dredging measures) for the long-term accumulation, it is necessary to establish a 3D model that is capable to simulate long-term periods in a reasonable computation time. For this purpose, a high-resolution 3D model was set up, whereby dynamic natural flow behaviour is modeled as detailed as possible using unsteady state simulations. However, due to the large number of cells in 3D model huge computation time is required for a simulation period till the year 2100. Therefore, 3D numerical models either need to be treated with reduced complexity or combined with extended approaches.

In the next step an optimization of the model was performed by reducing the computation time with only minor affects on the quality of the results. After coarsening the grid and increasing the time step size, the investigation was carried out to determine if 3D-flow effects, such as helical flow in the weir channel and secondary flows at the channel walls, could be taken into account. Additionally, restricting the number of grain

fractions to seven proved to be a meaningful simplification for representing the sediment material in the river Rhine, without negatively affecting the prognosis of the deposits and erosion volumes. The reduced 3D model contributed to large savings of computation time by 76 %, while the solution accuracy remains similar (5 % deviation) when compared to high-resolution results.

Moreover, the computationally time-consuming unsteady simulations were replaced by a precalculated series of simulations with stationary boundary conditions using an upscaling approach. The boundary conditions of the numerical model - the discharge and the suspended sediment concentration - are grouped into classes; in consequence not every single event has to be simulated separately. The amount of the deposition for a certain period can then be obtained by adding up the calculated daily depositions in each class. This procedure reduced the calculation time to 2.5 % of the unsteady calculations. For long-term simulations (years) deviations to the measurements were up to 20 %, while for short-term periods (months) much bigger deviations were determined. The choice of an appropriate class scale, by which discharge and concentration values should be grouped, is important. On one hand, a too large scale is not appropriate, since then calculated average values would no longer be representative for the entire group and this would adversely affect the accuracy of the results. On the other hand, this class scale should not be too small, in order to keep the computational time within reasonable bounds. The upscaling approach based on the classification of boundary conditions is especially useful for long-term simulations, since the consideration of long-term periods involves some averaging behaviour and also that extreme events are offset to some extent. It should be also noticed that the amount of volume change can be simulated efficiently, but the position of deposition or erosion cannot be assessed as accurately as with a numerical model.

For assessing the volume change in the future, a prediction of two important input parameters of the numerical model - discharge and suspended sediment concentration - are required. If this data were not available, both time-series analysis and synthesis and artificial neural networks (ANN) provide possibilities for forecasting future input parameters. The time series synthesis is a mathematical method which generates predicted values for a wide variety of parameters in a purely statistical way and provides possible time series. Its application is simple, but it requires a large number of measurements and it cannot account for non-unique relationships. Hence, this method is here used to improve the prediction of the temporal development of boundary conditions, e.g. discharge. However, the number of related variables should be kept low. Thus, short time steps, e.g. days, are rarely chosen, commonly months are applied. In this study, various

models are investigated to predict the monthly flow. The ARIMA model, a method of time series analysis, calculating trend and annual periodicity, presents the best results with determination of coefficient (DC) by 0.61.

Artificial neural network (ANN) is a black-box model which represents relationships between input and output variables including non-unique relationships. It is often used to compute a relationship between Q and SSC. For this work, the KLIWAS projected daily discharge was used. ANN was applied for the prognosis of long-term (until 2100) daily suspended sediment concentration values. The ANN model showed the best agreements in predicting the daily suspended sediment concentration and achieved a considerably good value of DC (0.52).

The predicted discharge and concentration values were then classified using the coupled upscaling approach. Morphological bed evolution of Iffezheim reservoir by deposition and erosion was calculated till the year 2100 based on bed level surveys and the reduced numerical model. The amount of riverbed changes is simulated with $10.849 \cdot 10^6$ m^3 using the developed simplified coupled concept in this work. In comparison to the present amount, the riverbed changes will increase by 33 % in the near future and by 63 % in the far future. This means that, under the assumptions of increased discharge until 2100, perfect maintenance of the riverbed and keeping the boundary conditions (e.g., the operation of the hydropower station and the weir control) more dredging management will be necessary in the future.

Recommendations for research and practitioners

The following recommendations are offered for further related research and practical applications.

1. The numerical model - SSIIM allows the simulation of key sediment transport processes and facilitates qualitative and quantitative impact assessment of measures in terms of both deposition and erosion in reservoirs. To estimate residence times of contaminant in the impounded section of Rhine River, an extension in the SSIIM program is recommended. This extension should have the ability to cover the characteristic of the existing cohesive sediments regarding the formation of flocculation (Klassen, 2017). In this manner the behaviour of containment concentrations over a long-term period could also be assessed. Particular attention should be paid to the number of sediment fractions. The sensitivity study carried out in section 5.3 should be further investigated.

2. Another way of reducing the computation time, related to chapter 5 (3D model reduction), is the implementation of a morphological factor in the SSIIM model, called MORFAC factor. The morphology then does not have to be updated after each hydraulic computation.

3. In order to make the prediction for the study area Iffezheim more realistic, it is recommended to consider the operation of the fifth turbine.

4. By using upscaling approach in chapter 6, an error correction factor was applied during the results evaluation. It had little positive effect on the calculations in this study. Nevertheless, its application and effect to other areas could be useful and it is suggested to be further investigated.

5. In chapter 7 (time-series analysis and synthesis) the monthly discharges are predicted based on exclusively historical discharge data.

6. A study comparing the different methods is recommended to be carried out: prediction of long-term monthly sediment volume changes using time-series analysis and synthesis of chapter 7 or ANN models of chapter 8 vs. the coupled concept of chapter 9, thereby the downscaling of predicted monthly discharges in daily discharges should first be carried out.

7. From a practical viewpoint, the developed coupled concept can be applied to other river sections in the Upper Rhine and to other rivers with barrages. Due to the considerable reduction of the computing time, large-scale study areas can likewise be investigated. The coupled concept could prove its practical applicability for the long-term assessment of fine sediment budget of the entire Upper Rhine, particularly in the area of the 10 barrages, where 3D currents have a significant influence. The river sections in the Upper Rhine between 2 barrages could be simulated with a 1D model and linked to the coupled concept for the barrage areas. This might improve the estimation of the sediment budget on a large scale.

8. With the long-term predictions methods of this work and similar comprehensive data bases, the extent of dredging measurements for the maintenance of waterways of other impounded rivers can be estimated.

References

Adamowski, J. and Chan, H. (2011). A wavelet neural network conjunction model for groundwater level forecasting. *Journal of Hydrology*, 407(1-4):28–40.

Addison, P. (2002). *The Illustrated Wavelet Transform Handbook: Introductory Theory and Applications in Science, Engineering, Medicine and Finance*. Crc press edition.

Aksoy, H. and Dahamsheh, A. (2009). Artificial neural network models for forecasting monthly precipitation in Jordan. *Stochastic Environmental Research and Risk Assessment*, 23(7):917–931.

Aljoumani, B., Sànchez-Espigares, J., Cañameras, N., Josa, R., and Monserrat, J. (2012). Time series outlier and intervention analysis: Irrigation management influences on soil water content in silty loam soil. *Agricultural Water Management*, 111:105–114.

Aljoumani, B., Zhang, Q., Hillebrand, G., Hoffmann, T., Sanchz, J., and Hinkelmann, R. (2017). Forecasting monthly inflow discharge of the Iffezheim reservoir using data-driven models.

Andale (2016). Parsimonious Model: Definition, Ways to Compare Models. [online] <http://www.statisticshowto.com/parsimonious-model/> [Accessed 22/06/2017].

Araghinejad, S. (2014). *Data-Driven Modeling: Using MATLAB® in Water Resources and Environmental Engineering*, volume 67 of *Water Science and Technology Library*. Springer Netherlands, Dordrecht.

ASCE (2000). Artificial neural Network in Hydrology. I: Preliminary Concepts. *Journal of hydrologic Engineering*, 5(2):115–123.

Astor, B., Gehres, N., and Hillebrand, G. (2014). Von der Quelle zur Mündung, eine Sedimentbilanz des Rheins. Technical report, Bundesanstalt für Gewässerkunde, Koblenz.

Baareh, A., Sheta, A., and Khnaifes, K. (2006). Forecasting River Flow in the USA : A Comparison between Auto-Regression and Neural Network Non-Parametric Models. *Journal of Computer Science*, 2(10):775–780.

BAW (1980). *Mitteilungsblatt Bundesanstalt für Wasserbau, Nr. 47.* Number 47. Karlsruhe.

Beale, M., Demuth, H., and Hagen, M. (2016). Neural Network Toolbox User' s Guide How to Contact MathWorks. *MathWorks*, (June):2–3.

Beckman Coulter Life Sciences (2017). Beckman Coulter Life Sciences [online] <http://www.beckmancoulter.de/> [Accessed 15/03/2017].

Bergström (1995). The HBV model. In Singh, V., editor, *Computer Models of Watershed Hydrology*, chapter 13, pages 443–476. Water Resources Publications.

BfG (2016). Sedimentbilanzen in Flussgebieten - von der Quelle bis zur Mündung. In *17. Gewässermorphologisches Kolloquium*, Koblenz.

BMVI (2015). KLIWAS-Auswirkungen des Klimawandels auf Wasserstraßen und Schiffahrt in Deutschland. Technical report, Bundesministerium für Verkehr und digitale Infrastruktur.

Boettcher, G. (2001). Geschiebezugabe am Rhein unterhalb Iffezheim. In *Kolloquium Geschiebebewirtschaftung an schiffbaren Flüssen, Untersuchungsmethoden und Wirkungsweise,*, Karlsruhe. Bundesanstalt für Wasserbau.

Box, G., Jenkins, G., and Reinsel, G. (1976). *Series Analysis Forecasting and Control.* Holden-Day, San Francisco, first ed. edition.

Brockwell, P. and Davis, R. (1987). *Time Series: Theory and Methods.* Springer.

Burg, J. (1967). Maximum entropy spectral analysis. In *37th Annual International SEG Meeting*, Oklahoma City.

Cannas, B., Fanni, a., Sias, G., Tronci, S., and Zedda, M. K. (2005). River flow forecasting using neural networks and wavelet analysis. 7.

Chen, J., Finlayson, B., Wei, T., Sun, Q., Webber, M., Li, M., and Chen, Z. (2016). Changes in monthly flows in the Yangtze River, China - With special reference to the Three Gorges Dam. *Journal of Hydrology*, 536:293–301.

Cheng, N.-S. (1999). Closure to "Effect of Concentration on Settling Velocity of Sediment Particles" by Nian-Sheng Cheng. *Journal of Hydraulic Engineering*, 125(3):317–317.

Chien, N. and Wan, Z. (1998). *Mechanics of sediment transport*.

Chien, N. and Wan, Z. (1999). *Mechanics of Sediment Transport*. American Society of Civil Engineers, Reston, VA.

Cigizoglu, H. (2003). Estimation, forecasting and extrapolation of river flows by artificial neural networks. *Hydrological Sciences Journal*, 48(3):349–361.

Cigizoglu, H. and Alp, M. (2006). Generalized regression neural network in modelling river sediment yield. *Advances in Engineering Software*, 37(2):63–68.

Cigizoglu, H. and Kisi, O. (2006). Methods to improve the neural network performance in suspended sediment estimation. *Journal of Hydrology*, 317(3-4):221–238.

Çimen, M. (2016). Estimation of daily suspended sediments using support vector machines Estimation of daily suspended sediments using support vector machines. 6667(August).

Dahamsheh, A. and Aksoy, H. (2013). Markov Chain-Incorporated Artificial Neural Network Models for Forecasting Monthly Precipitation in Arid Regions. *Arabian Journal for Science and Engineering*, pages 2513–2524.

Daubechies, I. (1992). *Ten Lectures on Wavelets*. SIAM, PHILADELPHIA.

Dickey, D. (1976). *Estimation and hypothesis testing in nonstationary time series*. Phd dissertation, Lowa State University.

Dietrich, W. (1982). Settling velocity of natural particles. *Water Resour. Res.*, 18(6):1615–1626.

Doeglas, D. (1968). Grain-Size Indices, Classification and Environment. *Sedimentology*, 10(2):83–100.

Dogan, E., Isik, S., Toluk, T., and Sandalci, M. (2007). Daily streamflow forecasting using artificial neural networks. *International Congress on River Basin Management*, pages 449–459.

Egiazaroff, I. (1965). Calculation of non-uniform sediment concentration. *Journal of the Hydraulics Division*, 91(4):225–247.

Einstein, H. (1950). The bed-load function for sediment transportation in open channel flow. Technical report, United States Department of Agriculture, Washington D.C.

Farajzadeh, J., Fakheri Fard, A., and Lotfi, S. (2014). Modeling of monthly rainfall and runoff of Urmia lake basin using "feed-forward neural network" and "time series analysis" model. *Water Resources and Industry*, 7-8(2014):38–48.

FGG Rhein (2015). Der Oberrhein. [online] <http://www.fgg-rhein.de/servlet/is/4264/> [Accessed 17/03/2017].

Fiering, M. (1972). *Streamflow synthesis*. Cambridge, Harvard University Press, Massachusetts.

Fischer-Antze, T., Olsen, N. R., and Gutknecht, D. (2008). Three-dimensional CFD modeling of morphological bed changes in the Danube River. *Water Resources Research*, 44(9):n/a–n/a.

FlowCam (2017). FlowCam dynamic imaging particle analysis [online] < http://www.fluidimaging.com> [Accessed 18/03/2017].

Folk, R. (1954). The distinction between grain size and mineral composition in sedimentary rock nomenclature. *Journal of Geology*, 62(4):344–359.

Folk, R. (1974). *The petrology of sedimentary rocks: Austin, Tex.*

Freiburg, W.-u. S. W. (2011). Sachstandsbericht oberer Wehrkanal Staustufe Iffezheim - Technische report - Upper weir channel of the Iffezheim hydropower reservoir. Technical report.

Frings, R., Gehres, N., Promny, M., Middelkoop, H., Schüttrumpf, H., and Vollmer, S. (2014). Today's sediment budget of the Rhine River channel, focusing on the Upper Rhine Graben and Rhenish Massif. *Geomorphology*, 204:573–587.

Gehres, N., Hoffmann, T., and Hillebrand, T. (2016). Von der Quelle zur Mündung, eine Sedimentbilanz. In *17. Gewässermorphologisches Kolloquium*, Koblenz.

Griffin, R. (1995). *Engineering and design - Sedimentation investigations of rivers and reservoirs*. Department of the army U.S. Army Corps of Engineers, Washington, DC.

Han, Q. (1979). A study on the non-equilibrium transport of non-uniformly graded suspended sediment. *Chinese Science Communication*, 17:808 (in Chinese).

Han, Y., Ye, Q., and Roelvink, J. (2014). Modeling on the estuarine turbidity maximum of Yangtze estuary before and after the regulation works using z-model. In *Coastal Engineering Proceedings*, pages 1–7.

Haun, S., Kjærås, H., Løvfall, S., and Olsen, N. (2013). Three-dimensional measurements and numerical modelling of suspended sediments in a hydropower reservoir. *Journal of Hydrology*, 479:180–188.

Henze, E. (1989). *Technik und Humanität: Johann Gottfried Tulla*. Mannheim, quadrate-b edition.

Hervouet, J. (2007). *Hydrodynamics of free surface flows: Modelling with the finite element method*. New York, wiley & so edition.

Hillebrand, G. (2008). *Transportverhalten kohaesiver Sedimente in turbulenten Stroemungen-Untersuchungen im offenen Kreisgerinne*. PhD thesis, Universität Fridericiana zu Karlsruhe.

Hillebrand, G. (2012). Sedimentation im Wehrkanal Iffezheim - räumliche und zeitliche Dynamik. In *Bundesanstalt für Gewässerkunde*, Koblenz.

Hillebrand, G., Klassen, I., Olsen, N., and Vollmer, S. (2012a). Modelling Fractionated Sediment Transport and Deposition in the Iffezheim Reservoir. In *10th International Conference on Hydroinformatics*, Hamburg.

Hillebrand, G., Otto, W., and Vollmer, S. (2012b). Findings from ADCP-Measured flow velocities and suspended sediment concentrations at the Upper Rhine. In *2nd IAHR Europe Congress*, Munich.

Hillebrand, G., Seidenkranz, U., and Noack, M. (2015). Untersuchungen zur Remobilisierbarkeit feiner Sedimente in der Stauhaltung Iffezheim am Oberrhein. In *Tagungsband des 45. IWASA*, pages 1–11, Aachen.

Hirt, C. and Nichols, B. (1981). Volume of fluid (VOF) method for the dynamics of free boundaries. *Journal of Computational Physics*, 39(1):201–225.

Ho, S. and Xie, M. (1998). The use of ARIMA models for reliability forecasting and analysis. *Computers & Industrial Engineering*, 35(1-2):213–216.

Huber, J. (2005). Die Umlagerung von Baggergut an der Staustufe Iffezheim und deren Wirkungen.

Hunziker, R. (1995). *Fraktionsweiser Geschiebetransport*. PhD thesis, Eidgenössischen Technischen Hochschule Zürich.

IPCC (2007). Fourth Assessment Report: Climate Change. Technical report.

Jacobsen, N., van Gent, M., and Wolters, G. (2015). Numerical analysis of the interaction of irregular waves with two dimensional permeable coastal structures. *Coastal Engineering*, 102:13–29.

Janhabi, M. and Ramakar, J. (2013). Time-series analysis of monthly rainfall data for the Mahanadi River Basin, India. *Sciences in Cold and Arid Regions*, 5(1):73.

Jia, D., Shao, X., Wang, H., and Zhou, G. (2010). Three-dimensional modeling of bank erosion and morphological changes in the Shishou bend of the middle Yangtze River. *Advances in Water Resources*, 33(3):348–360.

Jia, D., Shao, X., Zhang, X., and Ye, Y. (2013). Sedimentation patterns of fine grained particles in the dam area of the Three Gorges Project: 3D numerical simulation. *Journal of Hydraulic Engineering*, 139(6):669–674.

Joshi, R., Kumar, K., and Adhikari, V. (2016). Modelling suspended sediment concentration using artificial neural networks for Gangotri glacier. *Hydrological Processes*, 1366(November 2015):1354–1366.

Jothiprakash, V. and Vaibhav Gang, S. A. (2009). Artificial Neural Network. *J. Hydrol. Eng.*, 1(9):934 – 942.

Karamouz, M. and Araghineja, S. (2012). *Advance Hydrology*. Amirkabir University of Technology Press, Tehran, 1st edn. edition.

Karnahl, J. (2008). *2D numerische Modellierung von multifraktionalem Schwebstoff- und Schadstofftransport in Flüssen*. PhD thesis, Universität Stuttgart.

Karsoliya, S. (2012). Approximating Number of Hidden layer neurons in Multiple Hidden Layer BPNN Architecture. *International Journal of Engineering Trends and Technology*, 3(6):714–717.

Karunanithi, N., Grenney, W., Whitley, D., and Bovee, K. (1994). Neural networks for river low prediction. *Journal of Computing in Civil Engineering*, 8:201–218.

Khashei, M. and Bijari, M. (2010). An artificial neural network (p, d, q) model for timeseries forecasting. *Expert Systems with Applications*, 37(1):479–489.

Kheiashy, K., Mccorquodale, J., Georgiou, I., and Meselhe, E. (2010). Three dimensional hydrodynamic modeling over bed forms in open channels. *International Journal of Sediment Research*, 25(4):431–440.

Kisi, O. (2011). A combined generalized regression neural network wavelet model for monthly streamflow prediction. *KSCE Journal of Civil Engineering*, 15(8):1469–1479.

Klassen, I. (2012). Bericht der Iffezheim Staustufe. Technical report, Karlsruhe.

Klassen, I. (2017). *Three-dimensional numerical modeling of cohesive sediment flocculation processes in turbulent flows*. PhD thesis, Karlsruher Institut für Technologie (KIT).

Kopmann, R. and Schmidt, A. (2010). Comparision of different reliability analysis methods for a 2D morphdynamic numerical model of danube. In *River Flow*, page 6.

Köthe, H., Vollmer, S., Breitung, V., Bergfeld, T., Schöll, F., Krebs, F., and Landwüst, C. (2004). Environmental aspects of the sediment transfer across the Iffezheim barrage, River Rhine, Germany. In *Proc. 17th World Dredging Conference WODCON XVII*, Hamburg, Germany.

Kresser, W. (1964). Gedanken zur Geschieber und Schwebstofffführung der Gewässer. *Österreichische Wasserwirtschaft*, 16(1/2).

Kreus, A. (2008). *Fundamente Geographie*. Klett edition.

Krishna, B., Rao, Y. R. S., and Nayak, P. C. (2011). Time Series Modeling of River Flow Using Wavelet Neural Networks. *Journal of Water Resource and Protection*, 03(01):50–59.

Krumbein, W. and Aberdeen, E. (1937). The sediments of Barataria Bay [Louisiana]. *Journal of Sedimentary Research*, 7(1):3–17.

Kumar, D., Pandey, A., Sharma, N., and Flügel, W.-A. (2016). Daily suspended sediment simulation using machine learning approach. *Catena*, 138:77–90.

Labat, D. (2005). Recent advances in wavelet analyses: Part 1. A review of concepts. *Journal of Hydrology*, 314(1-4):275–288.

Langendoen, E., Mendoza, A., Abad, J., Tassi, P., Wang, D., Ata, R., El kadi Abderrezzak, K., and Hervouet, J. (2016). Improved numerical modeling of morphodynamics of rivers with steep banks. *Advances in Water Resources*, 93:4–14.

Legates, D. and McCabe Jr., G. (1999). Evaluating the Use of "Goodness of Fit" Measures in Hydrologic and Hydroclimatic Model Validation. *Water Resources Research*, 35(1):233–241.

Lesser, G., Roelvink, J., van Kester, J. A., and Stelling, G. (2004). Development and validation of a three-dimensional morphological model. *Coastal Engineering*, 51(8-9):883–915.

Lick, W. (2009). *Sediment and contaminant transport in surface waters*.

Liu, Q., Shi, Z., Fang, N., Zhu, H., and Ai, L. (2013). Modeling the daily suspended sediment concentration in a hyperconcentrated river on the Loess Plateau, China, using the Wavelet-ANN approach. *Geomorphology*, 186:181–190.

Liu, X. (2008). *Numerical models for scour and liquefaction around object under currents and waves*. PhD thesis, University of Illinois at Urbana-Champaign.

Liu, X. and Garcia, M. (2008). Three-Dimensional Numerical Model with Free Water Surface and Mesh Deformation for Local Sediment Scour. *Journal of Waterway, Port, Coastal, and Ocean Engineering*, 134(4):203–217.

Lohani, A., Goel, N., and Bhatia, K. (2011). Comparative study of neural network, fuzzy logic and linear transfer function techniques in daily rainfall-runoff modelling under different input domains. *Hydrological Processes*, 25(2):175–193.

Malcherek, A. (2006). *Sedimenttransport und Morphodynamik*. Diplom thesis, Fakultät für Bauingenieur- und Vermessungswesen.

Mallat, S. (1989). A Theory for multiresolution signal decomposition: The wavelet representation. *IEEE transactions on pattern analysis and machine intelligeence*, 11(7):555–560.

Malvern (2017). Malvern Particle Sizer [online] <www.Malvern.com> [Accessed 22/03/2017].

Maniak, U. (1997). *Hydrologie und Wasserwirtschaft: Eine Einführung für Ingenieure*. Springer-Verlag Berlin Heidelberg New York, 4 edition.

McCulloch, W. and Pitts, W. (1943). A logical calulus of the ideas immanent in neural nets. *Bull Math Biophys*, 5:115–33.

Mehta, A. (2013). *An introduction to hydraulics of fine sediment transport*. World Scientific Publishing Co. Pte. Ltd., University of Florida, USA.

Melesse, A., Ahmad, S., McClain, M., Wang, X., and Lim, Y. (2011a). Suspended sediment load prediction of river systems: An artificial neural network approach. *Agricultural Water Management*, 98(5):855–866.

Melesse, A., Ahmad, S., McClain, M., Wang, X., and Lim, Y. H. (2011b). Suspended sediment load prediction of river systems: An artificial neural network approach. *Agricultural Water Management*, 98(5):855–866.

MIKE (2017). Modelling all aspects of sediment processes in 1D, 2D and 3D [online] <https://www.mikepoweredbydhi.com/products/mike-21/sediments> [Accessed 30/06/2017].

Muller, B., Reinhardt, J., and Strickland, M. (1995). *Neural networks: an introduction*. New York, springer-v edition.

Nagy, H., Watanabe, K., and Hirano, M. (2002). Prediction of Sediment Load Concentration in Rivers using Artificial Neural Network Model. *Journal of Hydraulic Engineering*, 128(6):588–595.

Nash, J. and Sutcliffe, J. (1970). River Flow Forecasting Through Conceptual Models Part I - a Discussion of Principles. *Journal of Hydrology*, 10:282–290.

Nie, H., Sun, Z., and Xie, C. (2012). Simulating a typhoon storm surge using a nested Ecomsed model. *Procedia Engineering*, 31:775–780.

Nilson, E., Krahe, P., Lingemann, I., Horsten, T., Klein, B., Carabia, M., and Larina, M. (2014). Auswirkungen des KLimawandels auf das Abflussgeschehen und die Binnenschifffahrt in Deutschland. Technical report, Schlussbericht KLIWAS-Projekt 4.01. KLIWAS-43/2014., Koblenz.

Nilsson, P., Uvo, C., and Berndtsson, R. (2006). Monthly runoff simulation: Comparing and combining conceptual and neural network models. *Journal of Hydrology*, 321(1-4):344–363.

Noack, M., Gerbersdorf, S., Hillebrand, G., and Wieprecht, S. (2015). Combining field and laboratory measurements to determine the erosion risk of cohesive sediments best. *Water*, 7(12):5061–5077.

Noack, M., Schmid, G., and Wieprecht, S. (2014). Erosionsmessungen im Wehrkanal der Staustufe Iffezheim. Technical report, Lehrstuhl für Wasserbau und Wassermengenwirtschaftt, Universität Stuttgart, Stuttgart.

Nourani, V. and Andalib, G. (2015). Daily and monthly suspended sediment load predictions using wavelet based artificial intelligence approaches. *Journal of Mountain Science*, 12(1):85–100.

Nourani, V., Hosseini Baghanam, A., Adamowski, J., and Kisi, O. (2014). Applications of hybrid wavelet - Artificial Intelligence models in hydrology: A review. *Journal of Hydrology*, 514:358–377.

Nourani, V., Komasi, M., and Mano, A. (2009). A Multivariate ANN-Wavelet Approach for Rainfall-Runoff Modeling. *Water Resources Management*, 23(14):2877–2894.

Olsen, N. (2014). *A Three-Dimensional numerical model for simulation of sediment movements in water intakes with multiblock option*. Number June. Department of Hydraulic and Environmental Engineering the Norwegian University of Science and Technology.

Pantankar, S. (1980). *Numerical heat transfer and fluid flow*. New York, mcgraw-hil edition.

Partal, T. and Cigizoglu, H. K. (2008). Estimation and forecasting of daily suspended sediment data using wavelet-neural networks. *Journal of Hydrology*, 358(3-4):317–331.

Pohlert, T., Hillebrand, G., and Breitung, V. (2011). Trends of persistent organic pollutants in the suspended matter of the River Rhine. *Hydrological Processes*, 25(24):3803–3817.

Rajaee, T. (2011). Wavelet and ANN combination model for prediction of daily suspended sediment load in rivers. *Science of the Total Environment*, 409(15):2917–2928.

Rajaee, T., Mirbagheri, S., Zounemat-Kermani, M., and Nourani, V. (2009). Daily suspended sediment concentration simulation using ANN and neuro-fuzzy models. *Science of the Total Environment*, 407(17):4916–4927.

Reynolds, R., Stramski, D., Wright, V., and Woźniak, S. (2010). Measurements and characterization of particle size distributions in coastal waters. *Journal of Geophysical Research: Oceans*, 115(8).

Rouse, H. (1937). Modern conceptions of the mechanics of fluid turbulence. *Transactions, ASCE*, 102:1965.

Rumelhart, D., Hinton, G., and Williams, R. (1986). Learning Internal Representations by Error Propagation. In *Readings in Cognitive Science: A Perspective from Psychology and Artificial Intelligence*, chapter 8, pages 399–421.

Rüther, N. (2006). *Computational fluid dynamics in fluvial sedimentation engineering*. PhD thesis, Norwegian University of Science and Technology.

Salas, J. D., Markus, M., and Tokar, A. S. (2000). Streamflow Forecasting Based on Artificial Neural Networks. pages 23–51.

Schlee, J. (1968). Sand and gravel on the continental shelf off the northeastern United States: U.S. *Geological Survey Circular*, 602:9.

Schlichting, H. (1979). *Boundary layer theory*. New York, mcgraw-hil edition.

Schmitz, J., Zemp, R., and Mendes, M. (2006). Artificial neural networks for the solution of the phasestability problem. *Fluid Phase Equilib*, 245:83–7.

Schreider, S., Jakeman, A., Gallant, J., and Merritt, W. (2002). Prediction of monthly discharge in ungauged catchments under agricultural land use in the Upper Ping basin, northern Thailand. *Mathematics and Computers in Simulation*, 59(1-3):19–33.

Shepard, F. (1954). Nomenclature based on sand-silt-clay ratios: Journal Sedimentary Petrology. *Journal Sedimentary Petrology*, 24:151–158.

Shields, A. (1936). *Application of similarity principles and turbulence research to bedload movement*. Hydraulics laboratory, California Institute of Technology, Berlin: Wasserbau Schiffbau.

Simoes, F. (2014). Shear velocity criterion for incipient motion of sediment. *Water Science and Engineering*, 7(2):183–193.

Speckter, T. (2015). *Auswirkungen vergröberter räumlicher und zeitlicher Gitternetzauflösungen bei der hochaufgelösten Modellierung von Hydraulik und Sedimenttransport an der Staustufe Iffezheim*. PhD thesis, Technische Universität Berlin.

Stokes, G. (1850). On the effect of the internal friction of fluids on the motion of pendulums. pages 1–86.

Taylor, C. (2016). What is Kurtosis? [online] <https://www.thoughtco.com/what-is-kurtosis-3126241> [Accessed 22/06/2017].

Tayyab, M., Zhou, J., Zeng, X., and Adnan, R. (2016). Discharge Forecasting By Applying Artificial Neural Networks At The Jinsha River Basin, China. *European Scientific Journal*, 12(9):1857–7881.

Thomas, H. and Fiering, M. (1962). *Mathematical synthesis of streamflow sequences for the analysis of river basins by simulation*. Design of Water Resources Systems.

Tokar, A. and Johnson, P. (1999). Rainfall-Runoff Modeling Using Artificial Neural Networks. *Journal of Hydrologic Engineering*, 4(3):232–239.

Uenes, F., Yildirim, S., Cigizoglu, H., and Coskun, H. (2013). Estimation of dam reservoir volume fluctuations using artificial neural network and support vector regression. *Journal of Engg. Research*, 1(December):53–74.

Valipour, M., Banihabib, M., and Behbahani, S. (2013). Comparison of the ARMA, ARIMA, and the autoregressive artificial neural network models in forecasting the monthly inflow of Dez dam reservoir. *Journal of Hydrology*, 476:433–441.

van Rijn, L. (1987). *Mathematical modeling of morphological processes in the case of suspended sediment transport*. Ph.d thesis, Delft University of Technology.

van Rijn, L. (1989). *Sediment transport by currents and waves*. Delft, The Netherlands.

van Rijn, L., Davies, A., van de Graaff, J., and Ribberink, J. (2001). *Sediment transport modelling in marine coastal environments*. Aqua Publication, Amsterdam.

Villaret, C., Hervouet, J., Kopmann, R., Merkel, U., and Davies, A. (2013). Morphodynamic modeling using the Telemac finite-element system. *Computers and Geosciences*, 53:105–113.

Vollmer, S. and Goelz, E. (2006). Sediment monitoring and sediment management in the Rhine River. In *Sediment Dynamics and the Hydromorphology of Fluvial Systems*, number July, pages 231–240, Dundee.

Vollmer, S. and Kleinhans, M. (2007). Predicting incipient motion, including the effect of turbulent pressure fluctuations in the bed. *Water Resources Research*, 43(5):1–16.

Wang, W. and Ding, J. (2003). Wavelet network model and its application to the prediction of hydrology. *Nature and Science*, 1(1):67–71.

Warner, J., Sherwood, C., Signell, R., Harris, C., and Arango, H. (2008). Development of a three-dimensional, regional, coupled wave, current, and sediment-transport model. *Computers & Geosciences*, 34(10):1284–1306.

Wei, S., Yang, H., Song, J., Abbaspour, K., and Xu, Z. (2013). A wavelet-neural network hybrid modelling approach for estimating and predicting river monthly flows. *Hydrological Sciences Journal*, 58(2):374–389.

Wentworth, C. (1922). A scale of grade and class te rms for clastic sediments. *Journal of Geology*, 30:377–392.

Whipple, K. (2004). Course Notes. MIT Open Courseware [online] <https://ocw.mit.edu/.../4_sediment_transport_edited.pdf> [Accessed 30/01/2017].

Wieprecht, S., Tolossa, H. G., and Yang, C. T. (2013). A neuro-fuzzy-based modelling approach for sediment transport computation. *Hydrological Sciences Journal*, 58(3):587–599.

Wilcock, P., Pitlick, J., and Cui, Y. (2009). *Sediment Transport Primer Estimating Bed-Material Transport in Gravel-bed Rivers*. Number May.

Willis, D. and Krishnappan, B. (2004). Numerical modelling of cohesive sediment transport in rivers. *Canadian Journal of Civil Engineering*, 31(5):749–758.

Winterscheid, A. and Svenson, C. (2016). Morphologische Entwicklung und Sandbilanz der Elbe im Streckenabschnitt 'oberhalb des Wehres Geesthacht' bis 'Hamburg'. In *17. Gewässermorphologisches Kolloquium*, Koblenz.

Wright, L. and Thom, B. (1977). Coastal depositional landforms: a morphodynamic approach. *Progress in Physical Geography*, 1:412–459.

Wu, W., Rodi, W., and Wenka, T. (2000). 3D numerical modeling of flow and sediment transport in open channels. *Journal of Hydraulic Engineering*, 126(1):4–15.

Wu, W. and Wang, S. (2007). Formulas for sediment porosity and settling velocity. *J. Hydraul. Eng.*, 132(8):858–862.

Yalin, M. and da Silva, A. (1979). Inception of sediment transport. *Journal of the Hydraulics Division*, 105(11):1433–1443.

Yousif, A., Aswad, F., and Ibrahim, S. (2016). Performance of ARIMA model and Modified Thomas-Fiering Model for Predicting the Monthly Rainfall Data for Tallafar Station. 6(1).

Zanke, U. (1977). *Berechnung der Sinkgeschwindigkeiten von Sedimenten*. Band 46 der Reihe Mitteilungen des Franzium-Instituts für Wasserbau und Küsteningenieurwesen der TU Hannover.

Zanke, U. (1982). *Grundlagen der Sedimentbewegung*. Springer Berlin Heidelberg, Berlin, Heidelberg.

Zanke, U. (2003). On the influence of turbulence on the initiation of sediment motion. *International Journal of Sediment Research*, 18(1):17–31.

Zhang, G. (2003). Time series forecasting using a hybrid ARIMA and neural network model. *Neurocomputing*, 50:159–175.

Zhang, Q., Aljoumani, B., Hillebrand, G., Hoffmann, T., and Hinkelmann, R. (2017). Forecasting monthly inflow discharge of the Iffezheim reservoir using data-driven models. In *The EGU General Assembly*, Vienna, Austria.

Zhang, Q., Hillebrand, G., Klassen, I., Vollmer, S., and Olsen, N. (2013). Sensitivity analysis of flow field simulation in the Iffezheim reservoir in Germany with the 3D SSIIM model. In *35th IAHR World Congress 2013*, number 1.

Zhang, Q., Hillebrand, G., Moser, H., and Hinkelmann, R. (2015a). Simulation of Non-Uniform Sediment Transport in a German Reservoir with the SSIIM Model and Sensitivity Analysis. In *36th IAHR Wolrd Congress*, pages 1–9, Den Haag.

Zhang, Q., Hillebrand, G., Speckter, T., Hoffmann, T., Moser, H., and Hinkelmann, R. (2016a). Sensitivity of deposition and erosion to bed composition in the Iffezheim reservoir , Germany. In *13th ISRS*, number Olsen 2014, pages 810–816, Stuttgart. Taylor & Francis Group.

Zhang, Q., Hillebrand, G., Speckter, T., Moser, H., and Hinkelmann, R. (2016b). Reduction of a high-resolution numerical flow and sediment transport model. In *River Flow 2016*, St. Louis. Taylor & Francis Group.

Zhang, R. (1963). Discussion of gravitation theory and mechanism of sediment suspension. *Chinese J. of Hydraulic Reserach*, 3:11–23.

Zhang, X., Peng, Y., Zhang, C., and Wang, B. (2015b). Are hybrid models integrated with data preprocessing techniques suitable for monthly streamflow forecasting? Some experiment evidences. *Journal of Hydrology*, 530:137–152.

Zheng, J., Yan, Y., Tong, C., Lei, Z., and Zhang, C. (2012). Hydrodynamic and morphological processes in Yangtze Estuary: State-of-the-art research and its applications by Hohai University. *Water Science and Engineering*, 5(4):383–398.

Zhou, H., Peng, Y., and Liang, G. (2008). The research of monthly discharge predictor-corrector model based on wavelet decomposition. *Water Resources Management*, 22(2):217–227.

Zhou, X. (2011). *Morphodynamic response of Yangtze River estuary to sea level rise and human interferences*. Dissertation, Technische Universität Darmstadt.

Zhou, Z., Olabarrieta, M., Stefanon, L., D'Alpaos, A., Carniello, L., and Coco, G. (2014). A comparative study of physical and numerical modeling of tidal network ontogeny. *Journal of Geophysical Research: Earth Surface*, 119(4):892–912.

Zounemat-Kermani, M., Kisi, O., Adamowski, J., and Ramezani-Charmahineh, A. (2016). Evaluation of data driven models for river suspended sediment concentration modeling. *Journal of Hydrology*, 535:457–472.